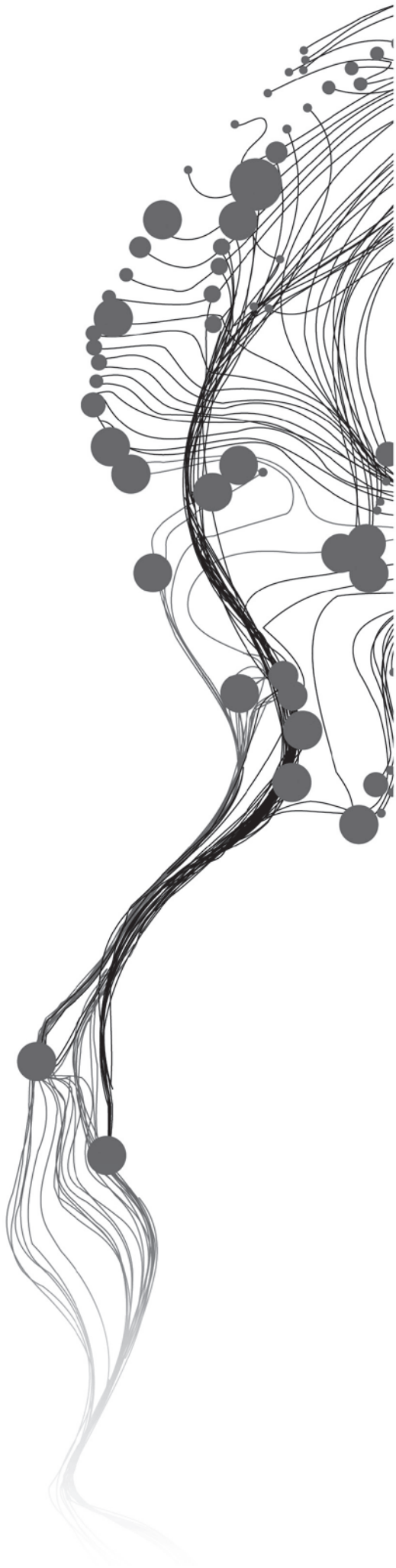


MAPPING ABOVE GROUND CARBON USING WORLDVIEW SATELLITE IMAGE AND LIDAR DATA IN RELATIONSHIP WITH TREE DIVERSITY OF FORESTS

YOGENDRA KUMAR KARNA
February, 2012

SUPERVISORS:
Dr. Y. A. Hussin
Ir. M.C. (Kees) Bronsveld



MAPPING ABOVE GROUND CARBON USING WORLDVIEW SATELLITE IMAGE AND LIDAR DATA IN RELATIONSHIP WITH TREE DIVERSITY OF FORESTS

YOGENDRA KUMAR KARNA

Enschede, The Netherlands, February, 2012

Thesis submitted to the Faculty of Geo-Information Science and Earth Observation of the University of Twente in partial fulfilment of the requirements for the degree of Master of Science in Geo-information Science and Earth Observation.

Specialization: Natural Resources Management

SUPERVISORS:

Dr. Y. A. Hussin

Ir. M.C. (Kees) Bronsveld

THESIS ASSESSMENT BOARD:

Chair: Dr. A. Voinov

External Examiner: Dr. T. Kauranne (Arbonaut Oy Ltd. and Department of Mathematics and Physics, Lappeenranta University of Technology, Finland)

DISCLAIMER

This document describes work undertaken as part of a programme of study at the Faculty of Geo-Information Science and Earth Observation of the University of Twente. All views and opinions expressed therein remain the sole responsibility of the author, and do not necessarily represent those of the Faculty.

ABSTRACT

Forests play a major role in global warming and climate change issues through its unique nature of carbon sinks and sources. Therefore, precise estimation of carbon stock is crucial for mitigation and adaptation of these issues through REDD+ carbon incentive program. Very high resolution (VHR) satellite imagery in combination with airborne LiDAR (Light Detection And Ranging) data using object based image analysis technique provide new opportunities to accurately estimate carbon stock of the forests. This study aims to develop species specific regression model using canopy projection area (CPA) and LiDAR derived tree height as predictor variables for accurate estimation and mapping of carbon stock in tropical forests of Chitwan, Nepal.

WorldView-2 image was co-registered to airborne LiDAR data. Lidar data was further processed to obtain the canopy height model (CHM) by subtracting digital terrain model (DTM) from digital surface model (DSM). Both the pan-sharpened image and CHM layers were used for tree crown delineation to extract CPA and height of the individual trees. Above ground carbon stock was calculated from field measured DBH and height using species-specific allometric equation and a conversion factor. Species wise multiple regression models were developed using CPA, Lidar height and field measured carbon stock for carbon mapping of the study area. Shannon diversity index of each community forests (CF) was calculated to find out the relationship between tree species diversity and carbon stock of CF.

LiDAR derived height showed overestimation of field height with RMSE of 3.84 m and was able to explain 76% of variability in height measurement. Multi-resolution segmentation resulted with overall accuracy of 76% in 1:1 correspondence and 67% segmentation accuracy (33% error) was observed from goodness of fit (D value). Transformed divergence indicated a good separation among different tree species with best average separability of 1970.99. NIR1, NIR2 and Red-Edge of WorldView-2 image were found to be the best bands for spectral separability. Tree species classification resulted in overall accuracy of 58.06% and Kappa statistics 0.47 for classifying six tree species. On average correlation coefficient of CPA and carbon, height and carbon and CPA and height was found to be 0.73, 0.76 and 0.63 respectively and indicated significant relationship for five dominant tree species. Species wise multiple regression models were able to explain 94%, 78%, 76%, 84% and 78% of variation in carbon estimation using CPA and LiDAR height for *Shorea robusta*, *Lagerstroemia parviflora*, *Terminalia tomentosa*, *Schima wallichii* and others respectively. A total of 188485 Mg C carbon stock was estimated with an average of 216 MgCha⁻¹. The relationship between tree diversity and carbon stock at CF level was not significant and indicated weak correlation.

WorldView-2 satellite imagery and airborne LiDAR data are very promising remote-sensing sources for estimating and mapping species wise above ground carbon stock of tropical forests. Further research is suggested to improve the carbon estimation by using non-linear multiple regression model and to explore the relationship between tree diversity and carbon stock at a broad scale of various forest types.

Keywords: Carbon Stock, CPA, LiDAR derived tree height, Co-registration, CHM, Allometric equation, Multi-resolution segmentation, Multiple regression models, Tree diversity, REDD+

ACKNOWLEDGEMENTS

I would like to express my gratitude to ITC, University of Twente and Netherlands Fellowship Program who provided me an opportunity to pursue MSc Degree and granted me the scholarship. I am very grateful to my organization Ministry of Forests and Soil Conservation, the Government of Nepal for giving the opportunity to study in abroad.

I am very much indebted and grateful to Dr. Yousif Ali Hussin, my first supervisor, for his continuous encouragement, invaluable suggestions, constructive feedback and comments from the very beginning till the completion of this research. Without his guidance, this research would hardly have come to fruition. Sincere thanks goes to my second supervisor, Ir. Kees Bronsveld, for his supervision and feedback which was really appreciative from the proposal writing to final submission of my thesis.

My sincere thanks goes to Dr. Alexey Voinov, for his constructive comments during the proposal and mid-term defence, which helped me to pave my way forward for a quality research. I am very much thankful to Dr. Michael Weir, Course Director NRM, for his advice, continuous support and feedback from the beginning of course to completion of research. Special thanks goes to Dr. Ir. T. A. Groen, Dr. D. G. Rossiter and Mr. Chandra Prasad Ghimire for their critical suggestion on statistical matter, Mr. Khamarrul Azahari Razak for guiding us in operating several LiDAR software and his critical comments in my proposal and thesis writing, and Dr. Kourosh Khoshelham and Willem Nieuwenhuis for RS data analysis.

I would like to acknowledge ICIMOD for providing logistic support during fieldwork. A special thanks goes to Mr. Hammad Gilani for his valuable suggestion in analysis of RS data, Himlal Shrestha for coordination and Eak Bahadur Rana for his logistic arrangement for field work and providing necessary documents during thesis writing. I wish to thank Dr. Indra Prasad Sapkota, DFO, Chitwan for providing valuable information and moral support to commence the fieldwork. I am grateful to Mr. Basanta Raj Gautam, Arbonaut Ltd, Finland for his incredible support to accomplish the research and Pem Narayan Kandel, FRA Nepal for providing Lidar data to carry out the research. I am very much thankful to Amrit Pant, ANSAB for initial coordination and providing GPS, FECOFUN members of study area for their kind support, and Man Bahadur Khadaka, Coordinator of REDD+ networking for logistic arrangement to carry out the fieldwork. I am really indebted to Tulka Giri and Sunbir Chepang for their fabulous support and hard work for data collection and completing the fieldwork on time.

I would like to extend heartfelt thanks to my fieldwork mates Pema, Sajana, Moon, Purity, Amado, Sola, Itoe and Tsikai who shared together the tough and cheerful moments. I wish to thank all the NRM classmates for fruitful time and enjoyment throughout the study period. I am very much thankful to all the Nepalese friends (Tika, Deepak, Susheel, Hari, Rehana, Shanti, Sudha, Dilli and Ragindra) for their tremendous support during the hard time and sharing joyful moments during 18 months stay at the Netherlands. My sincere appreciation goes to my colleague Dinesh Babu, Ram K. Deo, Sony and Kalyan Sir and Sharad Baral for their critical review and comments in thesis.

Last but not least, my everlasting gratitude goes to my loving mother, parents in law, family members, relatives and friends who always encourage me and wish my success. My very special thanks goes to my beloved wife Ruby who always sacrificed her interests and encouraged me for further study. I really missed my son Amit and daughter Aditi who always prayed for my success. I am very thankful for their endurance, courage and optimism during my long absence. I know they are eagerly looking up in the sky for my back to home with success.

Yogendra Kumar Karna
Enschede, the Netherlands
February, 2012

Dedicated to my Late Father Bal Krishna Lal Karna
"The ultimate source of inspiration"

TABLE OF CONTENTS

Abstract.....	i
Acknowledgements.....	ii
List of Figures.....	vii
List of Tables.....	viii
List of Equations.....	ix
List of Appendices.....	x
List of Acronyms.....	xi
1. Introduction.....	1
1.1. Background.....	1
1.2. Overview of techniques for above ground carbon estimation.....	2
1.3. What is Lidar and how does it work?.....	4
1.4. Application of Lidar data for above ground carbon estimation.....	5
1.5. Problem statement and justification.....	6
1.6. Research objectives.....	8
1.6.1. Specific objectives.....	8
1.7. Research questions.....	8
1.8. Research hypotheses.....	8
2. Description of the Study Area.....	9
2.1. Criteria for the selection of study area.....	9
2.2. Overview of Chitwan district.....	9
2.2.1. Geographical location and topography.....	9
2.2.2. Climate.....	9
2.2.3. Land use.....	10
2.2.4. Social, economic and demographic.....	10
2.2.5. Vegetation.....	10
2.3. Description of Kayerkhola watershed.....	10
3. Materials and Methods.....	13
3.1. Materials.....	13
3.1.1. Satellite data.....	13
3.1.2. Airborne Lidar data.....	13
3.1.3. Maps and other ancillary data.....	13
3.1.4. Field instruments.....	14
3.1.5. Software and tools.....	14
3.2. Methods.....	14
3.3. Image processing.....	16
3.3.1. Subset of image.....	16
3.3.2. Image fusion.....	16
3.4. Pre-fieldwork.....	16
3.4.1. Sampling design.....	17
3.4.2. Plot layout.....	17
3.5. Fieldwork.....	17
3.6. Secondary data collection.....	18

3.7.	Data analysis	18
3.7.1.	Fieldwork data analysis	19
3.7.2.	Tree diversity analysis.....	19
3.7.3.	Allometric equation and carbon stock calculation	19
3.7.4.	Manual delineation of tree crowns.....	20
3.8.	Species differentiation capability of image.....	21
3.8.1.	Transformed Divergence (TD).....	21
3.8.2.	Spectral separability of the tree classes.....	21
3.9.	Lidar data processing.....	22
3.9.1.	CHM generation	22
3.9.2.	Accuracy assessment of CHM.....	22
3.10.	Coregistration of image and Lidar data	22
3.11.	Layer stacking of image and CHM.....	23
3.12.	Image segmentation.....	23
3.12.1.	Multi-resolution segmentation.....	23
3.12.2.	Validation of segmentation	27
3.13.	Image classification and accuracy assessment	28
3.14.	Feature extraction	29
3.15.	Statistical Analysis	29
3.15.1.	Correlation analysis.....	29
3.15.2.	Multiple regression analysis.....	29
3.15.3.	Model calibration and validation	29
3.15.4.	Relationship of carbon stock and tree diversity.....	30
4.	Results.....	31
4.1.	Descriptive analysis of field data	31
4.2.	Shannon diversity index.....	32
4.3.	Carbon stock calculation from field data	33
4.4.	Species differentiation capability of image.....	33
4.4.1.	Transformed divergence (TD).....	33
4.4.2.	Spectral separability of tree classes.....	34
4.5.	CHM generation from Lidar data.....	35
4.6.	Accuracy assessment of Lidar derived tree height.....	35
4.7.	Image segmentaion	36
4.8.	Validation of segmentation.....	38
4.9.	Image classification and accuracy assessment	38
4.10.	Feature extraction	41
4.11.	Correlation analysis.....	41
4.12.	Model calibration and validation	42
4.13.	Carbon stock mapping of study area	43
4.14.	Relationship between tree diversity and carbon stock	45
5.	Discussions	47
5.1.	Canopy height model (CHM) generation and accurarcy assessment	47

5.2.	Image segmentation and accuracy assessment.....	48
5.3.	Image classification and accuracy assessment.....	50
5.4.	Modelling the relationship of CPA, height and carbon.....	51
5.5.	Carbon stock estimation.....	53
5.6.	Relationship between tree diversity and carbon stock.....	53
5.7.	Uncertainties and sources of error for carbon mapping.....	54
5.7.1.	GPS error occurred during navigation.....	54
5.7.2.	Uncertainty on tree level estimation.....	54
5.7.3.	Co-registration of image and Lidar data.....	55
5.7.4.	Sun elevation angle and off nadir view.....	55
5.7.5.	Summary of analysis of error.....	56
5.8.	Limitation of the research.....	56
6.	Conclusions and Recommendations.....	57
6.1.	Conclusions.....	57
6.2.	Recommendations.....	58
	List of References.....	59
	Appendices.....	65

List of Figures

Figure 1-1: Illustration of the conceptual differences between waveform and discrete-return Lidar	4
Figure 1-2: A typical operation of a Lidar survey (USDA, 2006)	5
Figure 2-1: Location map of the study area.	11
Figure 3-1: Flow diagram of research methods	15
Figure 3-2: Schematic representation of sample plot layout.....	18
Figure 3-3: Multi-resolution concept flow diagram: adapted from (Definiens, 2011).....	24
Figure 3-4: Segmentation processing steps and its corresponding ruleset	25
Figure 3-5: Interface of ESP tool for determining scale parameter	25
Figure 4-1: Species composition of study area	31
Figure 4-2: Box plot of DBH height and crown diameter of major tree species.....	32
Figure 4-3: Spectral separability of forest tree species.....	34
Figure 4-4: Lidar-derived images a) DTM, b) DSM), c) CHM, d) CHM visualized in 3D	35
Figure 4-5: Scatterplot and summary of fit for tree height measurements	36
Figure 4-6: a) Subset of pan-sharpened filtered image b) shadow and non-tree cover masking.....	37
Figure 4-7: Segmentation of pan-sharpened image and CHM.....	37
Figure 4-8: Measure of closeness (D value) for accuracy assessment of segmentation	38
Figure 4-9: Tree species classification map of study area	40
Figure 4-10: Scatterplot of observed and predicted carbon stock.....	43
Figure 4-11: Carbon stock map of Devidhunga CF and carbon stored by one tree (inset)	44
Figure 4-12: Species wise carbon stock of the study area	45
Figure 5-1: Errors in tree height measurements (Köhl <i>et al.</i> , 2006).....	48
Figure 5-2: a) Ground view and b) canopy view of clumped trees	49
Figure 5-3: WorldView-2 image a) cloud and huge shadow b) distortion in image	50
Figure 5-4: Error caused by co-registration.....	55
Figure 5-5: Tree crown shape from different angle of view (Li <i>et al.</i> , 2008).....	55

List of Tables

Table 2-1: Land cover types of Kayerkhola watershed.....	10
Table 2-2: Details of selected community forests (CFs).....	11
Table 3-1: Lidar data collection parameters for Leica ALS-40 sensor.....	13
Table 3-2: Field instruments used for the data collection	14
Table 3-3: List of the software and purpose of its use.....	14
Table 3-4: Number of sample plots measured in the field	18
Table 3-5: Model parameters and wood density of major tree species	20
Table 4-1: Descriptive statistics of sampled trees	31
Table 4-2: Diversity measures of CF.....	33
Table 4-3: Carbon stock calculated from field data.....	33
Table 4-4: Transformed divergence of WorldView-2 image.....	34
Table 4-5: Summary of statistics for tree height measurements.....	36
Table 4-6: Summary of statistical test	36
Table 4-7: Matching 1:1 correspondence of reference polygons to segmented polygons	38
Table 4-8: Summary of classification accuracy assessment	39
Table 4-9: User's and producer's accuracy of species classification	39
Table 4-10: Correlation among the variables of regression model.....	41
Table 4-11: Regression coefficients and summary statistics of model	42
Table 4-12: Summary of model validation and RMSE (kg/tree)	42
Table 4-13: Summary of species wise carbon stock (Mg C).....	44
Table 4-14: Summary of Pearson's correlation analysis	45
Table 4-15: Summary of one way ANOVA.....	46
Table 5-1: Several stages of sources of error and uncertainties	56

List of Equations

Equation 1: Lidar height measurement.....	4
Equation 2: Sample size determination.....	17
Equation 3: Shannon diversity index	19
Equation 4: Allometric volume equation.....	19
Equation 5: Calculation of stem biomass	20
Equation 6: Calculation of AGB from tree component biomass.....	20
Equation 7: Calculation of carbon stored by individual trees	20
Equation 8: Calculation of over segmentation	27
Equation 9: Calculation of under segmentation	27
Equation 10: Measure of closeness.....	28
Equation 11: RMSE calculation	30
Equation 12: Multiple regression model.....	42

List of Appendices

Appendix 1: Features of satellite image	65
Appendix 2: Printed image of sample plot.....	66
Appendix 3: Sample of data collection sheet.....	67
Appendix 4: Location of sample plots.....	68
Appendix 5: Name list of plant species found in the study area	69
Appendix 6: Descriptive statistics of trees for each CFs	70
Appendix 7: Details of outlier trees	71
Appendix 8: Segmentation of Panchromatic WorldView-2 image	71
Appendix 9: Accuracy assessment of species classification for each CFs.....	72
Appendix 10: Details of ANOVA table and regression parameters.....	73
Appendix 11: Carbon map of study area (CF wise).....	75
Appendix 12: Photographs from the field	79

List of Acronyms

AGB	Aboveground biomass
ANOVA	Analysis of variance
ANSAB	Asia Network for Sustainable Agriculture and Bio-resources
CBD	Convention on Biological Diversity
CF	Community Forest
CFUGs	Community Forest User Groups
CHM	Canopy Height Model
CO ₂	Carbon dioxide
CPA	Crown projection area
DBH	Diameter at breast height
DEM	Digital Elevation Model
DFO	District Forest Office
DoF	Department of Forests
DN	Digital Number
DSM	Digital Surface Model
D _T	Transformed divergence
DTM	Digital Terrain Model
FAO	Food and Agricultural Organization
FRA	Forest Resource Assessment
GHG's	Greenhouse gases
GPS	Geographic Position System
HCS	Hyperspherical Colour Sharpening
HPF	High Pass Filtering
ICIMOD	International Centre for Integrated Mountain Development
IHS	Intensity, Hue and Saturation
IPCC	Intergovernmental Panel on Climate Change
LiDAR	Light Detection and Ranging
MOFSC	Ministry of Forest and Soil Conservation
MSS	Multispectral data
NIR	Near Infrared band
NTFPs	Non-Timber Forest Products
OBIA	Object based image analysis
REDD+	Reducing carbon emission form deforestation and forest degradation and foster conservation, sustainable management of forests, and enhancement of forest carbon stocks
RGB	Red, Green and Blue
RMSE	Root Mean Square Error
UNFCCC	United Nations framework Convention on Climate Change
VDC	Village Development Committee
VHR	Very high resolution
WGS	World Geographical System

1. INTRODUCTION

1.1. Background

The growing concentration of greenhouse gases (GHGs) in the atmosphere increases temperature of the earth and have raised concerns about global warming and climate change issues. Carbon dioxide (CO₂) is one of the main contributors of greenhouse effect in the atmosphere along with other gases. The global atmospheric concentration of CO₂ has increased from 280 ppm in pre-industrial era (1970) to 379 ppm in 2005 at an average of 1.9 ppm per year which will further contribute to increase the temperature from 1.8°C to 4° C by the end of this century (IPCC, 2007). The sudden increase of CO₂ concentration is highly related with anthropogenic causes such as heavy use of fossil fuels, deforestation and degradation of land. Deforestation and forest degradation are responsible for about 20% of GHGs emissions, a major issue for climate change (World Bank, 2010)

Carbon is sequestered and stored by terrestrial and marine ecosystems. About 2,500 gigatonne carbon (Gt C) are stored in terrestrial ecosystems, compared to approximately 750 Gt C in the atmosphere (CBD, 2009). Healthy forests sequester and store more carbon compared to any other terrestrial ecosystem and are considered to be an important natural brake on climate change (Gibbs *et al.*, 2007). At present, forest covers around 31 percent of total global land area and stores a vast amount (289 Gt) of CO₂ in their biomass alone (FAO, 2010). Forests sequester CO₂ from the atmosphere through photosynthesis process and act as a carbon sink. At the same time, some areas of forests are being destroyed, overharvested or burned, and converted to non-forest use, consequently becoming the source of carbon emission. Tropical forests are a large pool of both the carbon sinks and sources, therefore the estimation of carbon stock is crucial for understanding the global carbon cycle and to reduce the global warming (Sierra *et al.*, 2007).

The Kyoto Protocol to the United Nations Framework Convention on Climate Change (UNFCCC) contains quantified and legally binding commitments to limit or reduce GHGs emissions at an average rate of 5% to 1990 level over the five-year period 2008-2012 (UNFCCC, 2011). All the contracting parties to the convention commit themselves to develop, periodically update, publish and report to the Conference of Parties (COP) about their national inventories to emissions by sources and removals by sinks of all GHGs using comparable methods (Houghton *et al.*, 1997). In addition, the Bali Action Plan (COP-13) of UNFCCC in 2007 opened windows of opportunity for developing countries to participate in forest carbon financing through the mechanism of "reducing emissions from deforestation and forest degradation" (REDD) (MOFSC, 2009). REDD is an international effort to create a financial value for the carbon stored in forests. It offers incentives for countries to preserve their forestland in the interest of reducing carbon emissions and investing in low-carbon paths of sustainable development (UN-REDD, 2009). The UNFCCC meeting of COP-15 introduced "REDD+" mechanism which is concerned with both reducing emissions and enhancing carbon stocks through actions that address deforestation, forest degradation, forest conservation and sustainable forest management (Cerbu *et al.*, 2011). To achieve the entire target in one hand, REDD+ will require the full engagement and respect for the rights of indigenous peoples and other forest-dependent communities.

Nepal is acknowledged and highly appreciated for its participatory forest management regimes. At present, approximately 39.6% of geographical area of the country is covered by forests, 25% of which are managed by local and indigenous community as a Community Forestry (DoF, 2010). The role of Community Forestry in REDD+ implementation is a central topic of discussion in Nepal's REDD process, and it is likely to be an important part both for environmentally effective and equitable approach (REDD net, 2009). Nepal, being a UNFCCC signatory and a member of UN-REDD Program, has recently submitted

the Readiness Preparation Proposal to participate in the Forest Carbon Partnership Facility. In order to further participate in the Carbon Finance Mechanism, Nepal has to show its current status of carbon stored by forests and emitted from deforestation and forest degradation (MOFSC, 2009). Therefore, it is crucial to precisely estimate the national forest carbon stocks in terms of biomass and sources of carbon emissions to determine a national reference scenario and to develop a national REDD strategies in Nepal.

1.2. Overview of techniques for above ground carbon estimation

FAO (2010) has defined biomass as "the organic material both above and below the ground, and both living and dead, tree, crops, grasses, dried litter, root etc" which is an important measure for analyzing ecosystem productivity. Above ground biomass (AGB), below ground biomass (BGB), dead wood, litter and soil organic matter is the main carbon pools in any forest ecosystem (FAO, 2010). AGB contains 47% of carbon which is defined as "all biomass of living vegetation, both woody and herbaceous, above the soil including stems, stumps, branches, bark, seeds and foliage (IPCC, 2007). Majority of biomass assessments are done for AGB of trees because these generally account for the greatest fraction of total living biomass in a forest and can be readily measured in the field (Brown, 1997). Others like the understory is estimated to be equivalent to 3% of above-ground tree biomass, dead wood 5-40%, and fine litter only 5% of that in the above-ground tree biomass. Hence, measuring AGB has received considerable attention in recent years because biomass can be readily converted to carbon storage, and quantifying carbon storage is important in understanding the carbon cycle (Malhi *et al.*, 2002).

There are different methods in practice to measure AGB and consequently the carbon stock of forests. Lu (2006) reviewed and summarized some approaches to estimate forest biomass based on field measurements, Remote Sensing (RS) and Geographic Information System (GIS). The AGB can be accurately estimated by destructive sampling (cutting and weighing) but it is not a practical approach because it is extremely costly, time consuming and labour intensive (Brown, 2002). Carbon estimation based on field measurements can be done by the measurements of diameter at breast height (DBH) alone or in combination with tree height which can be further converted to estimates of forest carbon stocks using allometric relationships (Gibbs *et al.*, 2007). Allometric equations statistically relate these measured forest attributes to destructive harvest measurements, and exist for most forests. Additionally, a sufficient number of field measurements are a prerequisite for developing AGB estimation models and for evaluating the AGB estimation results. GIS-based methods require ancillary data such as land cover type, site quality and forest age to establish an indirect relationship for biomass in an area (Lu, 2006). Such methods are difficult to implement because of problems in obtaining good quality ancillary data and the comprehensive impacts of environmental conditions on biomass accumulation (Brown, 2002; Lu, 2006). In RS based method, statistical relationship between satellite extracted tree parameters and ground based measurements is used in biomass estimation (Gibbs *et al.*, 2007). However, ground data is still necessary to develop the biomass predictive model (*i.e.* calibration) and its validation (Zianis *et al.*, 2005) because RS does not measure biomass, but rather it measures some other forest characteristics (*e.g.* spectral reflectance from the canopy).

The combination of above mentioned approaches provide an alternative to traditional methods which gives spatially explicit information and enable repeated monitoring, even in remote locations and in a cost effective way (Patenaude *et al.*, 2005). Therefore, with the advantage of having the capability to provide spatial, temporal and spectral information, remote sensing can be used as a tool for accurate estimation of carbon to meet the requirements of the Kyoto Protocol and UN-REDD Program (Andersson *et al.*, 2009; Rosenqvist *et al.*, 2003).

A range of satellite sensors from low to very high spatial resolution is available for mapping and monitoring forest resources. Andersson *et al.* (2009) has categorized the passive sensors as ultrafine (<5m), fine (10-100m), medium (100-250m) and coarse (>250m) on the basis of spatial resolution and further

explained their application in various field. For example, fine resolution satellite images are well suited for the land classification while ultrafine resolution are better adapted for measuring forest variable inputs for the allometric models (Andersson *et al.*, 2009) but medium to coarse resolution images are more suitable for monitoring changes in spatial extent of forests and identifying geographic areas. However, optical coarse resolution imageries are often used for biomass estimation at national, continental and global scales (Baccini *et al.*, 2004; Clark *et al.*, 2001). For example, NOAA-AVHRR data is probably most extensively used dataset to study vegetation dynamics on continental scale. It has shown its utility to represent net primary productivity for year 1982 (Warrick *et al.*, 1986). Coarse resolution pixels usually receive response from several stands, which makes the direct biomass estimation problematic (Muukkonen & Heiskanen, 2007) and tends to underestimate carbon stock. Lu (2006) reviewed that the AGB estimation based on coarse spatial resolution data is limited because of the common occurrence of mixed pixels and results in drawbacks in the integration of sample data and RS derived variables. In addition, Steininger (2000) faced problem of data saturation while estimating AGB in tropical regenerating forest using medium resolution Landsat TM data. Therefore, recognizing and understanding the strengths and weaknesses of different types of sensors and data are essential for selecting suitable sensor data for AGB estimation in a specific study (Lu, 2006; Tsendbazar, 2011).

Remote sensing based AGB estimation is a complex procedure in which many factors, such as atmospheric conditions, mixed pixels, data saturation and complex biophysical environments may interactively affect estimation performance (Lu, 2006). However, very high resolution (VHR) satellite images such as IKONOS, Quickbird, WorldView-2 and GeoEye-1 can be used to recognize, identify and delineate individual tree crown by object based image analysis (OBIA) (Gougeon & Leckie, 2006). Baral (2011) used OBIA method to compare the segmentation accuracy of tree crown and species classification accuracy and found better result of GeoEye than WorldView-2 images. Similarly, Tsendbazar (2011) demonstrated higher accuracy of tree crown delineation by region growing approach than valley following approach in mixed forest using the GeoEye images. However, effect of shadow, sun elevation angle and off-nadir viewing angle could not be overcome by the high resolution satellite images.

In principle, optical remote sensing technologies face the problem of frequent cloud cover which limits the acquisition of high quality RS data. In this situation, the use of Radar (Radio Detection and Ranging)/SAR (Synthetic Aperture Radar) becomes a feasible means for acquiring RS data in a given period of time irrespective of weather or light conditions (Ahamed *et al.*, 2011). Radar systems are active remote sensors operating in the microwave portion of the electromagnetic spectrum (ca. 1cm to 10m VHF). It generates their own source of electromagnetic radiation allowing to capture images independently of solar energy (Patenaude *et al.*, 2005). The Radar backscatter returned from the ground and tops of the trees are used to estimate tree height, which are then converted to forest carbon stock estimates using allometry (Gibbs *et al.*, 2007; Toan *et al.*, 2004). Although Radar backscatter has the capability to penetrate the clouds, it poses a saturation problem in tropical forest environments where AGB level generally exceed 200-250 Mg/ha (Ustin, 2004) and sometimes mountainous and hilly conditions also increase the errors (Toan *et al.*, 2004). To overcome this problem, active remote sensing sensor (*e.g.* airborne laser scanning or airborne LiDAR) is a promising mapping technique for estimating forest biomass, as no saturation is observed at high biomass levels (Patenaude *et al.*, 2005). Airborne LiDAR also offers the unique capability of measuring the three-dimensional vertical structure of vegetation in great detail which in itself is an advantage over high resolution satellite imagery (Song *et al.*, 2010). Moreover, forest structural characteristics such as canopy heights, stand volume, basal area and aboveground biomass can be accurately estimated directly by LiDAR data (Hyyppa *et al.*, 2008).

1.3. What is Lidar and how does it work?

LiDAR, is an acronym derived from LIght Detection And Ranging. As Lidar is a commonly used acronym, I will use 'Lidar' hereafter in this thesis. It is an active remote sensing technology that promises to both increase the accuracy of biophysical measurements and extend spatial analysis into the third (z) dimension (Lefsky *et al.*, 2002). The Lidar device directly measures the distance between the sensor and a target surface, obtained by determining the elapsed time between the emission of a short duration laser pulse and the arrival of the reflection of that pulse (the return signal) at the sensor's receiver. Multiplying this time interval by the speed of light results in a measure of the round-trip distance, and dividing that figure by two yields the distance between the sensor and the target (Bachman, 1979).

$$[\text{Distance} = (\text{Speed of light} * \text{Travelled time}) / 2] \dots \dots \dots \text{Equation 1: Lidar height measurement}$$

Lidar sensor, generally for terrestrial application, operates in the wavelengths range of 900–1064 nanometers where vegetation reflectance is high (Lefsky *et al.*, 2002) because in visible wavelengths, vegetation absorbance is very high and only a small amount of energy would be returned to the sensor. Lidar instruments can be categorized on the basis of two major characteristics *i.e.* the width of the laser beam and the way of return signal recorded in the devices. According to the first characteristics, it can be divided either as a large footprint or small footprint. Large footprint systems, such as Scanning Lidar Imagery of Canopies by Echo Recovery (SLICER) or the Laser Vegetation Imaging Sensor (LVIS), have a laser beam that is greater than 5 m in diameter, whereas small footprint systems use a more narrowly focused beam that is typically less than 50 cm in diameter (Dubayah & Drake, 2000b; Lefsky *et al.*, 2002). To date, all large footprint systems are experimental devices constructed by research institutions. Based on the second characteristics, Lidar sensor can be categorized into two forms as shown in Figure 1-1 *i.e.* Discrete-return device (DRD) and Waveform recording devices (WRD) (Lefsky *et al.*, 2002).

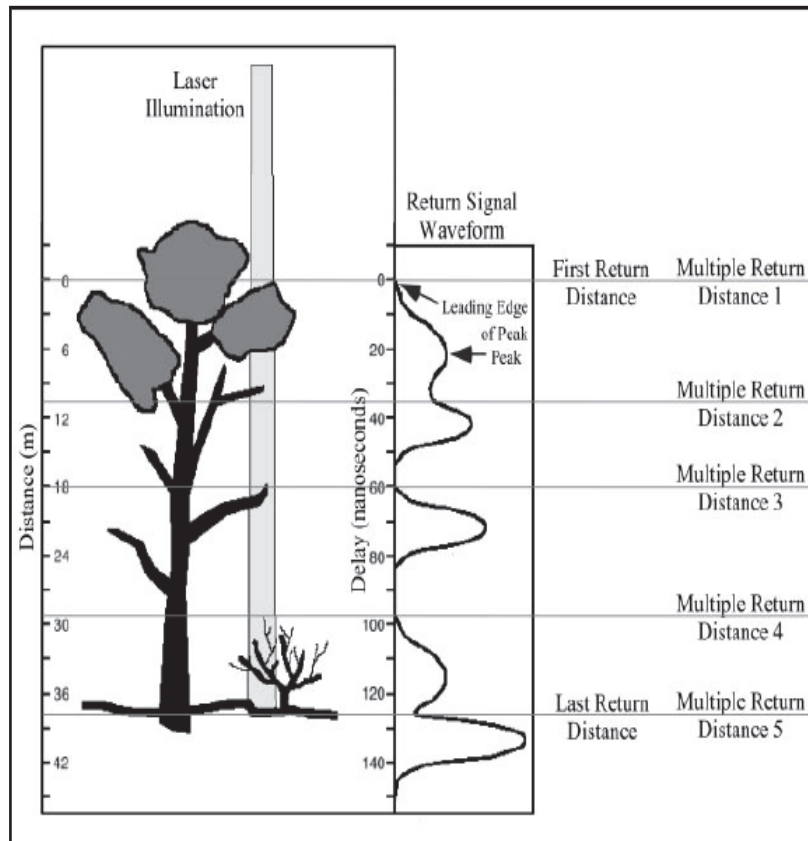


Figure 1-1: Illustration of the conceptual differences between waveform and discrete-return Lidar (Lefsky *et al.*, 2002)

Discrete-return Lidar devices measure either one (single-return systems) or a small number (multiple-return systems) of heights by identifying, in the return signal, major peaks that represent discrete objects in the path of the laser illumination (Lefsky *et al.*, 2002). While WRD records the time-varying intensity of the returned energy from each laser pulse, providing a record of the height distribution of the surfaces illuminated by the laser pulse (Dubayah *et al.*, 2000a; Harding *et al.*, 1994).

Both discrete-return and waveform sensors are typically used to measure the position of any x, y, z point on the Earth's surface from three sources: (i) the Lidar sensor, (ii) the Inertial Navigation System (INS) and (iii) Global Positioning System (GPS) (Figure 1-2). The Lidar measurements must be corrected for the pitch, roll and yaw of the aircraft by INS, and the GPS information allows the slant distances to be corrected and converted into a measurement of ground elevation relative to the WGS84 datum or local mapping system (Heritage, 2009). Combining this information with accurate time referencing of each source of data yields the absolute position of the reflecting surfaces for each laser pulse.

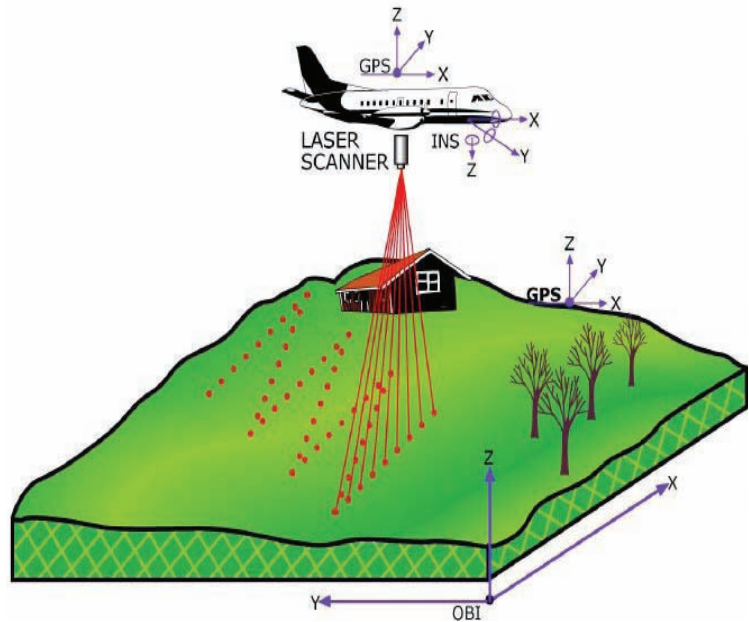


Figure 1-2: A typical operation of a Lidar survey (USDA, 2006)

1.4. Application of Lidar data for above ground carbon estimation

Lidar mapping can be done from both the platforms *i.e.*, airborne and space borne, but till the date it has been carried out based on airborne sensors data only, and there is yet no option before 2015 from the space (Gibbs *et al.*, 2007). Airborne Lidar data has capability to monitor forest biomass and volumes across ecosystems and aboveground biomass ranges. In contrast to optical remote sensing methods, Lidar has certain characteristics such as high sampling intensity, direct measurements of heights and precise geolocation, which enable it for directly assessing vegetation characteristics and deriving forest biomass at multiple scales, from individual trees to regional extents (Popescu, 2007). Lefsky *et al.* (2002) and Lim *et al.* (2003b) reviewed the potential of Lidar devices for retrieving forest parameters. The Lidar data were used to estimate Douglas fir western hemlock biomass (Lefsky *et al.*, 1999a; Means *et al.*, 1999), temperate mixed deciduous forest biomass (Lefsky *et al.*, 1999b), tropical forest biomass (Drake *et al.*, 2002), tree height and stand volume (Nilsson, 1996), stand height (Wulder & Seemann, 2003), tree crown diameter (Popescu *et al.*, 2003), and canopy structure (Lovell *et al.*, 2003). Similarly, Patenaude *et al.* (2004) estimated the above ground carbon content (AGCC) in a temperate deciduous woodland, by means of a discrete-return small-footprint airborne Lidar. They obtained a high correlation ($r = 0.85$) between field based estimates of AGCC and Lidar estimation from 20*20 m grid.

Very high resolution (VHR) optical imagery has been used extensively for forest inventory and health monitoring. The advancement of technology has extended the possibilities of using VHR imagery with other active remote sensing data (*e.g.* Lidar system). This system cannot provide all the information about the canopy structure and other forest parameters (basal area, volume *etc*) that is desired, however, it can be used to accurately assess biomass and height metrics. Combining these two types of complementary datasets is a very promising technique for improving forest classification (Ke *et al.*, 2010), species identification (Persson *et al.*, 2004), and individual tree crown analysis (Leckie *et al.*, 2003) and individual tree detection and carbon stock estimation (Kim *et al.*, 2010).

Furthermore, previous research indicated that either only use of Lidar data or in combination with other sensor or ancillary data, provide an important data source for forest parameter estimation (Drake *et al.*, 2003; Lim *et al.*, 2003b). For example, Popescu (2007) developed a method for assessing AGB for

individual pine trees using small footprint airborne Lidar data and found more accurate result ($R^2=0.88$) between model based and ground based measured biomass. Ke *et al.* (2010) found more accurate forest classification accuracy (Kappa =91.6%) using both spectral and Lidar data than using either spectral-based segmentation (88%) or Lidar-based segmentation (87%). Merging of Lidar and optical imagery and applying circular window filtering algorithm, Popescu *et al.* (2004b) claimed the improvement of volume and biomass estimates for pines and deciduous forest as opposed to use of Lidar data alone. Additionally, Holmgren *et al.* (2008) presented the benefits of integrating Quickbird multispectral imagery and high-density Lidar data for individual tree based classification, the accuracy increased from 88 to 96%. Similarly, Leckie *et al.* (2003) fused high-density Lidar data and digital camera imagery for suitable tree crown isolation and tree height measurement and the results showed between 80 to 90% good correspondence with ground reference tree delineations.

There are two methodological approaches for utilizing Lidar data for AGB assessment, (i) area-based approach and (ii) single-tree-based approach. Existing small footprint Lidar processing techniques follow one of the two approaches. In the first approach, distributional metrics such as the mean canopy height and the standard deviation of the canopy height are taken from either an interpolated grid corresponding to the height of the canopy a) canopy height model (CHM) or b) the raw returns. These metrics are then used in conjunction with regression equations to predict forest properties (Lim *et al.*, 2003a; Means *et al.*, 1999; Naeset & Bjerknes, 2001; Nelson *et al.*, 1988). The second approach is to use computer vision techniques to locate and measure the properties of individual trees using CHM (McCombs *et al.*, 2003; Persson *et al.*, 2002; Popescu *et al.*, 2003). It requires high point densities (>5 points/m²) Lidar data, and is mostly based on regression models focusing on a relationship between Lidar derived individual tree parameters (*e.g.* tree height, crown dimensions) and field based estimates of AGB. Whereas, area-based methods can also be used for lower point densities but require an extensive set of reference data (Jochem *et al.*, 2010). Several researches have been carried out for the estimation of AGB carbon based on area based approach or plot level (Jochem *et al.*, 2010; Nilsson, 1996; Patenaude *et al.*, 2004; Popescu *et al.*, 2004b) as well as single tree based approach (Kim *et al.*, 2010; Popescu, 2007; Popescu *et al.*, 2003).

1.5. Problem statement and justification

Several remote sensing based approaches have been developed for quantifying biomass and carbon stocks. However, most of the existing methods have considerable uncertainties for estimation results of carbon stocks and, thus reliable and accurate methods are required (Köhl *et al.*, 2009). In this context, integration of VHR satellite imagery such as WorldView-2 and Lidar data may provide more accurate estimation of carbon stock than other previous approaches. Airborne Lidar is a proven technology that can be used to accurately assess AGB but it cannot differentiate the species with low point density. Similarly it could not measure relative health of forest ecosystems which is relatively possible to extract from passive optical sensors. Individual tree and stand-level physical attributes such as tree height, canopy height, canopy closure, and density can be generated from Lidar data (Zimble *et al.*, 2003). In comparison to Lidar point cloud analysis, high resolution satellite image analysis does not provide 3D structural information of forest at either an individual tree or stand level for detailed biomass estimation. Therefore, integration of two technologies can be used for accurate estimation of AGB and carbon in tropical forests (Pilger, 2008) and also possible in Nepalese environment.

WorldView-2 is said to be the second generation satellite having a unique combination of various bands (DigitalGlobe, 2010). The spectral coverage of bands is: two bands of blue *i.e.* blue and coastal blue, followed by green, yellow, red, red edge and two bands of Near Infrared (NIR1 and NIR2). The yellow, Red-edge and two bands of NIR are regarded as important for vegetation study. The NIR1 band has a great potential to identify the vegetation type at species level (DigitalGlobe, 2010). Therefore, it is highly recommended by Baral (2011), who carried out her research in the same area, to use this image for further

explanation to estimate the amount of carbon stock since she could not achieve the good classification result due to geo-referencing and other artifacts.

DBH and tree height are crucial forest inventory attributes for calculating timber volume, above ground biomass, site quality and silvicultural treatment scheduling. Measuring of stand height or tree height by current manual photogrammetric or field survey techniques is time consuming and rather expensive (Popescu & Wynne, 2004a). DBH cannot be directly retrieved either from VHR satellite imagery or from low point density Lidar data. Therefore, relationship between DBH, crown diameter/crown projection area (CPA) and tree height should be established from regression analysis so that AGB can be estimated from remote sensing techniques (Popescu & Wynne, 2004a). However, crown diameter or CPA can be obtained from VHR satellite imagery whereas tree height can be easily obtained from canopy height model developed from Lidar data. Thus, the combination of VHR optical imagery and Lidar systems permit individual tree and canopy height information to be extracted along with the species, health, and other biophysical tree attributes (Leckie *et al.*, 2003). Besides, the integration of both spectral and Lidar data will be resulted in more accurate forest classification than using either of the data sources independently. Several studies (Andersen *et al.*, 2005; Gautam *et al.*, 2010; Hudak *et al.*, 2002; Kim *et al.*, 2010; Lu, 2006; Popescu *et al.*, 2004b) also showed that the integration of VHR satellite images and airborne Lidar data provides an accurate and efficient measurement of AGB in a variety of forest types and extensively larger areas. Furthermore, Shrestha (2011), Tsendbazar (2011) and Shah (2011), who already done their research in the same geographical location, highly recommended the integration of VHR images such as GeoEye and WorldView-2 with Lidar data for accurate estimation of AGB in the mountainous topography.

The UNFCCC and Convention on Biological Diversity (CBD) aim at addressing the global agenda of climate change and loss of biodiversity. The existence of potential synergies between the two conventions offers opportunities for implementing practices that aim at achieving the objectives of both conventions simultaneously (Caparros & Jacquemont, 2003). The relationship between tree species diversity and above ground carbon stock is of great concern among forest managers interested in estimation and mapping of carbon stock over a short time period and at a local level. But a few studies have been conducted to analyze this relationship. Sharma *et al.* (2010) conducted a research on twenty major forest types of India to assess the relationship between tree diversity and carbon stock and found a negative correlation between them. On contrary, Nakakaawa *et al.* (2010) found a strong positive correlation between carbon density and tree diversity in agro-ecosystem (afforestation/reforestation area) in south western Uganda.

Caparros & Jacquemont (2003) found that creating economic incentives for carbon sequestration may have negative impacts on biodiversity, especially for afforestation and reforestation programs. However, they also concluded that emphasis on carbon sequestered by means of forest management with economic incentives is not expected to have a great negative influence on biodiversity. Therefore, it is essential to assess the relationship between carbon stock and tree diversity of the tropical forests since Nepal is preparing for REDD+ implementation which addresses the issue of forest management and ensure the rights of indigenous community. In other words, a synergistic relationship between REDD+ and biodiversity conservation program should be considered before setting up the priorities for biodiversity protection and carbon sequestration. Thus, this study aims to explore the possibility of accurate estimation and mapping of carbon stock from the fusion of VHR satellite imagery and Lidar data in relationship with tree diversity which will be useful for mapping of carbon stock in tropical environment.

1.6. Research objectives

The main aim of this research is to develop an approach for accurate estimation of carbon stock using WorldView -2 satellite image and airborne LiDAR data and its relationship with tree diversity of tropical forests.

1.6.1. Specific objectives

1. To develop a canopy height model (CHM) for tropical broadleaved forests based on Lidar raw data and evaluate its accuracy.
2. To determine the relationship among CPA, height and carbon stock of different tree species.
3. To estimate/map carbon stock of study area using WorldView-2 image and airborne LiDAR data.
4. To evaluate the relationship between tree diversity and carbon stock of tropical broadleaved forests.

1.7. Research questions

1. How accurately the height of individual trees can be estimated from the Lidar derived CHM?
2. How accurately WorldView-2 image can differentiate tree species on the basis of spectral separability?
3. How accurate is the segmentation of CPA from WorldView-2 image in combination with Lidar data?
4. What is the relationship between CPA, height and carbon stock of dominant tree species?
5. How much carbon is stored by each major type of tree species in the study area?
6. What is the relationship between tree diversity and carbon stock of each community forests (CF)?

1.8. Research hypotheses

1. H_a : There is no significant difference between the height of tree measured from field and from Lidar.
2. H_a : There is a significant relationship between CPA, height and carbon stock of dominant tree species.
3. H_a : Worldview-2 image in combination with Lidar data using OBIA can accurately and significantly segment the CPA.
4. H_a : There is a difference between carbon stored by each major dominant tree species.
5. H_a : There is no significant relationship between tree diversity and carbon stock in the study area.

2. DESCRIPTION OF THE STUDY AREA

2.1. Criteria for the selection of study area

- **Nepal's first REDD+ pilot project**

Kayerkhola watershed is one of the three watersheds which have implemented the REDD+ pilot project through Community Forest User Groups (CFUGs) network in Nepal. The necessity of measuring the carbon stock in tropical forest of Nepal also gives the emphasis to choose this study area. The project area is fully financed by the Norwegian Agency for Development Cooperation (Norad) under the Climate and Forest Initiative. The project covers over 10,000 hectares of community-managed forest and has an outreach to over 16,000 households with over 89,000 forest-dependent people. It is one of the world's first carbon offset projects involving local communities in monitoring the carbon in their forests and providing the necessary training for them to do so. Now, the Forest Carbon Trust Fund provided an opportunity to claim reward for enhancement of carbon stock in pilot project. Norad provided a seed grant of US\$ 100,000 to initiate the fund (ANSAB, 2011).

- **Data availability**

Very high resolution satellite image *i.e.* WorldView-2 was only available for this watershed from ICIMOD and wall to wall mapping of Lidar data was provided from FRA project, Nepal for the research purpose in the same area. Lidar mapping in Nepal is the first practice in South Asia and hence it became important to choose the study area for carbon mapping of tropical forests. Other additional data such as detail delineation of CFUGs border (shape file), a landuse map and topographic map were also available from ICIMOD.

- **Accessibility**

The study area is fully accessible from the centre of the district so that the field has to be done on limited time and budget.

- **Diverse forest type**

The watershed constitutes of three different type of forest namely Sal (*Shorea robusta*) forest, mixed hardwood forest and Riverine forest which is one of the criteria to achieve the objective of this research.

2.2. Overview of Chitwan district

2.2.1. Geographical location and topography

Geographically, Chitwan district is located in lowland and Siwalik regions of the country. It is situated between 27°30'51"N - 27°52'01" N latitude and 83°55'27"E - 84°48'43"E longitude in central development region of Nepal. Chitwan is surrounded by Makwanpur district in the east and Nawalparasi in the west. Dhading, Gorkha and Tanahu are neighbouring district in the northern part while Parsa district and India are in the south. The district is around 70 kilometres south east (133°) of the approximate centre of Nepal and 80 kilometres south west (260°) of the capital Kathmandu. The altitude varies from 300m to 1200m above sea level. The land is characterized by many steep gorges and slope varies from 30% to more than 100%. The area is drained by Khayarkhola stream having many small tributaries feeding into it.

2.2.2. Climate

Chitwan has a diverse climate and rainfall over its landscape and land configuration. The district experiences tropical to sub-tropical type of climate which generally favours for the luxuriant growth of the vegetation. The average annual rainfall of the district is 1510mm/year. It is characterised as hot and wet during the summer and cool and dry during the winters. The average maximum and minimum temperature of the district is 30.3° and 16.6° Celsius respectively (Panta, 2003).

2.2.3. Land use

The district has a large amount of forested area as it constitutes two conservation areas *i.e.* Chitwan National Park, enlisted in world heritage site, covers an area of 970 km² and part of Parsa Wildlife reserve. Forest covers about 60% of the total land with an area of 128500 ha. Similarly agricultural land and urban area accounts for 40% covering 89500 ha.

2.2.4. Social, economic and demographic

Chitwan district is one of the most populated districts of Nepal with a total population of 623,677. The population density of the district is 9.17 km² and growth rate is 2.86%, which is higher than the average growth rate of Nepal. Chitwan district has several castes and ethnic groups, ranges from indigenous to elite people. Main centre of the district, Narayangadh, is renowned for the business activities although most of the people's occupation is in agriculture.

2.2.5. Vegetation

Basically, the study area has three dominant types of forest. They are Sal (*Shorea robusta*) forest, mixed hardwood forest and Riverine Khair-Sissoo forest (Panta, 2003). Sal is pre-dominant tree species found in the study area and occupies nearly 70% of forest composition. It is commercial woody species of Nepal and mainly found as Terai and hill Sal. Mixed hardwood forest is composed by Sal and other hardwood species. The major associate species are Asna (*Terminilia tomentosa*), Karma (*Adina cordifolia*), Botdhairo (*Lagerstroemia parviflora*) and Banjhi (*Anogeissus latifolia*). Riverine Khair-Sissoo forest is mainly distributed along the riverside of the study area and is mixed of Khair (*Acacia catechu*) and Sissoo (*Dalbergia sissoo*). Other associate tree species found in the study area are *Terminalia bellirica*, *Schima wallichii*, *Semicarpus anacardium*, *Mallotus philippensis*, *Cassia fistula*, *Cleistocalyx operculatus*, *Careya arborea*, *Holarrhena pubescens*, *Syzygium cumini*, *Aesandra butyracea*, *Terminalia chebula*.

2.3. Description of Kayerkhola watershed

Kayarkhola Watershed is located in north east part of Chitwan district and covers an area of 8002 hectare. Out of total area of watershed, 5821 ha is covered by forests which comprises 2381.96 ha as community forest managed by 16 CFUGs. 23223 people of 4163 households of 4 village development committees (VDCs), namely Shiddi, Shaktikhor, Chainpur and Pithuwa have been involved in the forest management activities and REDD+ pilot project. Within the CF 1902.72 ha is considered as dense forest whereas 479.19 ha are regarded as sparse forest type. Landuse profile of the watershed is mainly divided into five parts according to the classification done by ICIMOD. The area covered by each landuse type is given in Table 2-1.

Table 2-1: Land cover types of Kayerkhola watershed

Land cover types	Area (ha)	Area (%)
Close to open broadleaved (dense) forest	4119	51.48%
Open Broadleaved (sparse) forest	1702	21.27%
Natural water bodies	31	0.39%
Bare Soil	30	0.38%
Clouds	81	1.02%
Agriculture Land and built-up areas	2038	25.47%

Source: Land cover analysis report (ICIMOD, 2011)

The watershed is inhabited by socially and ethnically diverse forest-dependent indigenous communities such as Chepang and Tamang (ICIMOD, 2011). These ethnic groups are few of the most marginalized ethnic groups in the country. Chepang and Tamang communities practice shifting cultivation which puts

severe pressure on forest resources. The pilot project implemented in the area plays a major role to address the issues of forest degradation and deforestation by promoting sustainable forest management practices and linking it with REDD+ incentive mechanism. Out of 16 CFs of the watershed only 7 CFs from three different clusters have been selected for the research purpose in order to represent diverse type of forest structural attributes (Figure 2-1).

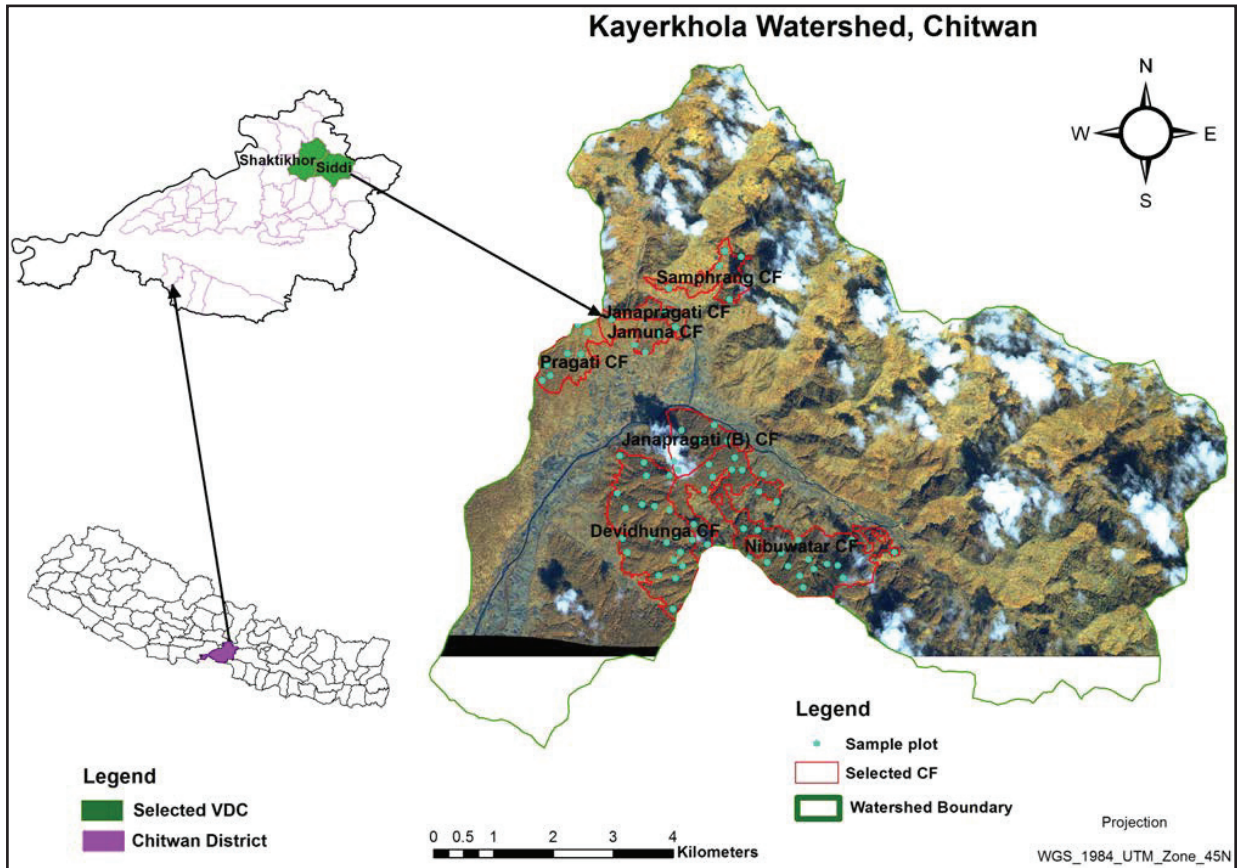


Figure 2-1: Location map of the study area.

Details of the CFs selected for this research is given in the Table 2-2.

Table 2-2: Details of selected community forests (CFs)

S. N.	Name of CFs	Location (VDC)	Area (ha)	Area in %
1	Samphrang	Shaktikhor -2	55.60	6.38
2	Janpragati	Shaktikhor -2	40.27	4.62
3	Jamuna	Shaktikhor -5	34.53	3.96
4	Pragati	Shaktikhor -6	79.06	9.08
5	Janpragati (B)	Shaktikhor -5	78.57	9.02
6	Devidhunga	Shaktikhor -8	253.86	29.14
7	Nibuwatar	Siddi – 2 & 3	329.18	37.79
Total			871.07	100

3. MATERIALS AND METHODS

3.1. Materials

3.1.1. Satellite data

Worldview-2 very high resolution satellite imagery obtained on 25th October 2010 was used for this study. It is the first commercial high-resolution satellite to provide 8 spectral bands in the visible to near-infrared range. The 8-bands multispectral of 1.84 cm spatial resolution has been resampled to 2 m, while panchromatic of 46 cm is resampled to 0.5 m. Metadata of the satellite image is given in Appendix1.

3.1.2. Airborne Lidar data

Lidar data were originally acquired for the purpose of national forest inventory of Nepal by Forest Resource Assessment (FRA) project under the Ministry of Forests and Soil Conservation. The data was collected by Arbonaut Ltd., Finland from 16 March to 2 April 2011 (leaf-off season) using a Leica ALS - 40 (Airborne Laser Scanner-40) sensor with aerial platform. A detail list of parameters for Lidar acquisition is given in Table 3-1.

Table 3-1: Lidar data collection parameters for Leica ALS-40 sensor

Parameter	Performance
Aerial Platform	Helicopter (9N-AIW)
Flying height (above ground level)	2200 m
Flying speed	80 knots
Laser pulse rate	52.9 khz
Field of view (FOV) half-angle	20 degrees
Sensor scan speed	20.4 lines/second
Swath width @ ground level	1601.47 m
Nominal outgoing pulse density @ground level	0.8 points per sq m
Point spacing	max 1.88 m across, max 2.02 m down
Beam footprint @ ground level	50 cm
Projection	UTM
Datum	WGS84
Sidelap	60 %
Side overlap	30 %
Average horizontal accuracy	45 cm
Average vertical accuracy	45 cm

3.1.3. Maps and other ancillary data

Topographic maps (2784-03C, 2784-03D, 2784-07A and 2784-07B) of the study area at scale of 1:25000 published by the Department of Survey, Government of Nepal in 1994 were used for this research. Similarly, other thematic map (local land use) was also used in the field during data collection. The watershed boundary, shape files of community forests (CF)and other infrastructure layers of study area

were obtained from ICIMOD, 2011. Besides, CF operational plan and District Forestry Sector Plan of the Chitwan districts were also used to obtain the detail information of forest management activities.

3.1.4. Field instruments

Various field equipments were used to collect the field data during fieldwork. Details of field instrument and its use are given in Table 3-2.

Table 3-2: Field instruments used for the data collection

S.N.	Instruments	Purpose
a.	Garmin GPS Map 60 CSx and iPAQ	Navigation or positioning
2.	TruPulse 360 B (laser technology)	Measuring the tree height
3.	Diameter tape (5m)	Measurement of DBH
4.	Measuring tape (30m)	Measuring radius of plot, crown diameter
5.	Spherical densiometer	Measuring the canopy density
6.	Field work dataset	Field data collection

3.1.5. Software and tools

Different softwares were used for the analysis of satellite image and airborne Lidar data during pre and post-field work. Specific use of software for data base creation, processing and analysis is depicted in Table 3-3.

Table 3-3: List of the software and purpose of its use

S.N	Name of Software	Purpose of usage
1.	Erdas Imagine 2011	Image processing and Coregistration
2.	ArcGIS 2010	GIS analysis
3.	PCI - Geomatica	Co-registration of image and Lidar data
4.	eCognition Developer 8.7	Object based image analysis
5.	LasTools	Processing of Lidar raw data
6.	Quick Terrain Modeler	Processing and visualization of Lidar data
7.	SPSS 16 and R stat	Statistical analysis
8.	Intersector.jar tools (in Java environment)	Segmentation accuracy assessment
9.	MS Office 2010	Data analysis and thesis writing

3.2. Methods

The method of this research mainly comprises of three parts: field work for data collection, satellite image and Lidar data processing, object based image analysis (OBIA), and model development. Panchromatic and MSS image of Worldview-2 were co-registered to intensity image obtained from Lidar point cloud. Co-registered panchromatic and multispectral images of WorldView-2 were fused to create pan-sharpened very high resolution image which was further smoothed to remove the noise. The Lidar data was further processed to obtain the canopy height model (CHM) by subtracting the digital terrain model (DTM) from the digital surface model (DSM). Both the pan-sharpened image and CHM layers were used for tree crown delineation and later the canopy projection area (CPA) and height of the individual tree can be extracted. Accuracy assessment of segmentation was performed and later used for species classification. After that, multiple regression models were developed using CPA and height as explanatory variables for carbon estimation/mapping. Field measured tree parameters were used to analyze tree species diversity and to estimate carbon stock of each tree and also for accuracy assessment of CPA, Lidar derived tree height and regression models. A flow diagram showing the research methodology is illustrated in Figure 3-1 and detailed explanations are described in the following sections.

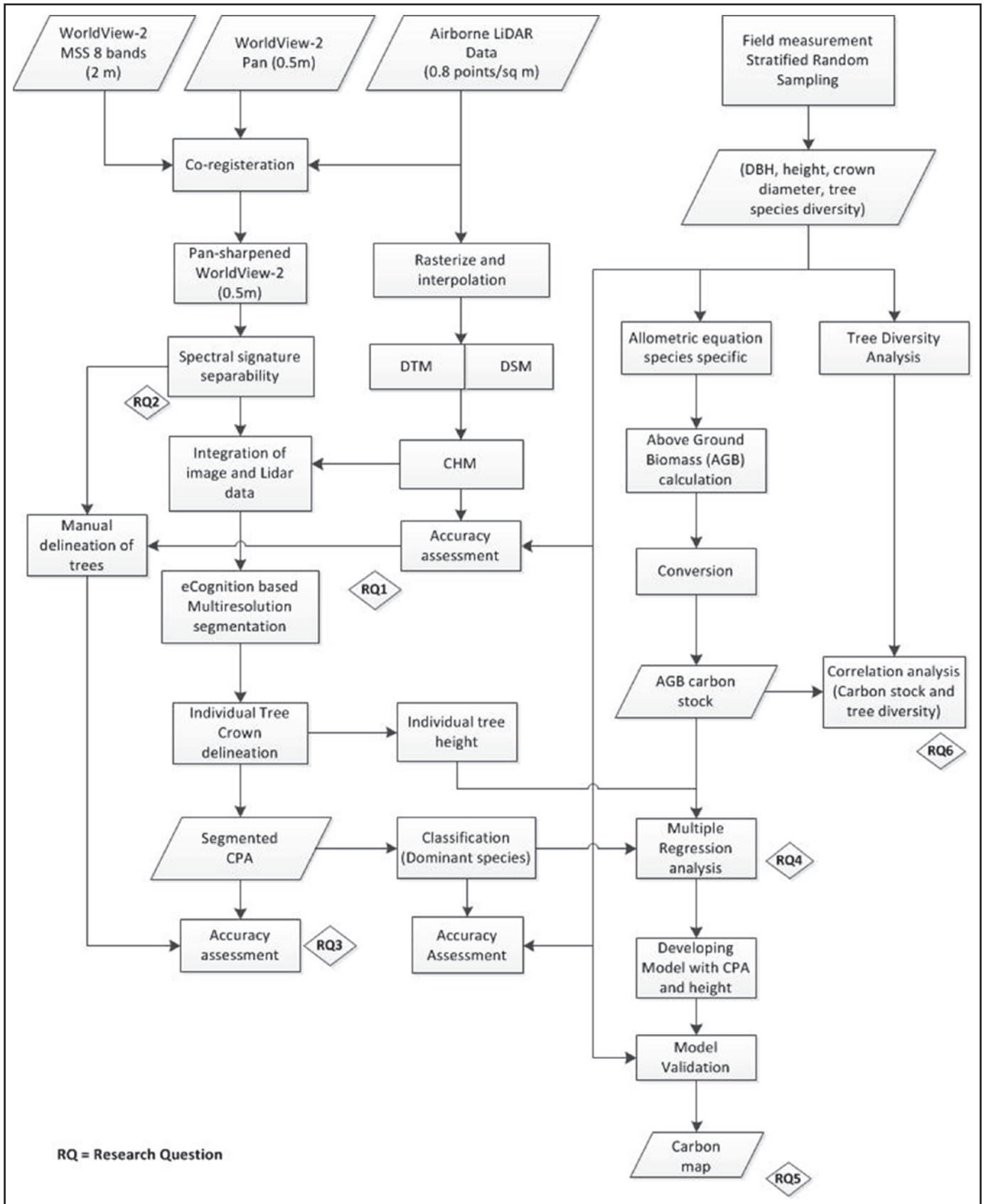


Figure 3-1: Flow diagram of research methods

3.3. Image processing

Image processing includes atmospheric, radiometric and geometric correction of the satellite image. The WorldView-2 image was already pre-processed for atmospheric and radiometric correction while geo-referencing and registration of the image was done to UTM 45 N zone projection and WGS 84 datum.

3.3.1. Subset of image

For this study only one image scene was required for the data processing although two images are needed for the entire Kayerkhola watershed. The subset of the selected CF area is selected for further processing. The study area from both the panchromatic and MSS image was extracted as a new subset using ERDAS Imagine 2011.

3.3.2. Image fusion

Image fusion is the combination of two or more different images to form a new image by using a certain algorithm. In general remote sensing fusion techniques can be classified into three levels *i.e.* pixel/data level, feature level and decision level (Pohl & Genderen, 1998). Pixel level fusion of optical images is mainly applied to improve spatial resolution, enhance structural and textural details and retain the spectral fidelity of the original multispectral data simultaneously. Therefore, it is also called as pan-sharpening (Zhang, 2010). Pan-sharpening is a pixel level fusion technique that combines the lower resolution colour pixels with the higher resolution panchromatic pixels to produce a high resolution colour image. Several pixel based image fusion methods like Intensity, Hue and Saturation (IHS), principal components analysis (PCA), high pass filter (HPF), Gramm-Schmidt (GS) and watershed transformations are commonly used for pan-sharpening.

In this study, a new pan-sharpening algorithm so called Hyperspherical Color Sharpening (HCS) is used as it is specifically developed for WorldView-2 imagery (ERDAS, 2011). This algorithm accepts any number of bands and handles both spatial and spectral recovery over a wide variety of scenes. Moreover, Padwick *et al.*, (2010) found that HCS algorithm maintains the best balance between spectral and spatial quality when compared among the 4 algorithms *i.e.* HCS, IHS, GS and PCA. This technique is based on the mathematics which required the forward and reverse transformations to and from the native colour space to the hyperspherical color space. A detail operation of the algorithm is applied for the hyperspherical transformation to pan-sharpening. Thus pan-sharpening quality index is calculated to measure both the spectral and spatial quality of pan-sharpened image, with respect to the original multispectral and panchromatic images.

WorldView-2 MSS image of 2 m resolution and panchromatic of 0.5 m resolution were fused to get a pan-sharpened image of 0.5 m spatial resolution with all multispectral information. The pan-sharpening process was carried out in ERDAS Imagine 2011. In the Hyperspherical Color Space Resolution merge dialog box the following options were checked: bilinear interpolation resampling technique, smoothing filter size 5, select layers 1 to 8 and unsigned 16 bit output data type. Bilinear interpolation technique was assigned because it reduces the alteration of spatial information and lead to smoother image compared to nearest neighbour resampling. For manual delineation of tree crowns and during the segmentation of images, a 5*5 low pass filter was used for smoothing the image.

3.4. Pre-fieldwork

Before the commencement of field work, different reference source data and images were collected and pre-processed. Pan-sharpened subset image was too large (1.68 GB) to upload in iPAQ for the field work. Therefore, this image was exported to enhanced compressed wavelet (ECW) format that reduced file size to 29.6 MB. The RGB 743 band combination was selected while exporting the image to ECW format so that output ECW image would be similar to pan-sharpened image (img format) in the same band

combination. For identification of recognizable tree on the image in the field, pan-sharpened image of each sample plot with its surrounding areas were printed in 1:1000 scale in JPEG format (Appendix 2). Apart from this, separate polygon shapefile for each 16 CFs were produced and a number of sample plots for each polygon were randomly generated in ArcGIS. Later these shapefiles were uploaded in the iPAQ. Road, river, high elevation point and contour information were also uploaded in the iPAQ in order to find out the selected plot without difficulty in the field. Field data collection sheet was prepared as its contents are given in Appendix 3. All necessary field equipment was borrowed from ITC field equipment section for the measurement of tree parameters.

3.4.1. Sampling design

Stratified random sampling procedure was adopted for sampling design. The study area, Kayerkhola watershed, consists of 16 CFs. Each CF has its own characteristics in terms of altitude, slope, aspect, age, species composition and stand structure. Stratification was done on the basis of these characteristics so that each CF will be one stratum and hence homogeneity prevails within CF. Stratified random sampling estimates population parameter of interest (mean or total) more precisely than non-stratified sampling for a given sample size or cost. Conversely, it will estimates population parameters as precise as simple random sampling or systematic sampling using a fewer plots for a lower cost (Shiver & Borders, 1996).

Total sample units were calculated using Equation 2 and second hand data of tree DBH already collected from the study area. It is almost impossible to determine the sample size of inventory without having some kind of prior knowledge of field therefore preliminary survey might be necessary to establish reasonable information of population parameters (Husch *et al.*, 2003).

$$N_{plots} = t^2 * CV^2 (1/E)^2 \dots\dots\dots \text{Equation 2: Sample size determination}$$

Where,

- N_{plots} = Minimum number of sample plots
- t^2 = Value of Student's t distribution for N_{plots} at desired probability
- CV^2 = Coefficient of Variation (in percent) of DBH of trees to be sampled
- E = Estimated allowable error or desired precision (in percent) for DBH of trees to be sampled, 20% is the common starting point for E (Husch *et al.*, 2003)

The number of sampling plots for each stratum was computed in proportion to the area of one stratum.

3.4.2. Plot layout

A circular plot of 500 m² area with a 12.62 m radius was chosen for the measurement of tree parameters. The circular plot is widely used as a single dimension, the radius, to define the perimeter and easy to measure in the forest. It has minimum perimeter for a given area without any predetermined orientation and consequently the lowest number of borderline trees will be selected (Husch *et al.*, 2003). For measurement of tree diversity, within the plot of 500 m² two more concentric plots were established with radius of 5.64 m (100 m²) and 2.68 m (25 m²).

3.5. Fieldwork

The center of each plot was demarcated in the forest according to the designed layout of sample plot on the map using iPAQ and Garmin GPS Map 60 CSx. The XY coordinate of centre of the plot and if possible coordinates of few measured trees were also located in the iPAQ. Within the circular plot, trees with DBH 10 cm or greater were only measured because trees with less than 10 cm diameter contribute little to the total biomass carbon of a forest (Brown, 2002). Hence, different tree parameters such as DBH, tree height, crown cover, canopy density and crown diameter were measured in the sample plot. The trees (DBH ≥ 10 cm) measured in the plot was also identified and recognized in the printed image

and was marked an outline with numeric notation. The numeric notations were also recorded in the data sheet as well. At least ten trees were recognized on the printed image coincide with the field measurement so that it can be used for development of regression model based on CPA and height.

In addition, all the species within the plot were recognized and noted on the sheet for analysis of tree diversity. For this purpose, trees of DBH 10 to 5 cm were measured within the radius of 5.64 m (100 m²) and sapling and regeneration of all the species below 5 cm DBH were only counted in radius of 2.68 m (25 m²) as shown in Figure 3-2. Furthermore, other important information such as aspect, slope, exposure and valuable species such as non-timber forest products (NTFPs) were also taken into consideration. During the measurement of plot radius and crown diameter, slope correction was performed in the areas more than 5° slope. In total 75 plots were measured in seven CFs although it was intended to measure 72 plots only. The details of the sampling plots measured are given in Table 3-4 and the coordinates of all the plots given in Appendix 4.

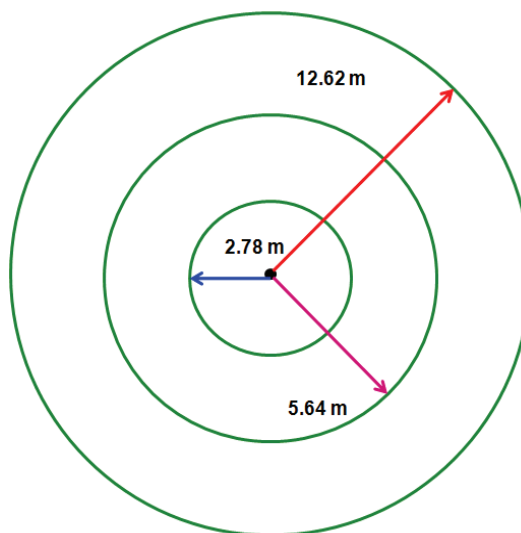


Figure 3-2: Schematic representation of sample plot layout

Table 3-4: Number of sample plots measured in the field

S. N.	Name of CFs	Area (ha)	No of plots measured	No of trees measured	Trees recognized in image
1	Samphrang	55.60	5	70	47
2	Janpragati	40.27	3	57	13
3	Jamuna	34.53	3	53	18
4	Pragati	79.06	7	99	32
5	Janpragati (B)	78.57	5	125	35
6	Devidhunga	253.86	28	436	96
7	Nibuwatar	329.18	24	307	102
Total		871.07	75	1147	343

3.6. Secondary data collection

Secondary information such as households benefitted from REDD+ program, management activities and involvement of local people for forest management and carbon mapping was collected from the concerned agencies such as district forest office (DFO), CFUGs, ICIMOD and ANSAB. The detail information about the proper CFs was obtained from their operational plan prepared by CFUGs and local people involved in the forest management and REDD+ program.

3.7. Data analysis

Data analysis stage comprises of data analysis (*e.g.* raw field data like DBH, height and crown diameter and other subsidiary information), descriptive analysis, calculation of field-based AGB estimation, and manual delineation of trees on the image.

3.7.1. Fieldwork data analysis

After fieldwork, all the collected field data were screened and sorted according to the data sheet and entered appropriately in an excel file. The missing information was either fulfilled from the inquiry or removed from the data sheet. The preliminary statistical analysis such as outlier detection and its removal, descriptive analysis and box plot was made for actual reflection of the field scenario. Scientific name of local species found in the study area was searched from literature and enlisted to get the idea of tree diversity as a whole. The list of species found in the study area is given in Appendix 5.

3.7.2. Tree diversity analysis

There are several measures of diversity known as “diversity indices” to describe complexity of a biological community. Each of these indices seeks to characterize the diversity of a sample or community by a single, quantitative value (Magurran, 1988). Common measures of diversity include counts of number of species (species richness) and use of indices such as Shannon-Wiener’s index (Shannon & Weaver, 1962) or the Gini-Simpson index. In this research, Shannon diversity index was used as an indicator of the tree species diversity because this diversity index is the most commonly used and acceptable indicator of biodiversity (Magurran, 1988). Moreover, this index reflects both evenness and species richness without favouring either dominant or rare species. Tree diversity was calculated based on Shannon diversity index using the general formula (Equation 3).

$$H' = - \sum p_i * \ln p_i \dots\dots\dots\text{Equation 3: Shannon diversity index}$$

Where,

- H' is Shannon diversity index,
- p_i is the proportion of individuals belonging to ith species, and
- ln is natural log (*i.e.* base 2.718)

In each plot, the number of tree species with DBH more than 10 cm, DBH less than 10cm to 5 cm and DBH less than 5 cm were counted. Similarly, seedlings and regeneration of all the species and NTFPs were also counted and recorded in the tally sheet (Appendix 3) in order to calculate the proportion of individual species in each plot.

3.7.3. Allometric equation and carbon stock calculation

The use of allometric equations is a crucial step in estimating above ground biomass (AGB) which can be used to estimate carbon stock of forests. In general AGB is estimated from volumetric and structural dimension of the trees for which DBH and height are considered as major parameters. In absence of species specific biomass equation of the trees, species specific volume equations developed by Sharma and Pukkala (1990) were used to estimate the AGB of forests. Total stem volume of individual trees was calculated from field measured DBH and tree height using the relationship in the following form (Sharma & Pukkala, 1990).

$$\ln (V) = a + b * \ln(\text{DBH}) + c * \ln(\text{Ht}) \dots\dots\text{Equation 4: Allometric volume equation}$$

Where,

- ln is natural logarithm to the base 2.71828
- V is the total stem volume with bark in m³, to obtain the volume in cubic meters the prediction is to be divided by 1000
- DBH is the diameter at breast height in cm
- Ht is the tree height in m
- and a, b and c are model parameters

The estimated parameter value of a, b and c for different species and wood density of the major tree species is given in Table 3-5.

Table 3-5: Model parameters and wood density of major tree species

Species	a	b	c	R ²	Wood density (Kg/m ³)
<i>Shorea robusta</i>	-2.4554	1.9026	0.8352	98.3	880
<i>Lagerstroemia parviflora</i>	-2.3411	1.7246	0.9702	97.5	850
<i>Adina cordifolia</i>	-2.5626	1.8598	0.8783	98.1	670
<i>Terminalia tomentosa</i>	-2.4616	1.8497	0.8800	98.9	950
<i>Schima wallichii</i>	-2.7385	1.8155	1.0072	98.3	689
<i>Albizia species</i>	-2.4284	1.7609	0.9662	97.8	673
<i>Syzygium cumini</i>	-2.5693	1.8816	0.8498	98.3	770
Miscellaneous in Terai	-2.3993	1.7836	0.9546	98.3	720

The obtained volume was multiplied with dry wood density (specific gravity) of the species to get air dry weight of stem biomass (Chaturvedi & Khanna, 1982) using the following formula (Equation 5). Species found in the study area other than mentioned above was categorized as Miscellaneous in Terai and volume was calculated accordingly (see Equation 5).

Stem biomass = Stem volume * Wood density.....Equation 5: Calculation of stem biomass

Due to absence of established biomass relationship of different tree components of individual tree species of sample forest types, this study used the relationship developed by Sharma (2011) for a single species of similar forest types of Nepal which was later adopted by Shrestha & Singh (2008) and Khanal *et. al.* (2011). The biomasses of branches and leaves (foliages) were estimated to be 42% and 8% of the stem biomass respectively (Sharma, 2011) to calculate the total biomass of trees. However, in case of *Shorea robusta* branch to stem and foliage to stem ratio was applied as suggested by Sharma & Pukkala (1990). Thus, the AGB of different tree species of the study area was calculated by sum of stem, branch and foliage biomass of the tree as shown in Equation 6.

Total AGB = Stem biomass + Branch biomass + Foliage biomass.....Equation 6: Calculation of AGB from tree component biomass

The total AGB thus obtained from the above equation were converted to carbon stock of the individual trees using conversion factor of 0.47 (about 47% of the dry biomass is assumed to be carbon for all parts of trees as a default value) as suggested by IPCC (2006) and is expressed in Equation 7.

Total Carbon Stock = Total AGB*0.47.....Equation 7: Calculation of carbon stored by individual trees

3.7.4. Manual delineation of tree crowns

Although large number of trees measured in the field, only one third of them could be recognized in the image for manual digitization/delineation due to the difficulties in identifying actual tree crown. The delineation of the recognized tree crowns was done for assessing the segmentation accuracy and validating the model. For this purpose, both panchromatic and 5*5 filtered pan-sharpen image were used in such a way that tree crown can relatively easy to be recognized. Both images were visualized in ArcGIS at several scales for the better view of tree crown using different band combinations such as 743, 876 and 632. Shape files of the sample plot and identified trees were also overlaid on the image for proper tree delineation. Finally, 1:400 scale and 743 band combination was selected for digitization of tree crown. The crown diameter of the trees was taken as a reference for delineation because the area of tree crown can be

estimated from it. Pan-sharpened and panchromatic images were checked and unchecked alternatively during the crown delineation for a better result. About 30% trees measured from field were delineated for accuracy assessment.

3.8. Species differentiation capability of image

Due to high spectral diversity of WorldView-2 image, the dominant and co-dominant trees of the tropical forest can be identified at species level through its new band like Red Edge, NIR1 and NIR2. Two NIR band of the image has potential to identify different vegetation types and enables broader vegetation analysis and biomass studies (DigitalGlobe, 2010). Therefore, following test was carried out to examine the potential of WorldView-2 image to differentiate tropical forest trees at species level.

3.8.1. Transformed Divergence (D_T)

Divergence is one of the first measures of statistical separability used in remote sensing data for feature selection (Jensen, 2005). Transformed Divergence (D_T) is an advanced divergence method, which calculates the statistical distance between the pairs of signatures to maximize the separability among the different classes. This statistic gives an exponentially decreasing weight to the increasing distance between the classes. It estimates the probability of correct classification between pair of classes. The class pairs with highest D_T maximize the likelihood of high classification accuracy.

The scale of the D_T values can range from 0 to 2000. The values greater than 1900 showed that the class can be separated. When D_T is between 1700 and 1900 it is said to be good separation but below 1700 is regarded as poor separation. A transformed divergence value of 2000 suggests excellent between-class separation (Jensen, 2005). In other words, if the calculated divergence is equal to upper bound then the signatures assumed to be totally separable in the bands being studied. It is based on the covariance. The mean vectors of the signatures are compared to determine which set of the band is most useful for classification.

The pan-sharpened image was used to evaluate the signature separability using D_T by overlaying training samples of tree classes before image classification taken place.

3.8.2. Spectral separability of the tree classes

A common way to represent the spectral separability of different tree species is by means of a spectral response/reflectance curve plot. An individual spectral response curve results from the quantitative measurement of the spectral properties of target object at one or several bands of the image (Amelinckx, 2010). There are different ways to present a spectral response data. The conventional representation is a 2-dimensional plot in which the recorded reflectance/emittance (y-axis) is plotted along a wavelength gradient/band (x-axis).

This technique was employed for the study to assess the potential of species differentiation of WorldView-2 image using ERDAS 2011. Vector layer of training samples of major tree species was overlaid on pan-sharpened image. Pixel values (DN) of each sample trees were extracted from the spectral profile viewer as each profile has its own DN value in each band of the image. In this way sufficient number of profiles was created for different type of species and the respective mean values was exported to excel sheet. The mean DN values were plotted in y-axis against eight spectral bands in x-axis on line graph. Thus, distinct separability of tree classes can be seen in the graph along the x-axis (bands). The band which has maximum separation among the tree classes (reflectance curve) were chosen as the best band for separability between the classes. Visual inspection of spectral profile curve would be the criteria to assess the potentiality of species spectral separability of image *i.e.* how distinctly each band of image can separate the tree classes.

3.9. Lidar data processing

Lidar point cloud was obtained from FRA, Nepal project in the las format which consists of 147 tiles for the whole watershed. Pre-processing of raw laser data was done in TerraScan software by Arbonaut Ltd., Finland. LasTools was used for further processing of data because it is easily available and open source. This software can be used for converting, filtering, viewing, gridding, and compressing Lidar point cloud data in different file formats. Thus, selected tiles of study area were imported in LasTools in order to get the detail information of laser point returns using *lasinfo* function. There are 5 returns in the point cloud, however only the first and last returns were used in this study. Tree canopy hits or first-return points are usually interpolated to a regular grid that corresponds to the DSM whereas last return or ground hits are interpolated as DTM.

Furthermore, ground (class 1) and non-ground points (class 2) from the point cloud were separated using *lasground* function. After that the ground points in laz format of each tile was merged into a single laz file (compressed las file) for subset area which was further converted into a DEM using *blast2dem* function. Similarly, canopy returns or non-ground points were converted into DSM using TIN (Triangulated Irregular Network) interpolation methods. Interpolation of elevation attributes from the point clouds of the first and last-returns to two spatially continuous surfaces was achieved in two stages. Firstly, a TIN based on a Delaunay triangulation was applied to each dataset. Secondly, a rectangular grid of pixels was extracted from each TIN using a linear interpolation method at a constant sampling interval of 0.5 m to generate the surfaces (Patenaude *et al.*, 2004).

Quick Terrain Modeler was used for the visualization and presentation of point cloud, DTM, DSM and CHM as it provides a better interpretability as compared to LasTools (*lasview* function). Since the QT Modeler is commercial software, only 15 days are given for a trial version. Noise filtering of some tiles and visualization and presentation of the surface models and CHM were performed using this software. Hence, most of the work (*e.g.* interpolation of DEM, gridding, generation of DTM and DSM) on Lidar data processing was done in LasTools.

3.9.1. CHM generation

The tree canopy height model (CHM) was computed as the difference between tree canopy hits and the corresponding Lidar-derived terrain elevation values. The same method was used by Popescu and Wynne, (2004a). The DTM and DSM created in LasTools were exported to ArcGIS and CHM was thus obtained by subtracting DTM from DSM using a raster calculator in order to get the height of individual tree. Height of individual tree was filtered from CHM as there was still some noise in data which showed different value of tree height *i.e.* greater than maximum field height and less than 0 even in negative value. Therefore, minimum and maximum value of the CHM was kept as 0 and 40 according to the field data. The height value out of 0-40 m range was filtered out using con function of raster calculator.

3.9.2. Accuracy assessment of CHM

Accuracy of CHM was quantitatively assessed on the basis of field measured height of individual tree taken as a test data. The Lidar derived tree height was extracted from CPA of same individual tree as a maximum pixel value from manually delineated CPA of the CHM. Lidar derived tree height was regressed against field height using least square method and thus validated using field measured data. Different statistical test such as Pearson's correlation test and one way ANOVA was done to find the significant difference between these two heights. Lidar derived height was regarded as response variable while field height was a predictor variable for regression analysis.

3.10. Coregistration of image and Lidar data

The basic idea for registration of a satellite image to a Lidar data is to utilize the Lidar intensity data and the satellite imagery to find the correspondence between image and image pairs acquired at different

times, perspectives or even from different sensors (Toth *et al.*, 2011). There are several methods for image to image registration such as map based registration and image-to-image registration. The latter method was adopted in this study. The principle of image-to-image registration is to use an already geo-referenced image with higher resolution as a master data in order to register the raw image so called slave (Du, 2008). In comparison to map based registration, this method provides one step process in which reference points on the master image and the corresponding points in the slave image can be found out simultaneously.

PCI Geomatica software was used to co-register the Lidar intensity data and WorldView-2 satellite image. The Lidar intensity map was generated in LasTools and prepared in tif format. *Lasgrid* function of LasTools was used for this purpose. The intensity data of point cloud was interpolated using 0.5 m pixel size and applying 5 pixels as a fill for rasterization. Lidar data is more accurate than satellite image as it has x, y and z coordinates of each point on the ground and already geo-referenced to WGS 1984 UTM Zone 45N. Therefore, in this study, Lidar intensity data was taken as a master image to register the panchromatic band (as slave) of WorldView-2 image. Then, this registered panchromatic band was used as a master image to register the multispectral bands of WorldView-2 satellite image. The Lidar-derived DSM was also used as an elevation model during the co-registration of image in Orthoengine tool of PCI Geomatica for removing the distortion of objects on the ground. Various common and prominent object features were collected as ground control points (GCPs) from both the image and thus the satellite image was registered based on the Lidar intensity data. Altogether 26 points were taken as GCPs that resulted in an overall RMSE of 1.2 m for panchromatic and 1.5 m for multispectral image.

3.11. Layer stacking of image and CHM

All bands of pan-sharpened image and Lidar derived CHM were stacked and used as a combined layer in eCognition software for segmentation purpose. The proposed segmentation method used a data fusion technique available from eCognition to identify objects with correlated characteristics in terms of reflectance and height. This was obtained by linking the CHM with reflectance values in MSS bands from the image of each segment. Multi-resolution segmentation was followed to partition the combined layer of image and CHM. This method identifies geographical features using scale and homogeneity parameters obtained from the spectral reflectance values in different bands from WorldView-2 image and the elevation values in the CHM (Suarez *et al.*, 2005).

3.12. Image segmentation

Image segmentation is the process by which an original image is partitioned into some homogeneous regions by subdividing, merging and reshaping operation of the image objects (Liu & Yang, 1994). It is a preliminary and critical step in segment based classification and assumed that the segmentation results directly affect the performance of the subsequent classification (Gao *et al.*, 2001). Although there are several types of segmentation techniques available, it can be divided either into boundary based/edge based or region based algorithms. In the other way, segmentation techniques can be grouped into top-down and bottom-up strategy. Top down strategy includes cutting big objects into smaller pieces such as Chessboard, Quadtree, Contrast filter and Contrast split segmentation. Whereas bottom up strategy includes merging of small pieces to get bigger objects based on homogeneity criteria that are also called as region based algorithm for example Multi-resolution segmentation. Region based algorithms extract information from the image by grouping spatially and spectrally similar pixels into homogenous area to form an image object. In this research, multi-resolution segmentation technique was applied to segment tree crown onto WorldView-2 image.

3.12.1. Multi-resolution segmentation

Multi-resolution segmentation, developed by eCognition Developer 8.7 software, is the process of delineating individual objects in the image based on homogeneity criteria such as colour, shape and

texture. For a given number of image objects, it minimizes the average heterogeneity and maximizes their respective homogeneity for producing meaningful objects.

The segmentation starts by considering each pixel as a separate object or seed and subsequently, pairs of image objects are merged to form bigger segments until the homogeneity is reached. The homogeneity criterion for multi resolution segmentation is defined by scale and shape parameters. The seed looks for its best-fitting neighbour for a potential merger. If best fitting is not mutual, the best candidate image object becomes the new seed image object and finds its best fitting partner. When best fitting is mutual, image objects are merged in each loop (Definiens, 2011). The loops continue until no further merging is possible and the procedure then starts with another image object.

Scale parameter is an important parameter in multi-resolution segmentation and is used to determine the upper limit for a permitted change of heterogeneity throughout the segmentation process. It also determines the average image object size. Therefore a higher scale parameter will allow more merging and consequently bigger objects, and vice versa (Rahman & Saha, 2008). The segmentation algorithm does not only rely on the single pixel value, but also on pixel spatial continuity (texture and shape) as well as their position within the hierarchical network. The homogeneity of the objects on which the scale parameter depends is called as composition of homogeneity *i.e.* mutually exclusive interaction between colour and shape. Colour refers to the spectral response of the objects, whereas shape conveys information about the semantic consistency of the objects. Shape is divided into two equally exclusive properties: smoothness and compactness. The value of shape field modifies the relationship between shape and colour criteria, (colour = 1-shape) so, decreasing the shape value will increase the colour criteria (Definiens, 2011). On the other hand, smoothness/compactness criteria is used when user wants to determine whether the objects should become more compact (fringed) or more smooth if the shape criterion is larger than 0. The relationship between scale parameter and composition of homogeneity is shown in Figure 3-3. By applying different scale parameter and colour/shape of combinations, the user is able to create a hierarchical network of image objects (Definiens Imaging, 2004).

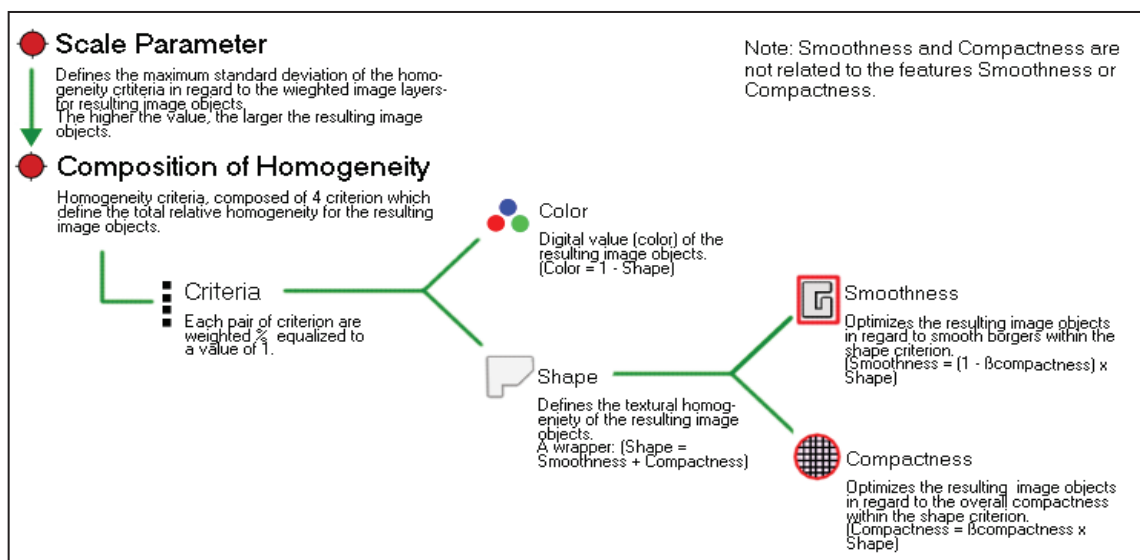


Figure 3-3: Multi-resolution concept flow diagram: adapted from (Definiens, 2011)

The success of multi-resolution segmentation depends on selecting the appropriate parameter combinations. In order to select the best parameter combinations, the panchromatic image was segmented 20 times iteratively using different parameter combination of scale, shape and compactness. Thus, the best combination of parameters was chosen as scale 21, shape 0.8 and compactness 0.6 for the segmentation. For the selection of best fit scale parameters, Estimation of Scale Parameter (ESP) tool was used in the

segmentation procedure. Figure 3-4 shows detail processing steps of multi-resolution segmentation and its corresponding rule set developed in eCognition.

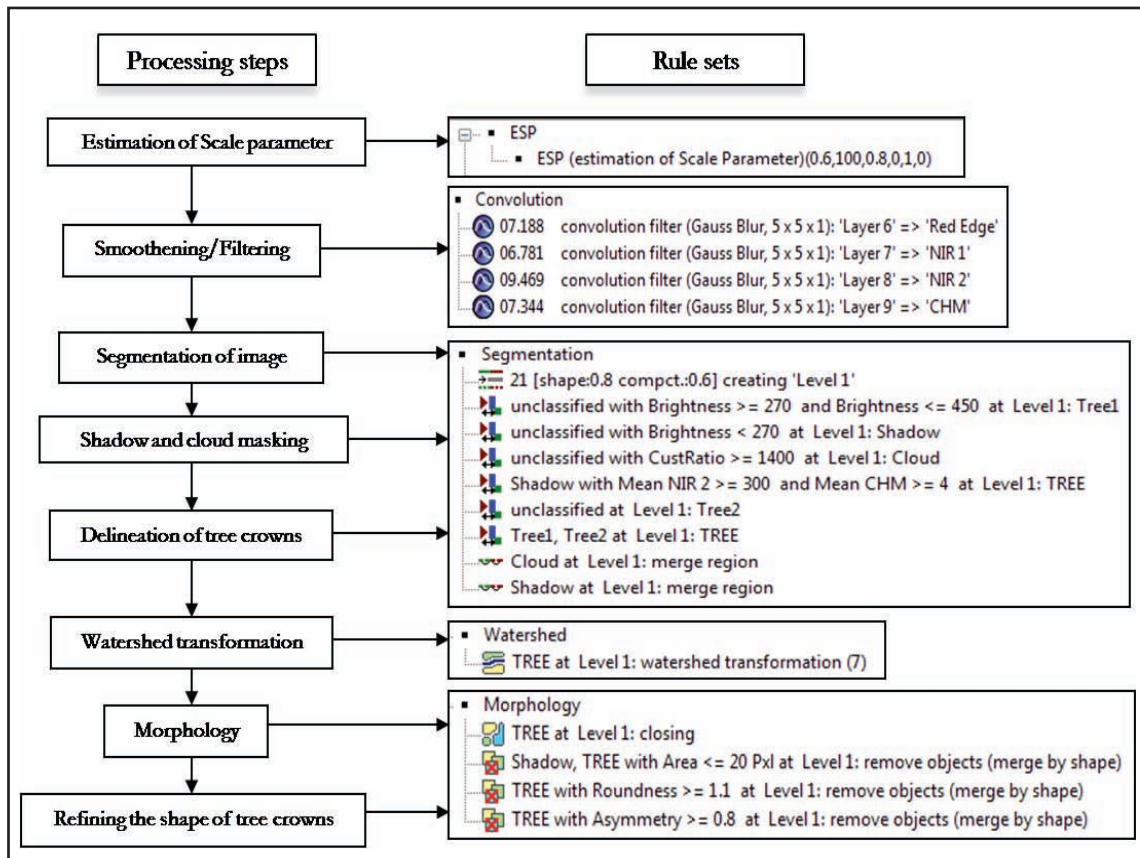


Figure 3-4: Segmentation processing steps and its corresponding ruleset

a. Estimation of Scale parameter

ESP tool is based on the idea of local variance (LV) of object heterogeneity within an image at multiple scales. It determines the upper limit of heterogeneity throughout the segmentation process. The variation in heterogeneity was explored by evaluating LV plotted against the corresponding scale. The thresholds in rates of change of LV indicate the scale levels at which the image can be segmented in the most appropriate manner (Dragut *et al.*, 2010). The ESP tool was downloaded from the website and loaded as a rule set in the process tree of the eCognition interface. Figure 3-5 shows the ESP tool to estimate the scale parameter.

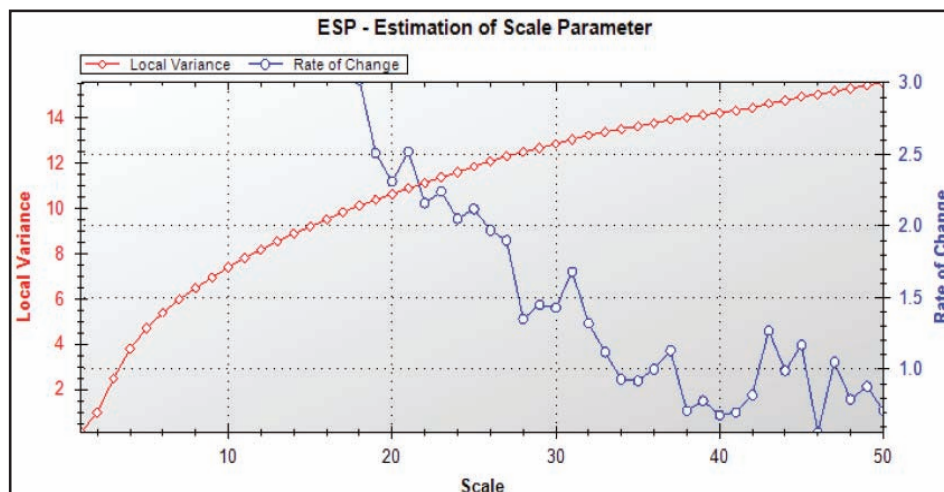


Figure 3-5: Interface of ESP tool for determining scale parameter

After that value of different parameters was set in the edit process dialogue box to choose the appropriate scale parameter. Since selecting scale parameter is an iterative process, it was done several times by keeping different value of each parameter.

b. Smoothing/Filtering

Filtering of WorldView-2 image was done in eCognition. Gaussian smoothing filter (Gauss Blur) of a 5*5 kernel was used for both the panchromatic and pan-sharpened image to remove the noise and smooth the appearance of image. After convolution filtering of image the processing time for segmentation also decreases. A convolution filter uses a kernel, which is a square matrix of a value that is applied to the image pixels and each pixel value is replaced by the average of the square area of the matrix centered on the pixel.

c. Segmentation of image

Segmentation of whole image was done using multi-resolution segmentation algorithm to partition the image pixel into smaller image objects. Out of eight spectral bands of pan-sharpened image, only three bands (NIR1, NIR2 and Red-Edge) and a CHM layer was given the higher weight *i.e.* 7, 6, 5 and 4 respectively for segmentation. It is because these bands were found to be the best bands for spectral separability of tree species and thus regarded as important for tree crown delineation. The segmentation was based on the thematic layer of panchromatic shape file that was already segmented and exported to shape file after validation. Segmentation process was done using 21 as scale parameter, 0.8 as shape and 0.6 as compactness value.

d. Shadow, cloud and open area masking

Due to the viewing angle and time of data acquisition, shadow and cloud were prominent on the image. Besides, there was some open and bare land in the study area. So such non-vegetated area needs to be masked from the image for better delineation of tree crowns. For masking out non-vegetated area, the reflectance values of vegetation and non-vegetation (shadow, cloud and open areas) was checked by updating the range of brightness value in a feature view window. Once the feature value identified for tree and non tree areas, the rule set was developed for masking of those area. For example, the pixels with CustRatio more than 1400 was regarded as cloud, values more than 450 as open areas and values less than 270 as shadow. Therefore, these areas were masked out accordingly to delineate the vegetated areas and tree crown delineation. However, the pixels value for shadow, cloud and open area are dependent on the subset of image.

e. Delineation of tree crown based on object features

Area other than non-vegetative class *i.e.* shadow, cloud and open areas were regarded as vegetative areas and the tree crowns were delineated using specific rule set developed for combined use of three bands of image and CHM. Certain threshold condition of brightness value and CHM value was given for the tree crown delineation for instance the pixels in between 270 and 450 and CHM greater than 4 was delineated as tree. Trees fall in the shadow area was delineated using the rule that if the CHM value is greater than 4 in shadow area it should be regarded as tree.

f. Watershed transformation

The watershed transformation algorithm is commonly used to separate image objects from others. This algorithm helps to split the overlapping tree crowns into individual tree crown based on splitting threshold. The threshold is given on the basis of expert knowledge and average crown diameter of tree measured in the field.

Watershed transformation considers the image to be processed as topographic surfaces and includes three basic notions: local maxima, catchment basins and watershed lines (Chen *et al.*, 2004). If the gray scale image is inverted the local maxima become the local minima and holes are punched at the local minima. In between the local maxima and minima there are catchment basins which correspond to the tree crowns. The watershed lines are the local maxima of an inverted image and image looks like a watershed

catchment. When water is introduced in the system each valley will collect water from local minimum until water spills over the watershed into an adjacent valley (Wang *et al.*, 2004). The watersheds surrounding the valleys constitute closed contours, which separate the whole area into different catchment basins and forms the desired boundaries of each object. In this way, when applying watershed transformation to the forest, tree clumps are treated as the catchment and under flooding water assumption, the trees (as valleys) touch each other and then those trees are separated into individual trees.

g. Morphology

Morphological operation was done to reshape the advanced object of image. The border of the image objects is smoothened by the pixel-based binary morphology operations *i.e.* opening or closing. Open image object removes pixels from an image which is completely separated from an image object while Close image object adds surrounding pixels to an image object (Definiens, 2011). Closing is defined as the complementary area to the surrounding area of an image object that can completely contain the mask. Close image object was applied in this study so that the smaller holes due to shadow and difference in spectral properties inside the area are filled. Another operation of morphology is to define the shape and size of mask. The mask is the structuring element, on which the mathematical morphology operation is based. Masking can be done either by circular or square as available in eCognition. Circular mask was created with 10 pixels size in this segmentation since the tree crowns are circular in shape.

h. Refining the shape of tree crowns

When the segmentation and other operations like watershed and morphology were completed, the tree crown of each segment was smoothened and refined by minor processing (*i.e.* removing smaller crowns on the basis of pixel number, roundness and asymmetry) so that the tree crown looks like natural tree. For this purpose, some unwanted segmentation such as tiny objects, noise and elongated objects from shadow and tree class were removed on the basis of roundness, asymmetry and area of pixels attributes. In addition, some temporary classes except tree crowns were merged to shadow class

3.12.2. Validation of segmentation

Accuracy assessment of image segmentation can be done by several methods. However, they are broadly based on visual and geometrical techniques. The visual assessment which is based on visual judgment of the degree of fit of segmented objects with that of known objects whereas the geometrical assessment is made with a comparison of segmented objects with training/reference objects in terms of various indices.

Möller *et al.*, (2007) developed an accuracy assessment method based on visual techniques, also known as relative area approach to validate the segmentation by using reference polygons from manual digitization. If the reference polygon is completely covered by segmented objects, best scores are given. On the other hand, Clinton *et al.*, (2010) developed a geometrical segmentation accuracy assessment of segmented outputs with reference to clearly defined training sets. The quality of segmentation outputs are defined in terms of over- and under segmentation as well as goodness of fit (D). Over segmentation and under segmentation as defined by Clinton *et al.*, (2010) are described as follows (Equations 8 and 9).

$$\text{Over segmentation}_{ij} = 1 - \frac{\text{area}(x_i \cap y_j)}{\text{area}(x_i)} \dots \text{Equation 8: Calculation of over segmentation}$$

$$\text{Under segmentation}_{ij} = 1 - \frac{\text{area}(x_i \cap y_j)}{\text{area}(y_j)} \dots \text{Equation 9: Calculation of under segmentation}$$

Where,

- x_i is the training objects or reference polygons, relative to which the segmentation to be judged
- y_j is the set of all segments in the segmentation.

The over and under segmentation forms ‘distance’ index (D) which indicates the quality of segmentation. D value is interpreted as the ‘closeness’ measure to an ideal segmentation result, in relation to a predefined reference set and ranges from 0 to 1 (Equation 10). As the value of D increases, the deviation of segmented objects and their respective reference object increases which indicated a high level of mismatch between objects. As the goodness of fit (D value) increases the degree of mismatch between the segmented and reference objects increases indicating minimum accuracy.

$$D_{ij} = \sqrt{\frac{\text{Oversegmentation}_{ij}^2 + \text{Undersegmentation}_{ij}^2}{2}} \dots \text{Equation 10: Measure of closeness}$$

In this research, the method proposed by Möller *et al.*, (2007) and Clinton *et al.*, (2010) was used for accuracy assessment of tree crown segmentation. Segmentation accuracy measures are also assessed by 1:1 spatial correspondence between the segmented and reference objects. These accuracy measures were calculated for segmented tree crowns of each CFs. 1:1 spatial correspondence was assessed by comparing the number of 1:1 corresponding tree crowns of the reference and segmented polygons with the total number of reference tree crowns. A higher percentage of 1:1 correspondence indicates a higher accuracy.

3.13. Image classification and accuracy assessment

Conventional pixel based classification approaches are poorly suited to very high spatial resolution imagery because within-class spectral variation increases with increased spatial resolution. Object based classification method uses not only spectral information but also considers texture (mean, variance, contrast, homogeneity and dissimilarity), spatial, contextual and semantic information to interpret an image (Definiens, 2011). There are two different kinds of classification approaches in eCognition *i.e.* membership function and nearest neighbour. Both are the supervised classification scheme. While the first can be edited directly and enable the user to formulate knowledge about the image content, the latter needs appropriate sample objects to determine the desired class properties. Samples can be selected manually (click and classify) or based on training area masks (Definiens Imaging, 2004).

The nearest neighbour classification is applied to selected object features and trained by samples. In comparison to pixel based training, the object based approach of the nearest neighbour requires fewer training samples. Samples are image objects which are the result of the segmentation process. After a representative set of sample objects has been declared for each class, the algorithm looks for the closest sample object in the feature space for each image object. If an image object's closest to sample object belongs to Class A, the object will be assigned as Class A (Definiens Imaging, 2004).

The supervised nearest neighbour classification was applied to classify the tree crowns at the species level. The image objects (tree crown) was classified into six species altogether on the basis of training data collected from field. The tree that was clearly recognized and annotated in the image and field both was used as training sample for classification. 70% of sample trees recognized in the image were used as training samples while the rest 30 % as a test data for accuracy assessment in case of each major dominant species. The mean value of NIR1, NIR2 and Red-Edge band of pan-sharpened image and maximum value of CHM was chosen in object features for the classification.

A classified image of eCognition was exported to ERDAS 2011 using export thematic raster files algorithm and export type as classification in edit process window of eCognition. The exported raster file should be changed to thematic layer as data type was in continuous layer. Accuracy assessment was carried out on the basis of allocated test samples. Confusion matrix, Kappa statistics and overall accuracy report was generated to calculate complete statistical measures.

3.14. Feature extraction

The procedure employed for the extraction of the relevant objects like point, line or polygon from the image is called feature extraction. Feature extraction could be manual by visual image interpretation, semiautomatic by using different filtering algorithms and techniques in addition to automatic by using segmentation and classification. In this study, mainly two types of feature *i.e.* canopy projection area (CPA) and tree height from the particular CPA were extracted using multi-resolution segmentation in eCognition software. The rule set for image segmentation and CHM was developed for individual crown delineation and tree height extraction from the same segment in terms of maximum pixel value contained in CHM. Feature extraction was only carried out after the complete process of segmentation and object based classification of the image in eCognition. The required object features were exported as a vector and raster format to ArcGIS 2010.

3.15. Statistical Analysis

Statistical analysis is vital for any scientific research therefore, it was carried out for both types of data either collected in the field or extracted from remote sensing technique. The major statistical analysis includes correlation and regression analysis of two variables *i.e.* response and explanatory, model development and its validation based on the regression results.

3.15.1. Correlation analysis

A scatter diagram of related two variables was depicted in order to see the relationship between them for instance the field measured CPA and image CPA, field height and Lidar derived height, carbon and CPA, carbon and Lidar derived height. Correlation coefficients and coefficient of determination (R^2) was calculated which showed the percentage of variation in one variable which associated to other variables and can be explained by the given regression. Analysis of variance (ANOVA) test was also used to calculate the mean difference of different variables.

3.15.2. Multiple regression analysis

The regression analysis has intensively been used for modelling the relationship between remotely sensed data and field measurements. The objective of regression analysis is to quantify the relationship between response variable and one or more explanatory variables. It determines the relationship between dependent and independent variable and works on the cause and effect relationship. The change in independent variable resulted the changes in dependent variable (Husch *et al.*, 2003). After calculating aboveground carbon stock using DBH and height of tree and using species specific allometric equations, relationship among carbon stock and CPA and height was developed using multiple regression analysis. Multiple linear regression analysis was employed using field measured carbon stock as response variable and CPA and Lidar derived height as an explanatory variable. In order to avoid multi-collinearity amongst the explanatory variables (*i.e.* CPA and height), a tolerance limit of the variance inflation factor [$VIF = 1 / (1 - R^2)$] was used, where R^2 is the multiple correlation of the variable with all other explanatory variables in the regression model.

3.15.3. Model calibration and validation

The classified individual trees that have 1:1 spatial correspondence with reference and delineated tree crowns were used for model development and validation since misclassified trees cannot be used for evaluation (Pouliot *et al.*, 2002). Apart from this, few outliers were also removed which is the prerequisite of regression models to establish a robust model. Thus, the number of observations becomes less than the number of trees collected from the field or recognized on the image. Only 264 trees (25%) from the total trees recognized in the field were used for the modelling.

The model thus obtained was validated with 30% of field measured data in case of each major dominant species. The R² and root mean square error (RMSE) was used to assess the performance of the model. RMSE explains the difference between model predicted values and the calculated values. Equation 11 shows the RMSE in kg per tree. Similarly, RMSE in percentage was calculated from the ratio of RMSE and average calculated carbon.

$$RMSE = \sqrt{\sum_{i=1}^n (Y_i - \hat{Y}_i)^2 / n} \dots\dots\dots\text{Equation 11: RMSE calculation}$$

Where,

- RMSE is root mean square error of the model
- Y_i is the measured/calculated value of carbon
- Ŷ_i is the predicted carbon value by the model
- n is the number of samples

Carbon stock of whole study area was calculated for each CF and species wise on the basis of validated regression model.

3.15.4. Relationship of carbon stock and tree diversity

Pearson’s correlation analysis and t-test was applied to explore the relationship between tree diversity (Shannon diversity index) and carbon stock of each CF calculated from field data. One way ANOVA was used to test whether there was statistically significant difference between the mean value of tree diversity and Shannon diversity index.

4. RESULTS

4.1. Descriptive analysis of field data

Forest stand parameters (DBH, height and crown diameter) of each individual sampled tree were measured in every sampling plot for all seven CFs of the study area. In total DBH for 1147 trees were measured while height and crown diameter of 727 and 497 trees were measured respectively in 75 plots. Descriptive statistics of each parameter for whole study area and for each CF are shown in Table 4-1 and Appendix 6 respectively.

Table 4-1: Descriptive statistics of sampled trees

Statistic	DBH (cm)	Height (m)	Crown Diameter (m)
Mean	26.07	12.93	4.96
Minimum	5	2	1
Maximum	152	37	20
Standard Deviation	19.86	6.73	3.11
Number of Trees	1147	727	497

Kayarkhola watershed has immense tree species diversity with a total of 72 species encountered during forest inventory. 73% of the forest is covered by only six species and *Shorea robusta* contributes most with 42% followed by *Lagerstroemia parviflora* 12% and other major three species with 5% each. Similarly, *Semecarpus anacardium* contributes 4% in species composition. Other four major identified tree species has 8% contribution whereas the rest of the species is categorized as Miscellaneous with 19% as shown in Figure 4-1.

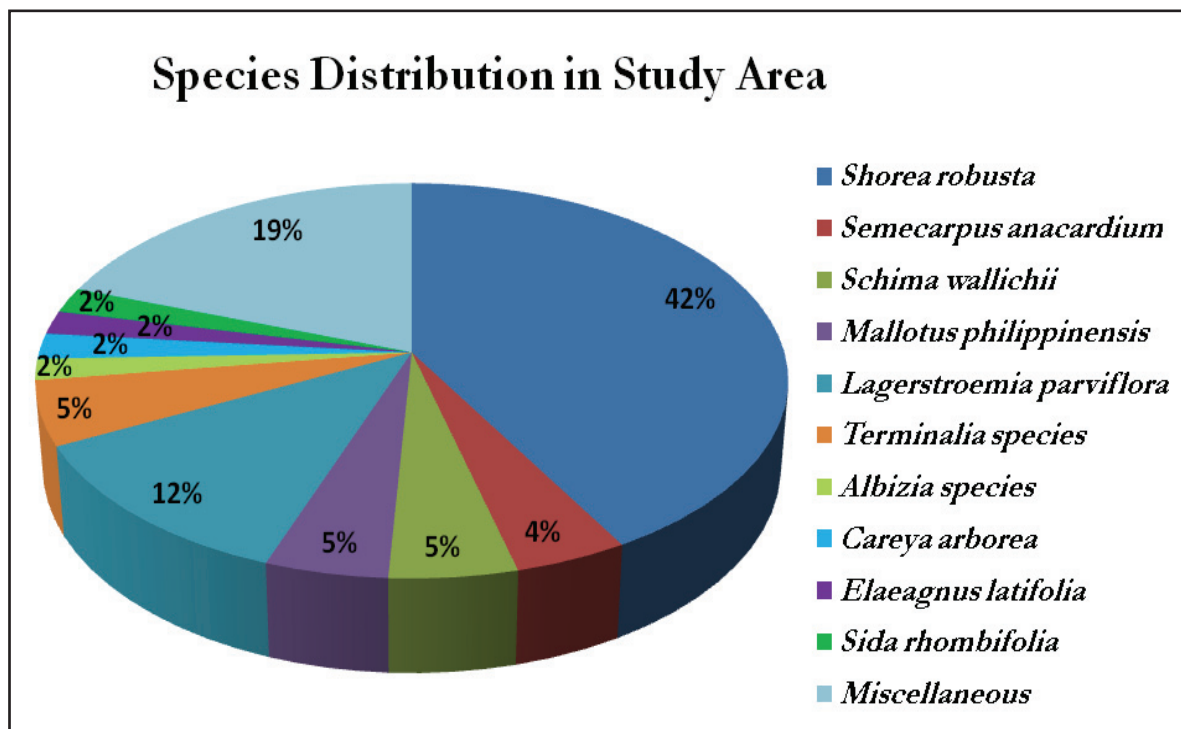


Figure 4-1: Species composition of study area

DBH, height and crown diameter of each major dominant tree species was analyzed and presented in Box-whisker plot to identify the outliers and further processing of the data as shown in Figure 4-2 (abc). Detected outliers were removed from raw data and presented in Appendix 7.

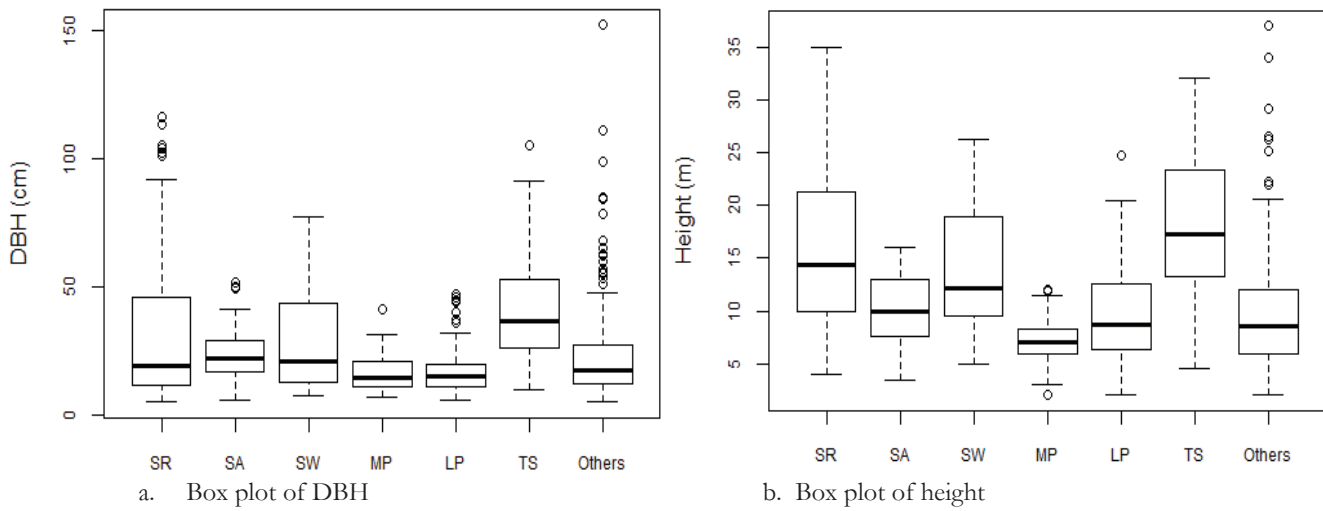
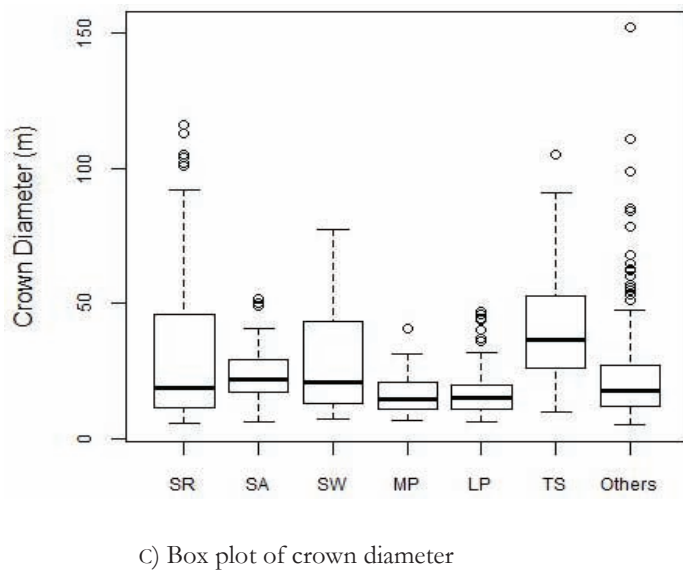


Figure 4-2: Box plot of DBH height and crown diameter of major tree species

On average, others species category had the largest DBH and was the tallest followed by *Shorea robusta* and *Terminalia species* whereas *Terminalia species* had the largest crown diameter followed by *Shorea robusta*, *Schima wallichii* and others. Moreover, these species have the highest variability in terms of DBH and height as well as crown diameter. On the other hand, DBH, height and crown diameter of *Semecarpus anacardium*, *Mallotus philippinensis* and *Lagerstroemia parviflora* were smaller than remaining tree species. In particular, DBH of these species were not more than 50cm in average and also the height and crown diameter was reported less than the other species.



(SR = *Shorea robusta*, SA = *Semecarpus anacardium*, SW = *Schima wallichii*, MP = *Mallotus philippinensis*, LP = *Lagerstroemia parviflora*, TS = *Terminalia species*)

4.2. Shannon diversity index

Tree species diversity for all seven CFs was assessed by Shannon diversity index. Number of regeneration (seedlings), saplings and trees found in each sampling plot were counted individually and summarised for each CF per ha. Janpragati B CF has the highest stem density with all forms *i.e.* regeneration, sapling and tree density whereas Samphrang CF has least stem density with equal contribution of saplings and regeneration.

Shannon diversity index, species richness, stem density per ha and number of plots measured for each CF is presented in Table 4-2. Shannon diversity index was calculated for every plot and then made average for each CF. Shannon diversity index ranges from 0 to 4.5 whereas species richness showed the exponential

value of Shannon index. Samphrang is most diverse CF with 1.898 diversity index (DI), 6.944 species richness and 2320 stem density followed by Devidhunga with 1.536, 4.897 and 8591 respectively. On the other hand, Japragati CF has least number of species with 0.888 DI, 2.616 species richness and 6680 stem density.

Table 4-2: Diversity measures of CF

Community Forest	Tree Diversity Index	Species Richness	Stem Density per ha	No of plots (500 m ²)
Devidhunga	1.53	4.89	8591	28
Nibuwatar	1.47	4.91	10427	24
Janpragati (B)	0.98	2.78	17140	5
Samphrang	1.89	6.94	2320	5
Jamuna	1.21	4.17	9253	3
Janpragati	0.88	2.61	6680	3
Pragati	1.20	3.36	10383	7

4.3. Carbon stock calculation from field data

Above ground carbon stock was calculated from field measured DBH and height by using species specific allometric equation as described in Section 3.7.3 for whole study area. Carbon stock of individual trees was calculated species wise then total carbon of trees measured in the sampling plots were calculated and averaged (e.g. per plot) for each community forest. After that, carbon stock per ha was calculated by extrapolating the carbon stock from plot (500 m²) to ha. The carbon stock (MgCha⁻¹) for each CF is shown in Table 4-3.

A total of 91141Mg C was found in the study area with 104.63 Mg C per ha. Nibuwatar CF has highest carbon stock of 41817 with 127.03 MgCha⁻¹ followed by Janpragati B with 101.52 MgCha⁻¹. Janpragati has least carbon stock among all CFs with 36.83 MgCha⁻¹ followed by Jamuna with 40.54 MgCha⁻¹ while Pragati and Samphrang has less than average carbon stock with 83.37 and 98.05 MgCha⁻¹.

Table 4-3: Carbon stock calculated from field data

Name of Community Forest	No of plots	Carbon in all plots	Average Carbon per plot	Carbon per ha in Kg	Carbon per ha (MgCha ⁻¹)	Area of CF	Total carbon in CF (Mg C)
Devidhunga	28	142124	5076	101517	101.52	253.86	25771
Nibuwatar	24	152440	6352	127033	127.03	329.18	41817
Janpragati B	5	26355	5271	105421	105.42	78.57	8283
Samphrang	5	20842	4168	83368	83.37	55.60	4635
Jamuna	3	6082	2027	40544	40.54	34.53	1400
Janpragati	3	5524	1841	36827	36.83	40.27	1483
Pragati	7	34317	4903	98049	98.05	79.06	7752
Total	75					871.07	91141

4.4. Species differentiation capability of image

4.4.1. Transformed divergence (TD)

Transformed divergence was calculated on the basis of field training dataset of different major tree species to assess the potentiality of WorldView-2 image for differentiating tree species as shown in Table 4-4. All

eight bands of pan-sharpened image were used to extract the value of transformed divergence. Table 4-4 shows the best average separability of 1970.99 which indicates an image with a good separation among the several species. Excellent separability between *Semecarpus anacardium* and *Mallotus philippinensis*, *Schima wallichii* and *Terminalia tomentosa*, *Mallotus philippinensis* and *Schima wallichii*, and *Semecarpus anacardium* and *Terminalia tomentosa* was found with D_T of 2000. *Shorea robusta* and *Lagerstroemia parviflora* has best separability with rest of the species as shown in table because all the values are greater than 1900, which indicated that these species can be separated distinctly. The segmented image was classified into six classes as recognized in the table although *Semecarpus anacardium* and *Mallotus philippinensis* could not be classified for all CF due to lack of sufficient observations. Moreover, one general class known as others which could not be categorized as any of these classes was also classified on the image.

Table 4-4: Transformed divergence of WorldView-2 image

Signature Name	<i>Lagerstroemia parviflora</i>	<i>Terminalia tomentosa</i>	<i>Shorea robusta</i>	<i>Schima wallichii</i>	<i>Mallotus philippinensis</i>	<i>Semecarpus anacardium</i>
<i>Lagerstroemia parviflora</i>	0	1907.41	1911.88	1998.25	1947.53	1996.7
<i>Terminalia tomentosa</i>	1907.41	0	1908.29	2000	1999.14	2000
<i>Shorea robusta</i>	1911.81	1908.29	0	1984.51	1933.01	1996.34
<i>Schima wallichii</i>	1998.25	2000	1984.51	0	2000	1982.64
<i>Mallotus philippinensis</i>	1947.53	1999.14	1933.01	2000	0	2000
<i>Semecarpus anacardium</i>	1996.7	2000	1996.34	1982.64	2000	0
Best Average Separability : 1970.99						

4.4.2. Spectral separability of tree classes

The mean DN values of six major tree species and one other class were plotted against eight band of WorldView-2 image for assessing the potential of image spectral separability before the classification process. Spectral profile of each species was extracted from pan-sharpened image and later the reflectance curve against each band was analyzed (Figure 4-3).

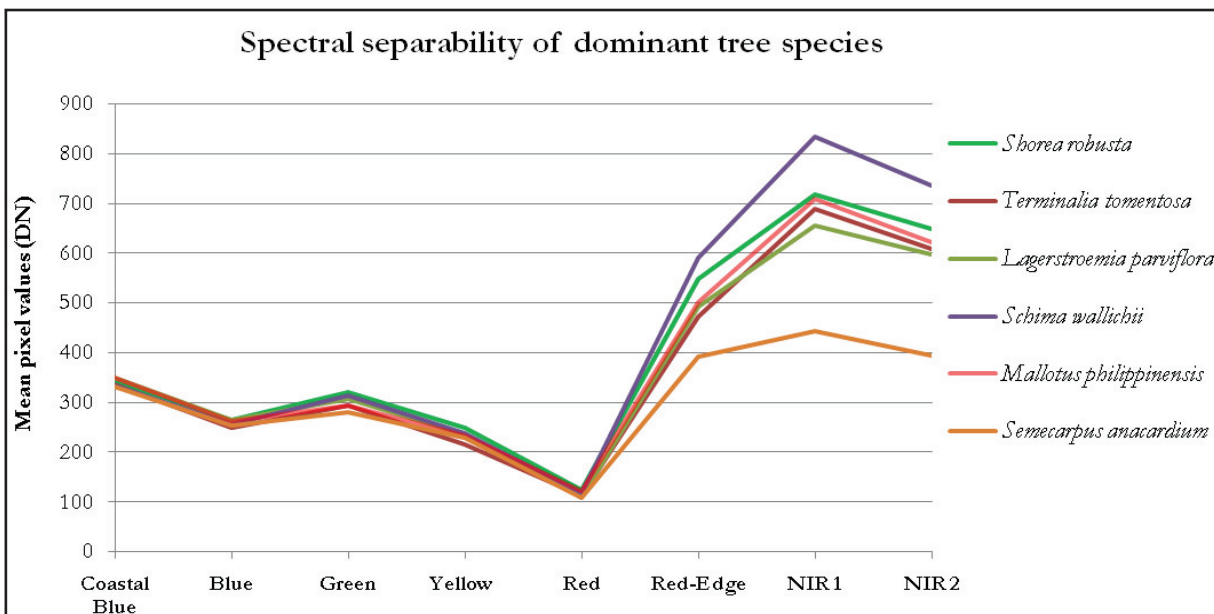


Figure 4-3: Spectral separability of forest tree species

Figure 4.3 demonstrates that all the species can be separated in NIR1, NIR2 and Red-Edge bands because the separation between the classes, which is higher in near infra-red bands compared to the visible bands of the image. *Semecarpus anacardium* and *Schima wallichii* was in distant from the rest of all species which was followed by *Shorea robusta*. It also shows that all six classes of different tree species can be separated from WorldView-2 image.

4.5. CHM generation from Lidar data

Lidar data was processed to obtain the CHM as shown in Figure 4-4. The extracted ground points were interpolated for generating a DTM, while DSM was created by interpolating the first return points which are often located on top of the trees (Figure 4-4 (a) & (b)). Figure 4-4 (c) shows the CHM which was obtained from subtraction of DTM from DSM. The actual tree height in 3D view is shown in Figure 4-4 (d).

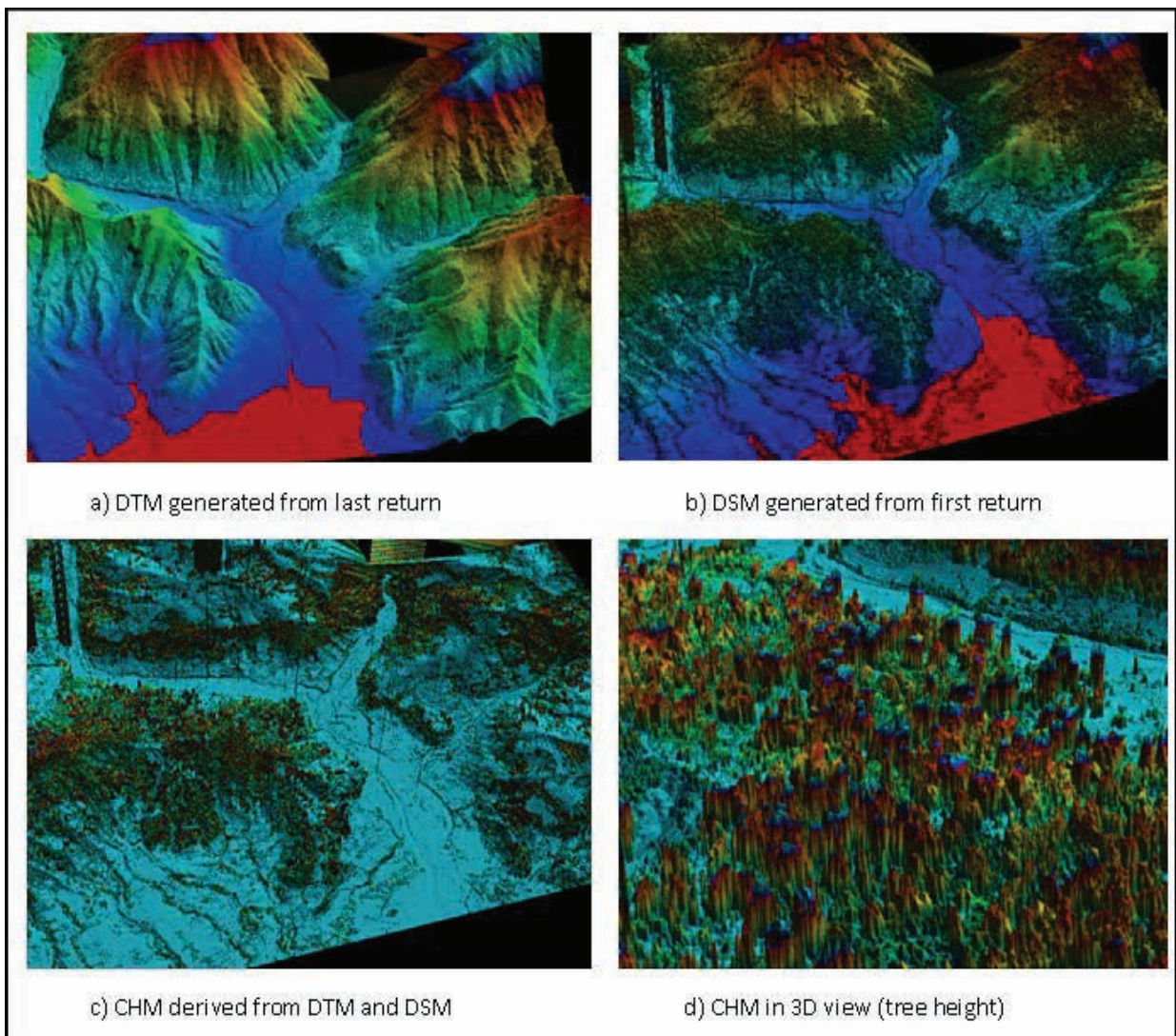


Figure 4-4: Lidar-derived images a) DTM, b) DSM, c) CHM, d) CHM visualized in 3D

4.6. Accuracy assessment of Lidar derived tree height

Tree height collected from the field and the one derived from Lidar was evaluated using Pearson's correlation coefficient and one way ANOVA. A total of 205 tree height measured in field and corresponding Lidar height extracted from the manual delineation of tree crown were used as a sample dataset. Summary of statistics for both height performances is given in Table 4-5. On average mean value

of Lidar derived height was 0.14 m greater than the field height, which was explained by about 111 trees were overestimated and 94 underestimated.

Table 4-5: Summary of statistics for tree height measurements

Statistic	Field height (m)	Lidar derived height (m)
Mean	14.64	14.78
Minimum	3	3.13
Maximum	30.5	34.78
Standard Deviation	6.31	6.19
Observations	205	205

Best of fit between field and Lidar-derived tree height was analyzed in R stat. Summary of regression equation was depicted in Figure 4-5. Field height was considered as independent variable, whereas Lidar derived height as dependent variable for linear regression. R square and adjusted R square showed that Lidar derived height was best predicted at 76 % with 3.84 m RMSE. .

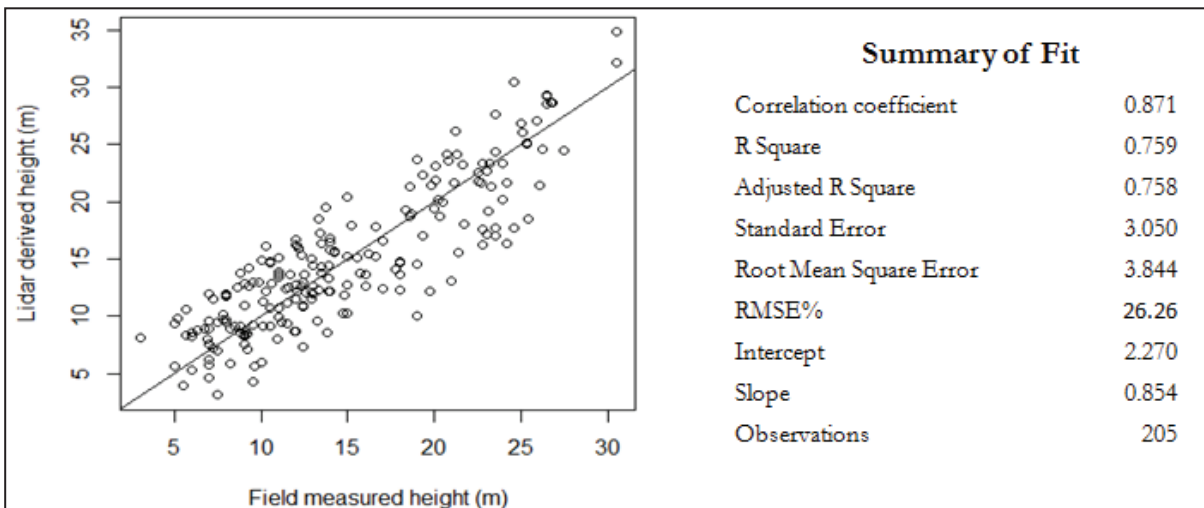


Figure 4-5: Scatterplot and summary of fit for tree height measurements

Pearson’s Correlation test and one way ANOVA was applied to test the hypothesis and conclusion made that there is no significant difference between height measured from field and derived from Lidar. Different test statistic and conclusion is presented in Table 4-6.

Table 4-6: Summary of statistical test

Test	df	Test stat	P value	Test critical
Pearson’s correlation	203	0.871	0.527	0.178
One way ANOVA	1, 408	0.051	0.820	3.864

Conclusion: r statistic is greater than critical value of r so null hypothesis is rejected *i.e.* there is statistically significant relationship between height measured from field and derived from Lidar (P<0.05)

Conclusion: F statistic is less than F critical so two means are not statistically significant different *i.e.* there is no significant difference between height measured from field and derived from Lidar (P<0.05)

4.7. Image segmentaion

Image segmentation was done in two steps. Firstly, multi-resolution segmentation was performed in panchromatic image by using the best multi-resolution segmentation parameter combinations (scale, shape

and compactness) for each subset area of forest. The best segmentation parameter combination for panchromatic image, after an iterative process, was found at scale 21, shape 0.8 and compactness 0.6. The output of multi-resolution segmentation of panchromatic band is shown in Appendix 8.

Secondly, the output of panchromatic segmentation was used as a thematic layer to segment the pan-sharpened image and CHM in order to get the same size and shape of crown. Convolution filter of 5*5 was used to filter pan-sharpened image as well as CHM as shown in Figure 4-6 a. Shadow, cloud and non-tree cover was masked out from the image before segmentation process so that the overestimation of the crown projection area can be avoided. The masked image visualized as a red border and blue surface as shown in Figure 4-6 b.

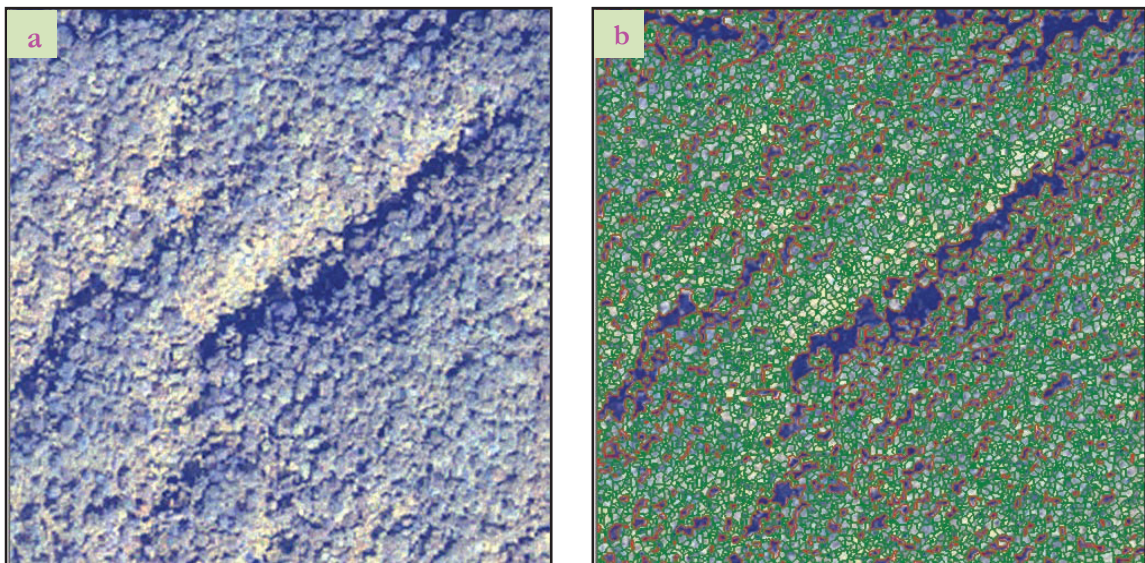


Figure 4-6: a) Subset of pan-sharpened filtered image b) shadow and non-tree cover masking

The CHM and pan-sharpened images were used as a different layer for segmentation. The different weights were given to the NIR1, NIR2, Red-Edge and CHM layers. The filtered image was segmented using the same scale, shape and compactness as used in the panchromatic band. Rule set for segmentation was applied according to the brightness of near-infrared band and height threshold of CHM. After watershed transformation, morphology and refining the shape of tree crown, the final output of segmentation was obtained as shown in Figure 4-7.

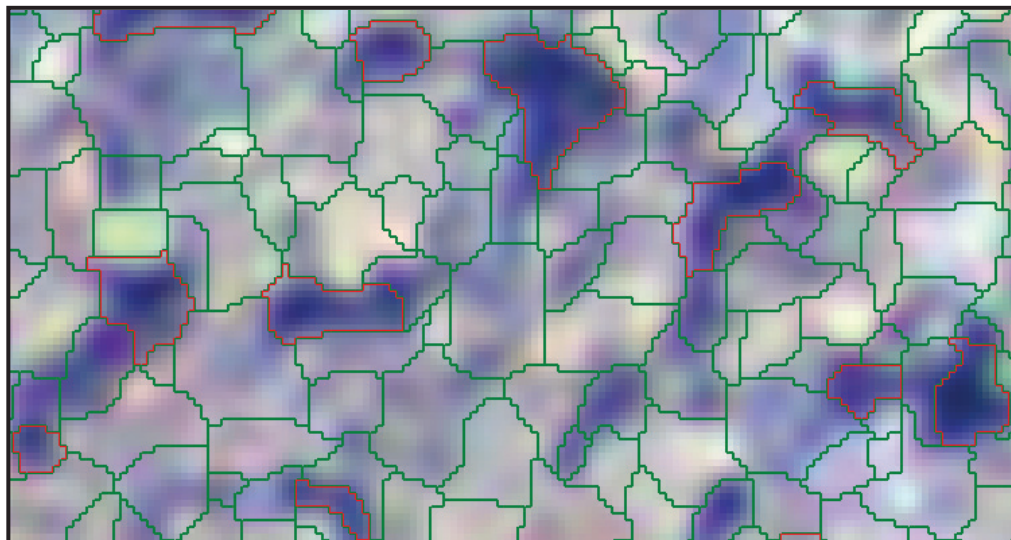


Figure 4-7: Segmentation of pan-sharpened image and CHM

4.8. Validation of segmentation

Validation of tree crown segmentation was obtained using accuracy measures of D and 1:1 spatial correspondence for 344 manually delineated reference tree crowns. Figure 4-8 shows accuracy measures of D of segmented crowns for each CF. Overall, the over-, under-segmentation, and D were 0.29, 0.34, and 0.33, respectively. Total accuracy of tree crowns delineation was about 67% which means 33% of segmentation error. In Jamuna CF, D value was the lowest (0.29), as it implied a lower over segmentation error, whereas Janpragati and Pragati CF have a higher D value of 0.40 and 0.39 respectively.

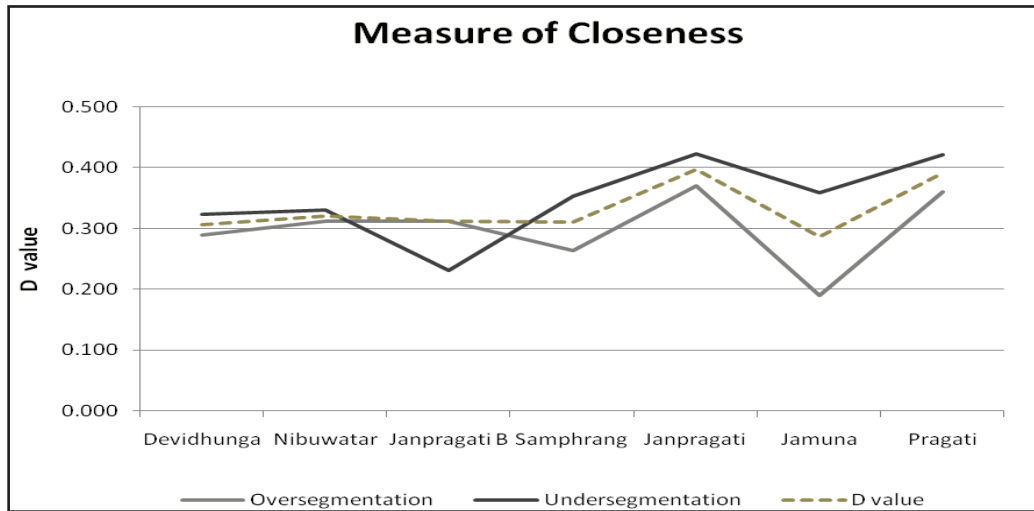


Figure 4-8: Measure of closeness (D value) for accuracy assessment of segmentation

For accuracy measure of 1:1 spatial correspondence, matching of reference and segmented polygons was observed on one to one basis. Out of 344 reference polygons obtained from manual delineation, only 261 automatic polygons obtained from segmentation had one to one relationship as shown in Table 4-7. Put differently, only 76% of the total reference crowns were matching to the segmented tree crown thus the reported accuracy of segmentation was 76%.

Table 4-7: Matching 1:1 correspondence of reference polygons to segmented polygons

CF Name	No of Reference polygons	1:1 Correspondence	Correctly Segmented CPA (%)
Devidhunga	97	75	77.32
Nibuwatar	102	73	71.57
Janpragati B	32	25	78.13
Samphrang	47	39	82.98
Janpragati	13	9	69.23
Jamuna	18	12	66.67
Pragati	35	28	80.00
Overall Accuracy	344	261	75.87 %

4.9. Image classification and accuracy assessment

Segmented tree crowns were classified into six major dominant species *i.e.* *Shorea robusta*, *Lagerstroemia parviflora*, *Terminalia tomentosa*, *Schima wallichii*, *Mallotus philippinensis* and one general class so called others. Classification was performed on the pan-sharpened image using nearest neighbourhood classifier in eCognition. All seven CFs were segmented in 4 clusters *viz.* Devidhunga, Nibuwatar, Janpragati B and Samphrang, Jamuna, Janpragati and Pragati because all above mentioned species were not common in each CF and eCognition could not process large dataset at one run. Therefore, the output segmented

image was classified for each of four clusters with different number of species (Figure 4-9). A total of 228 (Devidhunga - 67, Nibuwatar - 63, Janpragati B - 22 and Samphrang, Jamuna, Janpragati and Pragati – 76) observations were used to train the image and 101 observations (Table 4-8) to assess the accuracy of the classified image. Table 4-8 shows number of species classified, an overall classification accuracy and Kappa statistic for each cluster. Detail of confusion matrix, users and producers accuracy for each cluster is supplied in Appendix 9.

Table 4-8: Summary of classification accuracy assessment

Name of CFs	Number of species classified	Reference/ classified Totals	Correctly classified	Overall Accuracy (%)	Kappa statistics
Devidhunga	6	31	18	58.06	0.47
Nibuwatar	5	27	15	55.56	0.43
Janpragati B	3	11	8	72.73	0.62
Samphrang, Janpragati, Jamuna and Pragati	5	32	20	62.50	0.48

The classification of CFs resulted as Janpragati B CF with the highest overall accuracy and Kappa statistic with three species whereas Nibuwatar CF implied a lowest rank based on an overall accuracy and Kappa statistics with 5 numbers of species classified. 18 out of 31 reference polygons of Devidhunga CF were correctly classified with overall accuracy of 58.06% and 0.47 Kappa statistics and six species could be classified. A moderate overall accuracy (62.50%) and Kappa statistics (0.48) was obtained from group of four CFs with five classified species. Table 4-9 shows users and producers accuracy of species classification for each species.

Table 4-9: User's and producer's accuracy of species classification

Species name	Devidhunga		Nibuwatar		Janpragati B		Samphrang, Jamuna, Janpragati and Pragati	
	User accuracy	Producer accuracy	User accuracy	Producer accuracy	User accuracy	Producer accuracy	User accuracy	Producer accuracy
<i>Shorea</i>	66.67	85.71	75	50	100	60	71.43	62.50
<i>Terminalia</i>	100	25	42.86	50	-	-	100	75
<i>Lagerstroemia</i>	75	75	100	50	-	-	50	50
<i>Mallotus</i>	100	66.67	-	-	-	-	66.67	40
<i>Semecarpus</i>	100	50	-	-	-	-	-	-
<i>Schima</i>	-	-	50	100	66.67	100	-	-
Others	35.71	62.50	33.33	50	50	66.67	56.25	66.67

Shorea robusta, *Lagerstroemia parviflora*, *Mallotus philippinensis* and *Semecarpus anacardium* have 100% user's accuracy in case of Janpragati B CF, Nibuwatar CF, Devidhunga CF and Devidhunga CF respectively. *Terminalia tomentosa* achieved 100% user's accuracy in case of Devidhunga and group of four CFs. *Schima mallichii* and other class have lower user's accuracy in comparison to the rest of the tree classes for all CFs. However, *Shorea robusta* could be classified in all four cluster of CFs with more than 65% user's accuracy.

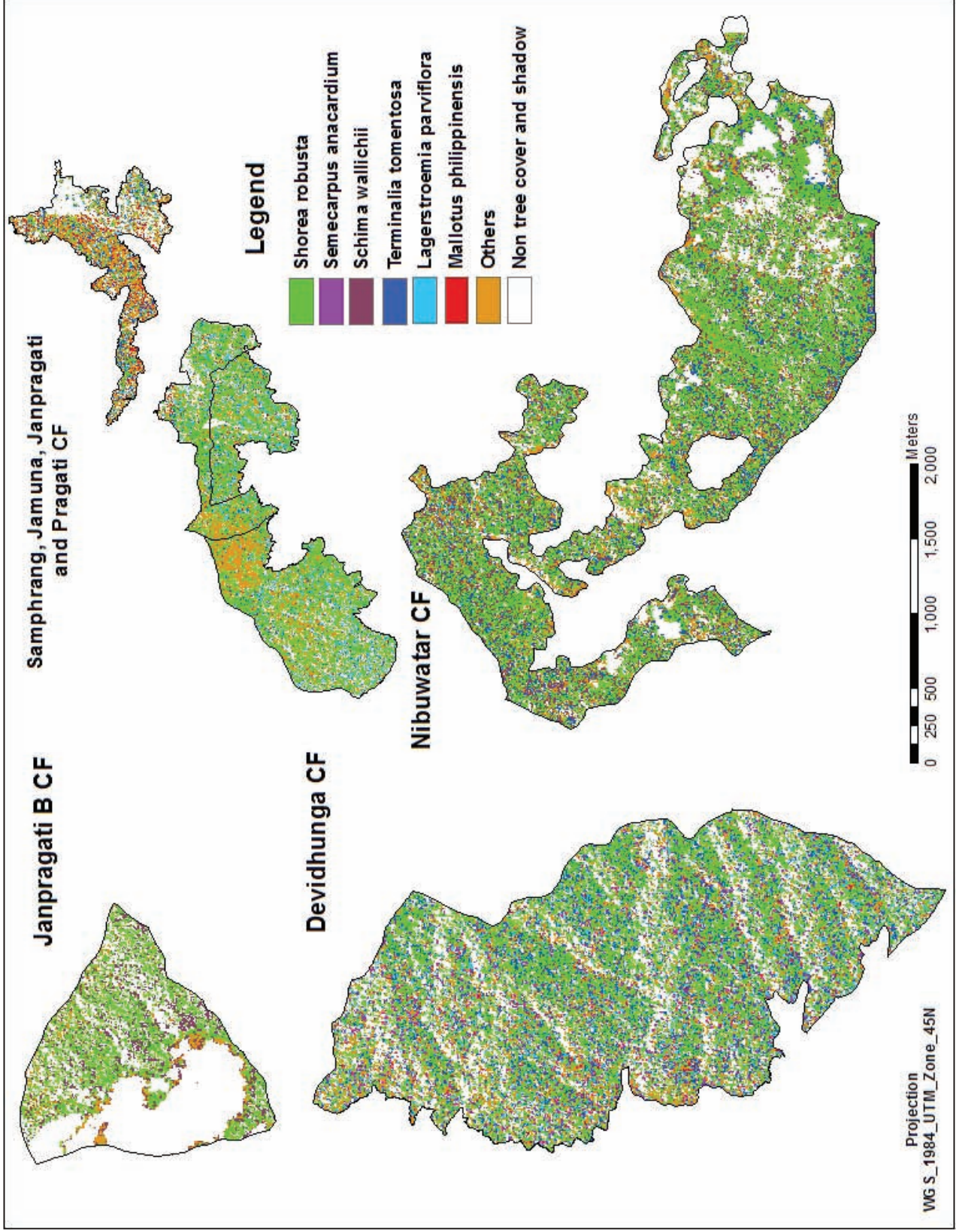


Figure 4-9: Tree species classification map of study area

4.10. Feature extraction

After classification and accuracy assessment of classified image, different features like CPA and maximum height of tree within each segment was extracted using an export algorithm in eCognition for further analyses. Attribute CF table provides attributes such as class name, CPA_image, CHM_ht and mean reflectance value of different bands of pan-sharpened image. Thus, CPA and maximum value of tree height within each segment were used to develop and validate the regression model as well as for calculation of carbon stock for each tree species in the study area

4.11. Correlation analysis

Pearson’s product-moment correlation coefficient was calculated using SPSS software to analyze the strength of linear relationship between the variables *i.e.* CPA, Lidar derived tree height (written as height in the table) and carbon stock of trees. The relationships among 3 variables were calculated for each of five species as shown in Table 4-10. The datasets for five species were randomly divided into 70% for model calibration and 30% for validation.

Table 4-10: Correlation among the variables of regression model

Species Name	Variables	df (n-2)	t- statistic	r	R Square	P value
<i>Shorea robusta</i>	CPA and carbon	60	6.89	0.70	0.49	< 0.01
	Height and carbon	60	8.58	0.77	0.60	< 0.01
	CPA and height	60	6.56	0.68	0.47	< 0.01
<i>Lagerstroemia parviflora</i>	CPA and carbon		5.46	0.62	0.38	< 0.01
	Height and carbon	29	7.97	0.75	0.56	< 0.01
	CPA and height	29	5.70	0.63	0.40	< 0.01
<i>Terminalia tomentosa</i>	CPA and carbon	16	9.16	0.79	0.63	< 0.01
	Height and carbon	16	11.90	0.86	0.74	< 0.01
	CPA and height	16	6.47	0.68	0.46	< 0.01
<i>Schima wallichii</i>	CPA and carbon	23	10.75	0.84	0.70	< 0.01
	Height and carbon	23	6.83	0.70	0.49	< 0.01
	CPA and height	23	5.51	0.62	0.38	< 0.01
<i>Others</i>	CPA and carbon	49	6.64	0.69	0.47	< 0.01
	Height and carbon	49	7.33	0.72	0.52	< 0.01
	CPA and height	49	4.66	0.55	0.31	< 0.01

There are strong positive correlations (>0.70) between tree height and carbon in all five species. The correlation between them are highly significant (P<0.01). In general, the correlation coefficient of CPA with carbon and CPA with height was found less than that of height with carbon. The correlation coefficient between CPA and carbon is more than 0.70 in particular the *Schima wallichii* and *Terminalia tomentosa*. The lowest r value was found for CPA and height of others relationship. However, on average correlation coefficient of CPA and carbon, height and carbon and CPA and height was found to be 0.73, 0.76 and 0.63 respectively. It indicates that the relationship between tree height and carbon was the highest and statistically significant for all five species. According to the result of correlation coefficient and t-statistics, the null hypothesis was rejected and concluded that there is significant relationship between CPA, height and carbon stock of study area at 95% confidence level.

4.12. Model calibration and validation

Multiple regression models were developed for five tree species in such a way that the carbon stock can be properly estimated. CPA and height were used as explanatory variables to estimate the carbon stock of individual trees. Linear regression model in Log form as shown in Equation 12 was developed for each species because it can describes the relationship between CPA, height and carbon stock. The relationship between these variables was also significant at 95% confidence level. Besides, in order to avoid multi-collinearity amongst the explanatory variables (*i.e.* CPA and height), collinearity test was done using a variance inflation factor (VIF) and it was less than 10 for all five species. Summary statistics and regression coefficient of variables is given in Table 4-11 and details of ANOVA table and other parameter estimates are given in Appendix 10

$$\text{Ln Carbon} = \beta_0 + \beta_1 * \text{Ln (CPA)} + \beta_2 * \text{Ln (Height)} \dots \dots \text{Equation 12: Multiple regression model}$$

Where,

- Ln is natural logarithm to the base 2.71828
- Carbon is above ground carbon stock per tree in Kg
- β_0 is intercept
- β_1 is coefficient of CPA
- β_2 is coefficient of Lidar derived tree height

Table 4-11: Regression coefficients and summary statistics of model

Species	β_0	β_1	β_2	R Square	Adjusted R square	Standard error	Observations
<i>Shorea robusta</i>	-0.877	0.597	1.873	0.66	0.65	0.90	62
<i>Lagerstroemia parviflora</i>	0.205	0.370	1.494	0.60	0.57	0.58	31
<i>Terminalia tomentosa</i>	-0.126	0.458	1.848	0.82	0.80	0.37	18
<i>Schima wallichii</i>	-0.144	1.124	0.883	0.75	0.73	0.61	25
Others	0.044	0.616	1.396	0.64	0.63	0.57	51

Model for each species and regression coefficient was tested using F-test and t-test respectively. All the models and regression coefficients showed statistically significant at 95% confidence level.

Multiple regression models were validated using randomly selected 30% of independent datasets (total 77) in case of each species as described in Table 4-12. Observed and predicted carbon stock from regression models were plotted against each other as shown in Figure 4-10 and co-efficient of determination (R^2) was calculated to see goodness of fit. A root mean square error (RMSE) and RMSE percentage (average field measured carbon divided by RMSE) were calculated. *Shorea robusta* described the best fit of model with 94% of variation explanation and 24.85% of RMSE. For all species R^2 values was greater than 75% which means carbon stock of individual trees estimated by the regression model were able to explain up to 75% the carbon stock measured from the field. However, model error varies from 22.48 to 289.68 kg/tree depending on the species and calculated mean carbon stock and 24.85 to 49.75% of RMSE.

Table 4-12: Summary of model validation and RMSE (kg/tree)

Species	Coefficient of determination	Calculated mean carbon	RMSE	RMSE %	Observations
<i>Shorea robusta</i>	0.94	849.39	211.12	24.85	25
<i>Lagerstroemia parviflora</i>	0.78	80.98	22.48	27.77	11
<i>Terminalia tomentosa</i>	0.76	865.93	289.68	33.80	10
<i>Schima wallichii</i>	0.84	198.21	75.24	37.96	11
Others	0.78	163.36	81.27	49.75	20

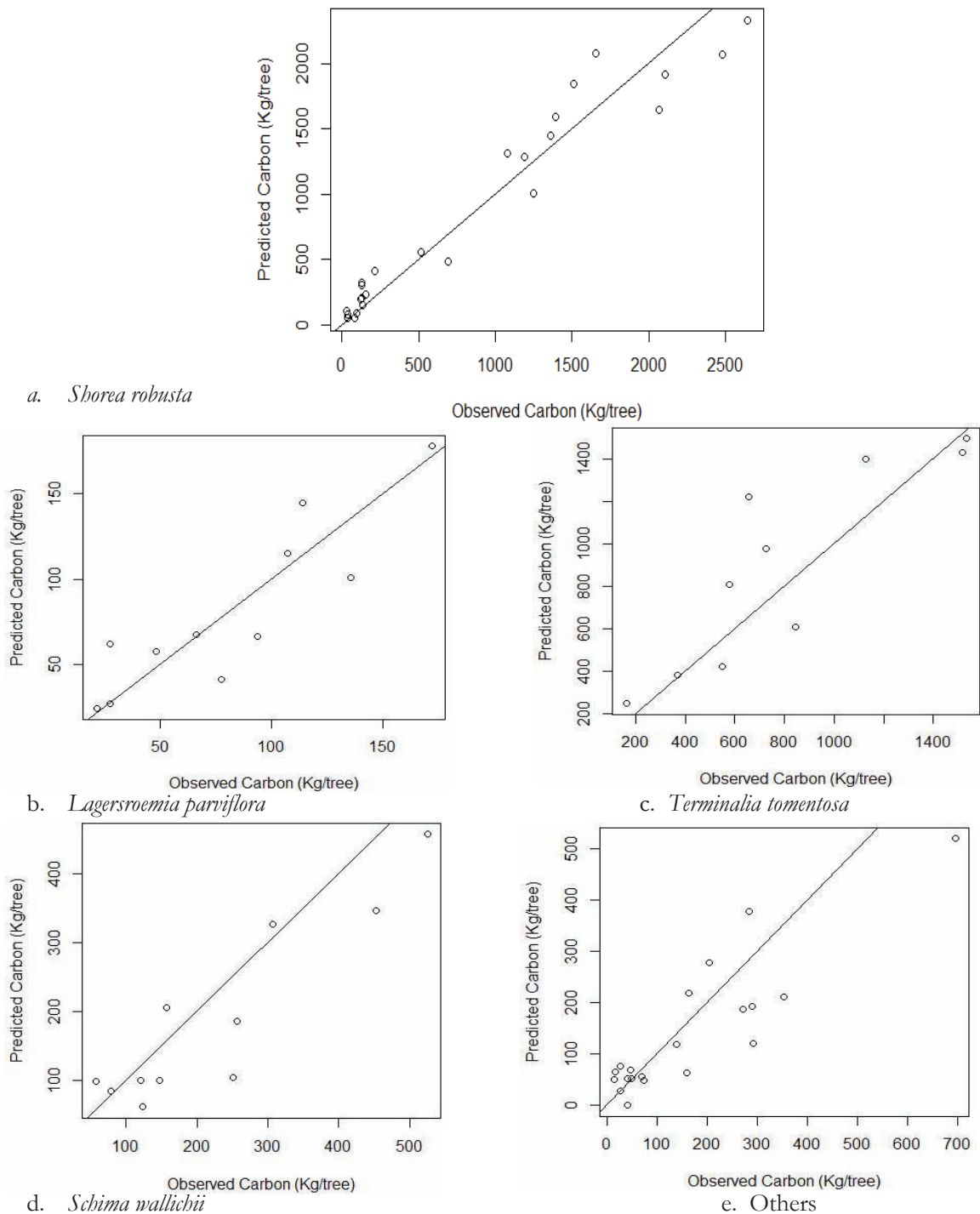


Figure 4-10: Scatterplot of observed and predicted carbon stock

4.13. Carbon stock mapping of study area

Multiple regression model developed for each species was used to estimate total carbon stock of study area. Species wise model was used to estimate amount of carbon stock of major dominant tree species for all seven CFs and later a carbon map was produced using ArcGIS 2010. Carbon map produced for each CF is presented in Appendix 11 and for Devidhunga CF at tree level is shown in Figure 4-11. The amount of carbon per tree varies from less than 500 kg/tree to more than 2000 kg/tree. Few big trees with large CPA and height have even more the 5000 Kg, with a good indication reported for the *Shorea robusta* and *Terminalia tomentosa*. *Lagerstroemia parviflora*, *Schima wallichii* and most of the species from others category have less carbon stock within a range of 500 to 1500 kg per tree.

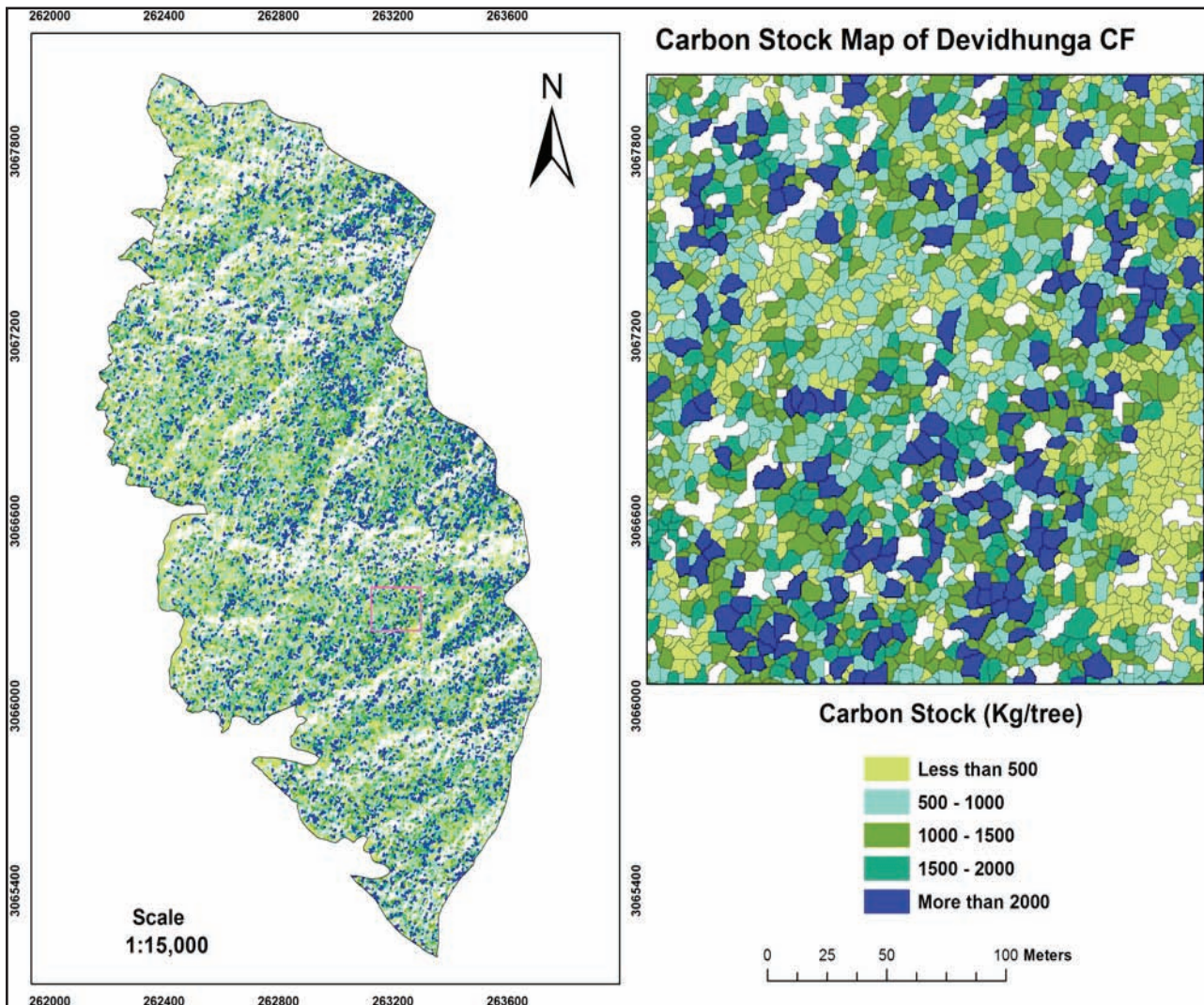


Figure 4-11: Carbon stock map of Devidhunga CF and carbon stored by one tree (inset)

A total of 188485 Mg C carbon was estimated in the study site which covered an area of 871.07 ha and thus on average 216.38 Mg C per ha was found as shown in Table 4-13. Nibuwatar CF has the highest carbon stock (86391 Mg C) with major five species followed by Devidhunga CF (58373 Mg C) whereas Jamuna CF has the least carbon stock with four tree species.

Table 4-13: Summary of species wise carbon stock (Mg C)

CF Name	Species Name					Total Carbon	Area of CF (ha)	Carbon Per ha
	<i>Shorea robusta</i>	<i>Lagerstroemia parviflora</i>	<i>Terminalia tomentosa</i>	<i>Schima wallichii</i>	Others			
Devidhunga	33969	2139	12582		9683	58373	253.86	229.94
Nibuwatar	56055	402	12276	10510	7147	86391	329.18	262.44
Janpragati (B)	5682			1925	682	8290	78.57	105.51
Samphrang	2392	286	2414		3219	8311	55.60	149.48
Janpragati	3403	208	407		2297	6314	40.27	156.78
Jamuna	2627	255	374		1159	4415	34.53	127.85
Pragati	8509	428	893		6562	16392	79.06	207.34
Total	112637	3717	28945	12436	30749	188485	871.07	216.38
Per ha	129.31	4.27	33.23	14.28	35.30			

The percentage carbon stock of each CF is presented in Figure 4-12. It shows that 60% of carbon stock of the study area was contributed by *Shorea robusta* except in the case of Samphrang CF. *Schima wallichii* is mainly found in the Janpragati B and Nibuwatar CF which constitutes about 20 and 10% respectively. Other species was found in all the CFs but the percentage coverage of carbon stock varies from 10% to 40% whereas *Lagerstroemia parviflora* contributed less than 10% of carbon stock except in Samphrang CF.

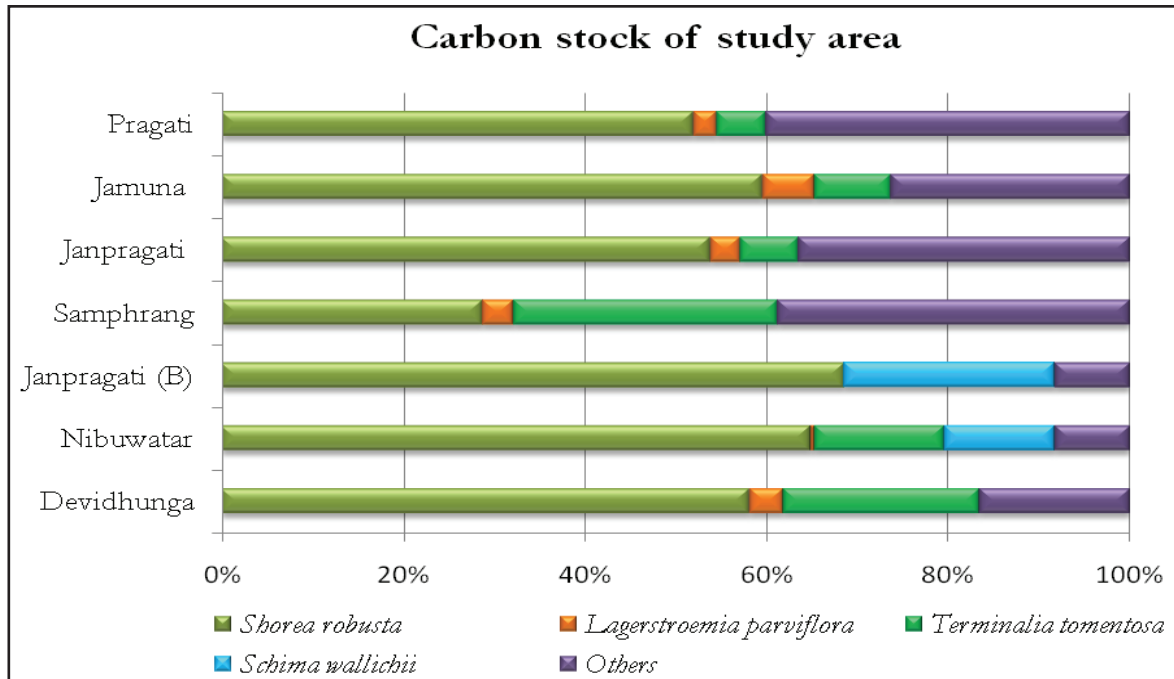


Figure 4-12: Species wise carbon stock of the study area

4.14. Relationship between tree diversity and carbon stock

The strength of relationship between tree diversity and carbon stock was depicted after plotting these two independent samples in scatter plot diagram. Pearson’s correlation coefficient and one way ANOVA test was employed for the correlation of tree diversity and carbon stock. Table 4-14 shows the result of Pearson’s correlation. According to the table, correlation between tree diversity and carbon stock was not statistically significant at 95% confidence level for all of the CF except Janpragati CF. The result of Jnparagati CF was statistically incorrect due to insufficient degrees of freedom. Pragati CF and Nibuwatar CF have negative correlation between tree diversity and carbon stock while rest of five CFs have positive correlation but not statistically significant.

Table 4-14: Summary of Pearson's correlation analysis

F Name	Pearson Correlation	Coefficient of determination (R ²)	df	t-stat	t critical	Critical values for Pearson's r
Nibuwatar	-0.290	0.084	22	-1.422	2.074	0.404
Devidhunga	0.109	0.012	26	0.557	2.056	0.374
Janpragati B	0.349	0.122	3	0.645	3.182	0.878
Samphrang	0.506	0.256	3	1.016	3.182	0.878
Janpragati	1.000	0.999	1	33.305	12.710	0.997*
Jamuna	0.877	0.769	1	1.826	12.710	0.997
Pragati	-0.576	0.332	7	-1.865	2.365	0.666
Overall	0.566	0.321	7	1.817	2.000	0.666

One way ANOVA as shown in Table 4-15 indicated that there is statistically significant difference between the mean values of tree diversity and carbon stock for each of the seven CFs with different P value because in each of the cases F statistic is greater than the F critical. Thus, there is no significant relationship between tree diversity and carbon stock of CF.

Table 4-15: Summary of one way ANOVA

CF Name	F Stat	P-value	F crit
Nibuwatar	85.36848	4.73E-12	4.051749
Devidhunga	47.76784	5.74E-09	4.019541
Janpragati B	19.6368	0.002193	5.317655
Samphrang	11.48234	0.00952	5.317655
Janpragati	20.90318	0.010245	7.708647
Jamuna	14.18708	0.019663	7.708647
Pragati	6.937025	0.021821	4.747225

5. DISCUSSIONS

5.1. Canopy height model (CHM) generation and accuracy assessment

Canopy height model (CHM) generation and its accuracy assessment were described and reported in this study. It showed that 54% field measured tree height was overestimated and 46% was underestimated by Lidar height. Tree height extracted from CHM was evaluated by plotting against field measured height of 205 sampled trees in scatterplot. The coefficient of determination (R^2) of estimated tree height was 0.76, with RMSE of 3.84 m. The Pearson's correlation test and F test revealed that there is statistically significant relationship between tree height measured from field and the one derived from Lidar.

Several studies have been done for the estimation of tree height from Lidar data and reported different results. Kwak *et al.*, (2007) obtained 0.77, 0.80 and 0.70 coefficient of determination (R^2) for two coniferous and one deciduous species respectively by using 1.8 m point density, whereas Lim *et al.*, (2003a) found 0.68 R^2 value for leaf-on hardwood stands of Ontario, Canada. Similarly, Brandtberg *et al.*, (2003) obtained an accuracy of field and Lidar height within 1.1 m mean standard error and 0.69 coefficient of determination using high sampling density (*e.g.*, 12 points/m²) in deciduous forest of North America. In another study Heurich *et al.*, (2003) found mean differences of 0.53 m between ground measurements and the Lidar height for all species while for deciduous trees the mean differences was 0.37 m with a standard deviation of 1.43 m. In both the cases it was overestimation. In addition, Takahashi *et al.*, (2005a) observed an overestimation of Lidar derived tree height with an average error of 0.90 m in mountainous (steep slope >38°) area of Sugi plantation in Japan.

In this study, the reported accuracy of tree height is within acceptable range as the previous studies carried out by Kwak *et al.*, (2007), Lim *et al.*, (2003a), Heurich *et al.*, (2003) and Takahashi *et al.*, (2005a). Nevertheless, comparison cannot be done directly due to different forest types, densities, composition of tree species, topographic features and quality of the Lidar data. In this study, the percentage difference of overestimation and underestimation of tree height is very small and there is a tendency for the heights of smaller trees to be overestimated and those of tall trees to be underestimated. Different types of error can be attributed due to the following reasons: interpolation of the point cloud data into a grid-based canopy height model, precision of laser height measuring instruments (TruPulse 360 B), random errors introduced by the field personnel during height measurements. Complexity of the landscapes (undulating, rugged, steep slope) and uneven forest age may contribute to the error propagation found in this study.

Lidar data (0.8 m point density) used for the study is sufficiently beneficial for estimating tree height at a plot level but not particularly recommended for an individual tree level. The point cloud data has numerous noises arises from external object and sensor itself which cannot be overcome by simple interpolation like TIN. The reason behind is that the interpolation is a prediction of what is not known. TIN interpolation techniques make the prediction using the direct/close neighbours of three points on the triangle and fit them into a model therefore the larger the distance between the points, higher the chance of error in estimating elevation of tree height. It may also be biased when interpolation done in the elevation for steep slope and irregular surface. Thus another method should be tried for better noise removal because LasTools only uses the TIN methods for interpolation. Noise could be one of the prominent reasons for overestimation of tree height because maximum height of the tree on the ground was up to 37 m but Lidar height showed beyond this range. It might be occurred due to the low quality (unfiltered) raw Lidar data.

Several literatures (Leckie *et al.*, 2003; Naesset & Bjercknes, 2001; Persson *et al.*, 2002) showed that Lidar under-predicts the tree height in plot level *i.e.* mean height of the plot and mostly in coniferous stands of temperate region in relatively flat terrain. Persson *et al.*, (2002) found 0.99 correlation coefficients and 0.63 RMSE in a coniferous forest and further explained that low laser sampling density caused tree height underestimation in their study. Furthermore, they argued that because the uppermost parts of the tree tops were not likely to be hit when using small footprint airborne LiDAR, the estimates of tree heights would consequently be underestimated. But in case of our study, the terrain is rugged and hilly with tropical natural broadleaved forests and tree height was estimated on individual crown basis not on plot level as usual. Therefore, the failure to sample tree tops because of an insufficient laser sampling density is likely to be of greater relevance in coniferous forests where crown shape is more conical than in broadleaf forests where crowns are more rounded.

Error in height measuring instruments could be attributed for overestimation of tree height because the laser instruments (TruPulse 360 B) used in the field have precision of 0 to 1.67 m (Clark *et al.*, 2004). Another reason for overestimation in steep slope is the horizontal positional error between the tree top and stem because Lidar height calculated from the distance between tree top and the ground surface would be overestimated. Apart from that, it is difficult to measure the exact top of the trees in dense deciduous forest due to intermingling or overlapping between tree canopies. It is often challenging in the field to decide on the highest point of the crown as there is no distinct peak, especially when trees are leaning or have large crowns as shown in Figure 5-1. In addition sometimes the peak is hidden behind a green wall of leaves because the branches of different trees are mixed. Therefore, more detailed research about the overestimation of tree heights in mountainous deciduous forest like Chitwan is suggested

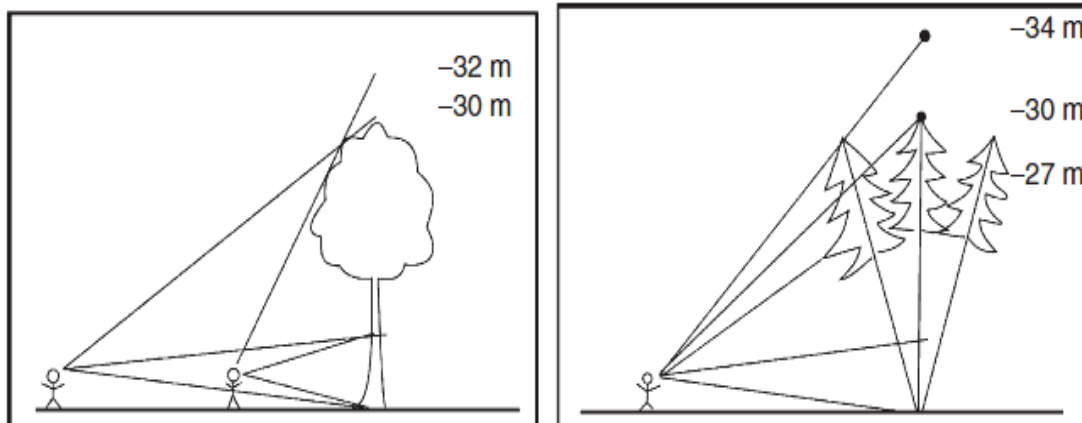


Figure 5-1: Errors in tree height measurements (Köhl *et al.*, 2006)

5.2. Image segmentation and accuracy assessment

Multi resolution segmentation was chosen for the segmentation of WorldView-2 image in this study. 1:1 spatial correspondence and measure of closeness *i.e.* goodness of fit between reference polygons and segmented polygons was employed for accuracy assessment of segmentation. Results thus obtained from measure of closeness showed 67% accuracy with 0.33 D value whereas from 1:1 spatial correspondence 76% accuracy was obtained. Measure of closeness gives the ‘distance index’ while the latter is based on positional accuracy of the reference polygons to segmented polygons *i.e.* if there was overlap of at least 50% between these two polygons then the segmentation was regarded as correctly classified as done by Zhan *et al.*, (2005). The reason for difference between two methods of accuracy is due to different approach of assessment while some of the segmentation error is caused by the slight discrepancies in the co-registration of image and Lidar data which could not be overcome during the image registration. Therefore, further research will be needed to address the issue of co-registration.

The finding of this study can be compared with different study done by several researchers (Baral, 2011; Wang *et al.*, 2004; Workie, 2011). Our study is very similar to Baral, (2011) who obtained segmentation accuracy of 74.4 % using WorldView-2 image and 77.6 % with GeoEye in the same study area by applying 1:1 correspondence method. Similarly, Workie (2011) achieved relatively low segmentation accuracy in broadleaved forest (67%) compared to the coniferous (73%) using measure of closeness methods while on the basis of 1:1 correspondence the study reported 71% accuracy for coniferous and 55% for broadleaved forest in the Netherlands. In addition Wang *et al.*, (2004) obtained 75.6% segmentation accuracy for the spruce and fir forests. In comparison to above studies, results obtained in this research are relatively higher due to the combined use of satellite imagery and Lidar data. Because, it is possible to delineate the tree crown in shadow and low structured vegetation using height information of CHM which cannot be addressed by satellite images. Holmgren *et al.*, (2008) found an accuracy increase up to 8% in tree crown segmentation by integrating data from the laser-based sensor and optical satellite imagery.

In this study, the multi-resolution segmentation coupled with watershed transformation was implemented for delineating tree crown with respect to its capability to segment highly heterogeneous forest (Kim *et al.*, 2010) and captivating more than one band during the segmentation process (Ke & Quackenbush, 2011). Other tree crown delineation algorithms considered trees that have conical shape and treetop to be the brightest point of the tree (Culvenor, 2002; Gonzalez *et al.*, 2010; Wang *et al.*, 2004). Compared to coniferous tree crowns, the within-crown brightness variation for broadleaved trees tends to be greater due to the large branches and non-conical shape of the crown. Since, this study area is natural broadleaved forest type with several age gradation and different species composition, multi-resolution segmentation technique was performed to fully explore the information content of VHR satellite images. In addition, Lamonaca *et al.* (2008) discovered that multi-resolution segmentation is preferable for segmenting heterogeneous forest and to explore the dimension of forest structural attributes.

The success of multi-resolution segmentation depends upon several parameters including weights given to image layers, a colour/shape ratio associated with the spectral/shape criterion of homogeneity, a compactness/smoothness ratio associated with object shape and a scale parameter. Therefore, higher weight was given to NIR2, Red-Edge and CHM, while fine scale *i.e.* 21 and shape and compactness value of 0.8 and 0.6 was chosen by iterative process during the segmentation. However relatively lower accuracy was obtained when assessed from measure of closeness “D value”. Overall D value (segmentation error) in this research was higher mainly due to under segmentation (0.34) of big trees and large number of clumped trees (Figure 5-2).



Figure 5-2: a) Ground view and b) canopy view of clumped trees

This might be due to improper splitting up of bigger crowns into actual trees using the multi-resolution segmentation and also images still affected by the cloud, huge light shadow and distortion (Figure 5-3).

Other sources of error such as co-registration of image and CHM and viewing nadir angle is described in Section 5.7.



Figure 5-3: WorldView-2 image a) cloud and huge shadow b) distortion in image

5.3. Image classification and accuracy assessment

Segmented tree crowns were further used for classification of dominant tree species as described in Section 3.13 and results are shown in Section 4.9. A nearest neighbourhood classifier was used in eCognition which resulted in different accuracy for different cluster of CFs.

Species classification resulted in overall accuracy of 58% and Kappa 0.46 for classifying six species, overall accuracy of 56% and Kappa 0.43 for five species, overall accuracy of 63% and Kappa 0.48 for five species and overall accuracy of 73 % and Kappa 0.62 for three species depending on the cluster of CFs as shown in Table 4-8. Thus, it depicted that classification accuracy increased when the number of classified species decreased. The user's accuracy of *Shorea robusta* was higher (more than 66% in each case) and distinctly classified whereas others category implied a relatively low accuracy (below 63% in each case) than remaining species. But for *Lagerstroemia parviflora*, *Schima wallichii*, *Terminalia tomentosa* and *Mallotus philippinensis*, the user's accuracy varies from 25% to 100% depending on the cluster and number of species classified (Table 4-9). A higher user's accuracy of *Shorea robusta* was obtained due to a significant number (ca. 42%) of this tree species found in the field. The obtained result is comparable to Baral (2011) with an overall classification accuracy of 66.7% and Kappa 0.32 for two classes *i.e.* *Shorea robusta* (user's accuracy 76.47%) and others (user's accuracy 58.33%), using the same satellite imagery in the same study area. With regards to the number of species classified by Baral (2011), this study revealed that the integration of Lidar and imagery data is significantly improved the accuracy of tree classification in the tropics. Best average separability of transformed divergence (Table 4-4) also proved that WorldView-2 image has huge potential to separate different species on the basis of spectral signature and thus classification accuracy was improved. Moreover, NIR1, NIR2 and Red-Edge were found to substantially improve the classification results of the dominant tree species which also observed from spectral separability analysis of the image (see Figure 4-3).

Tree species classifications based on high resolution satellite imagery and Lidar data have been widely used. For example, Tsendbazar (2011) achieved relatively low accuracy of 64.5% and Kappa 0.48 for four species classes of *Alnus nepalensis*, *Pinus roxburghii*, *Schima wallichii*, and others using GeoEye image, the accuracy increased to 90.3% and Kappa 0.80 when species were generalized into broadleaf and needle leaf species. Waser *et al.*, (2011) achieved an overall accuracy of 76% and 84% with kappa 0.70 and 0.73 when classifying 7 species and 4 species by using airborne digital sensor 40 of 0.25 m resolution and Lidar with 0.8 m point density. Voss & Sugumaran, (2008) obtained an accuracy of 57% and 56% when classified 5 deciduous and 2 evergreen tree species from two hyperspectral dataset. The accuracy was increased up to

19% when combined with 0.6 m posting of Lidar data. Holmgren *et al.*, (2008) obtained an overall accuracy of 96% when classifying groups of Norway spruce, Scots pine, and deciduous trees, using autumn multispectral aerial images (0.1m panchromatic and 0.6 m colour infrared) and very high-resolution LiDAR data (50 points per m²) whereas only 88 and 91% accuracy was obtained from either Lidar or aerial imagery alone. Nevertheless, the range of previously reported accuracy value suggests that the species classification in this study is comparatively successful because six broadleaved tree species were classified using WorldView-2 (2m MSS and 0.5 panchromatic) imagery and 0.8 m Lidar point density data.

The classification accuracy reported from different researchers reveals that accuracy increased in four cases i) lower the number of species classified higher the accuracy obtained (Baral, 2011; Tsendbazar, 2011), ii) use of very high resolution aerial camera imagery (Waser *et al.*, 2011), iii) the combination of Lidar with images (Voss & Sugumaran, 2008), and iv) the type of forest either plantation or needle leaf (Holmgren *et al.*, 2008). In general, research showed that classification accuracy of planted coniferous trees is relatively higher than broadleaved natural forest. Although WorldView-2 image has a great potential for the species differentiation as described in Section 4.4, higher accuracy could not be achieved due to several reasons: a) Automatic tree crown delineation errors during image segmentation; b) Time difference between the season of image acquisition from image and Lidar data, image was acquired in autumn (October, 2010) while Lidar mapping was done in March, 2011; c) Less number of samples given to the classifier as a training data and also for validation because insufficient trees were recognized in the image; and d) Effect of shadow and cloud on remotely sensed image at both tree level and landscape level (see Figure 5-2)

Quality of tree crown segmentation also affects species classification results. The higher classification accuracy would be obtained if the tree crown delineation is more precise. Erikson (2004) and Brandtberg (2002) discussed that delineation error of tree crowns can affect the classification system and with better segmentation, the classification can most probably be better. Leckie *et al.*, (2005) investigated the influence of quality of tree crown delineation and noted that classification accuracy was higher (40-70%) for well delineated tree crowns, while classification accuracy was much lower for all crowns when poorly delineated ones are included.

5.4. Modelling the relationship of CPA, height and carbon

The relationship between CPA and carbon, CPA and height and height and carbon was evaluated by correlation analysis and t-test. Correlation analysis demonstrated that the strength of linear relationship between height and carbon were strong ($r > 0.70$) and highly significant ($P < 0.01$) for all five species whereas correlation coefficient of CPA with carbon and CPA with height was found less than that of height with carbon. The linear relationship (r value) between CPA and carbon was 0.70, 0.84 and 0.79 for *Shorea robusta*, *Schima wallichii* and *Terminalia tomentosa* respectively which is very similar to the results of the study done by Shah (2011). He obtained r value of 0.80, 0.73 and 0.79 for *Shorea robusta*, *Schima wallichii* and *Terminalia tomentosa* respectively. *Terminalia tomentosa* resembles the same value while other two species have big difference. It could be due to the variability of sample correlation coefficient which depends on sample size and data outliers. This result is comparable to Kuuluvainen (1991) who modeled the relationship between CPA and AGB of Norway spruce plantation and obtained R^2 of 0.79. Moreover, Hemery *et al.*, (2005) found close linear relationship ($R^2 > 0.80$) between crown diameter and stem diameter from 20 to 50 cm DBH for different species of broadleaved trees.

Multiple regression models were employed to get the combined effect of both predictor variables to estimate carbon stock which ensures better prediction (Ketterings *et al.*, 2001) and higher coefficient of determination (Cairns *et al.*, 2003). CPA and Lidar height were used to predict the carbon stock of different tree species as VIF was less than 10 and no multi collinearity existed. A log transformed multiplicative model was preferred to predict the carbon stock as indicated by previous studies which

found that such models are suitable for predicting the stand tree volume and biomass of the trees (Bartelink, 1996; Holmgren *et al.*, 2003; Means *et al.*, 2000; Sharma & Pukkala, 1990; Takahashi *et al.*, 2005b). Log transformation is explicitly recommended when the standard deviation is proportional to mean and the variables typically showed skewed distribution which can often be made symmetric using transformation (Keene, 1995). Watt & Kirschbaum (2011) found linear relationship of 0.73 R^2 between height and DBH of even aged coniferous stands when both the variables have been log transformed. Bartelink, (1996) demonstrated the relationship between stem dimensions and biomass of needle leaf forest using log transformed regression equation which explained 94% of variation. In natural forest, tree parameters such as DBH, CPA and height have wide range of distribution and they often does not show the normal distribution therefore response and predictor variables were log transformed in order to address extreme value of tree parameters. In this study, Lidar derived tree height and CPA of individual tree showed heteroscedasticity and positively skewed, so regressions were fit to the natural logarithm to develop multiple regression models. Moreover, the allometric equations used for estimation of AGB also based on log transformed linear equations (Section 3.7.3) so that it fits well with the model developed to predict the carbon stock. Thus, carbon stock predicted from such models give higher accuracy than the models developed using only one variable *i.e.* CPA and can be used for wide range of CPA and height.

Species wise regression models developed for this study was significant at $P < 0.05$ and showed R^2 value of 0.66 for *Shorea robusta*, 0.60 for *Lagerstroemia parviflora*, 0.82 for *Terminalia tomentosa*, 0.75 for *Schima wallichii* and 0.64 for others. The results is in line with the study of Takahashi *et al.*, (2010) who achieved R^2 of 0.73 for the tree canopy area, height and volume of Japanese Cedar using low density Lidar data and QuickBird panchromatic imagery using log transformed linear regression. Thus it can be said that our result is satisfactory for the model development. However, no study has been done to estimate the carbon of broadleaved species using CPA and Lidar height in combination with satellite image and airborne Lidar data. Results of this study is relatively higher in comparison to Baral (2011) who found R^2 of 0.64 for *Shorea robusta* and 0.80 for other species using GeoEye image in the same study area. Moreover, Holmgren *et al.*, (2003) found 0.90 R^2 and 37 m^3/ha RMSE between Lidar derived tree height and canopy area using 6.8 points/ m^2 Lidar data. They estimated stand volume of three coniferous trees species from Lidar height and canopy area measured at plot level using log transformed regression model. The reason for achieving lower R^2 value in case of this study was the effect of shadow which influenced the relationship of carbon stock of broadleaf tree and CPA.

The coefficient of determination (R^2) and RMSE show how accurately carbon stock of the forest can be predicted from the regression model. Validation of the models resulted in least value of RMSE (22.48 kg/tree) for *Lagerstroemia parviflora* and highest (289.68 Kg/tree) for *Terminalia tomentosa* whereas highest R^2 for *Shorea robusta* (0.94) and lowest for *Terminalia tomentosa* (0.76). The results can be compared to Baral (2011) who obtained lower R^2 for *Shorea robusta* (0.77) and almost same value for others (0.79). Higher result obtained in this study is due to interaction of CPA and Lidar derived height which can better explain the variation of carbon stock in the field. RMSE value per tree is a relative measure and it depends on the mean carbon stock of the individual tree species. For example, mean carbon stock of *Lagerstroemia parviflora* was 80.98 Kg/tree so the RMSE value is lowered compare to rest of the tree species. Regression models developed for *Shorea robusta* were able to explain up to 94% of variability associated with carbon stock of individual trees however there was 24.85 % RMSE error in carbon stock estimation. In terms of values of R^2 , it indicated that on average carbon stock can be predicted with 82% variability and 35% RMSE from the model developed for each species. Thus, it can be highlighted that carbon stock can be predicted more accurately from regression models of this study which composed of both CPA and height than the use of CPA or tree height alone.

5.5. Carbon stock estimation

Above ground carbon stock of different dominant tree species was estimated using multiple regression models. The models predicted higher carbon stocks for trees which have higher CPA and height than the trees which have lower CPA and height. The result showed 188485 Mg C carbon stock with an average of 216.38 Mg C per ha in total study area. There is a variation of carbon stock per ha in case of each major species and CFs. Nibuwatar CF had highest carbon stock (262.44 MgCha⁻¹) whereas least carbon stock was in Janpragati B with 105.51 MgCha⁻¹. Similarly, carbon stock constituted by *Shorea robusta* is 129.31 MgCha⁻¹ but *Schima wallichii* showed 35.30 MgCha⁻¹ (Table 4-13). All the CFs except Samphrang was constituted by 60% of carbon stock with *Shorea robusta*.

The result thus obtained is relatively higher than the other study done so far (Baral, 2011; Baral *et al.*, 2010; ICIMOD, 2011; Kaul *et al.*, 2010). Comparison with other forests of similar ages indicates that the present estimates of carbon stock for study area are evidently higher such as Kaul *et al.*, (2010) reported 156 MgCha⁻¹ carbon stock for slow growing long rotation forests *e.g.* *Shorea robusta* of India. Result of this study is also comparable to the study done by ICIMOD, (2011) in the same study area *i.e.* Kayerkhola watershed. They reported a mean above ground carbon stock of 153.10 Mg C per ha which is lower estimate than our study. However, Baral (2011) achieved relatively lower result of 70 MgCha⁻¹ in the same study area whereas Baral *et al.*, (2009) found 96.6 MgCha⁻¹ in the same forest types of Nepal. Both the results are much lower than this study. Usuga *et al.*, (2010) obtained 99.6 MgCha⁻¹ for *Pinus patula* and 85.7 MgCha⁻¹ for *Tectona grandis* in a commercial plantation in Columbia. Thus, it is evident that tree species found in the study area were slow growing and tend to have larger long-term carbon storage in forest biomass compared to the fast growing and short rotation tree species. Estimation of carbon stock of several tree species using species specific allometric equation can be one of the reasons for higher estimation than the previous studies because they have used different allometric equation for different studies. Nevertheless, higher RMSE and RMSE percentage calculated for each species showed error in model which could also be attributed for higher estimation.

5.6. Relationship between tree diversity and carbon stock

Present study revealed that there was no significant relationship (weak relationship) between tree species diversity and carbon stock of forest at small scale and local level *i.e.* community forests. Out of seven CFs, two CFs indicated negative correlation (Nibuwatar -0.29, Pragati -0.57) between tree diversity and carbon stock. Overall correlation between tree diversity and carbon stock for all seven CFs was 0.57 indicating positive relationship but statistically not significant at 95% confidence level.

This study can be compared with the result of Sharma *et al.*, (2010). They obtained a correlation coefficient of -0.25 between Shannon diversity index and total carbon density of several forest types of India and implied that natural forests with higher diversity are not rich in carbon density. On the contrary, Nakakaawa *et al.*, (2010) discovered that there was a strong positive correlation between the carbon density and tree species diversity, a study carried out in plantation farmland of Uganda. The relationships between carbon storage and tree species diversity of natural forest at small scale are still unclear. It is because tree carbon storage generally increases with increasing tree species richness but for stands with same species richness, tree carbon storage varies dramatically Chen, (2006). He also observed that different tree species have different carbon storage abilities therefore, the evenness of same main tree species is important to control the stand tree carbon storage at small scale when tree species are similar. Hence, it can be said that carbon stock of forest depends on the composition of forest and regime of management because carbon stored by species is almost half of its biomass. Manmade forest always produces more carbon than the natural forest because plantation forests has even aged monoculture plantation but natural forest has a diverse type of species which have different capacity of carbon sequestration.

It is evident that climate change and biodiversity loss are two crises of global magnitude each posing individual as well as synergistic risks to human well-being (Strassburg *et al.*, 2010). There is still a debate of setting priority between reducing carbon emissions and increasing biodiversity conservation. Therefore, understanding the relationships between biodiversity and carbon sequestration owing to international interest is important aspect both in preserving terrestrial carbon pool and conserving biodiversity. Although this study showed a weak relationship between tree diversity and carbon stock at local level, attention should be given to the conservation of tree species diversity along with the carbon stock enhancement of natural forest. Focusing only to afforestation or reforestation program for forest carbon could be counterproductive to biodiversity conservation, because forests are managed as “carbon farms” with the application of intensive silvicultural management that could homogenize diverse forests of the country. Conservation of forests having large amount of carbon stocks is also a valuable way to reduce CO₂ emission as it may be more beneficial than afforestation in the short term. Sharma *et al.*, (2010) revealed that preserving old growth stands may not only maintains large amounts of stored carbon but could be continued to sequester much more carbon than artificial forests. In this context, REDD+ provides unique opportunity for conservation of natural forests along with biodiversity conservation. Hence, attention should be given not only for the carbon stock measurement but also for the conservation of tree species diversity which will further preserve our forests and reduce carbon emissions. Moreover, REDD+ also addresses the rights of indigenous and local communities who have played a significant role in conserving biodiversity and cultural value through customary laws or other effective means which are not usually included in official records (Khatun, 2011).

5.7. Uncertainties and sources of error for carbon mapping

There are several uncertainties associated with the estimation of above ground carbon in the tropical forest of Nepal. These uncertainties depends on the different sources of error occurred from field measurement to data acquisition, image processing, and model development for carbon mapping. Different sources of errors introduced at several steps of research are discussed in the following subsections.

5.7.1. GPS error occurred during navigation

Printed image and coordinate of each sample plot was used to navigate plot location in the forest using GPS. Precision and accuracy of GPS depends upon various factors such as density of forest, topographic features, atmospheric conditions, satellite position, noise in the radio signal and natural barriers to the signal. In the forested mountainous area, GPS signal is often not properly work and may lead to inaccurate positional reading. Although accuracy of GPS Map 60 CSx has up to 3 m in a clear sky condition, it could not be used to collect exact plot locations in Kayerkhola watershed. Noise can create an error between 1 to 10 meters and results from static or interference from something near the receiver or something on the same frequency. However, barriers between the satellite and the receiver can produce error up to 30 m (maps-gps-info.com, 2012).

5.7.2. Uncertainty on tree level estimation

Chave *et al.*, (2004) summarized the sources of error in AGB estimation of tropical forests which mainly includes the uncertainties on tree level AGB estimation, allometric model selection error, sampling uncertainties for one plot and estimation of AGB of the whole forest. Tree DBH and total tree height are the most commonly used variables to predict AGB and introduces the error at initial stage. Tree level error propagates from measurement of DBH for individual trees in the field for example, measuring DBH for trees of higher diameter like 150 cm could be wrong due to the deformity of trunk at 1.3 m or irregular shaped-trunk. Similarly, actual tree height of individual trees might be measured wrongly due to personnel and instrumental error of measurement as described in section 5.1. Thus, overall estimation of carbon stock for individual tree would be affected if those parameters were not measured correctly.

5.7.3. Co-registration of image and Lidar data

Registration of two types of data sources is a crucial step in order to extract the required information from both the data at one time. The co-registration of panchromatic and multispectral band of WorldView-2 image was done with Lidar intensity image which resulted with RMSE of 1.5 m. Due to random error of object shift in image it could not be corrected for less than 1.5 m RMSE. Thus, error introduced during the co-registration process is inevitable which subsequently leads to the segmentation error in height extraction from the tree segments and species classification. Figure 5-4 shows the corner of buildings before and after co-registration of image (colour) and Lidar intensity image (black and white). Even after co-registration there is still small shift of few pixels which could not be correctly adjusted.

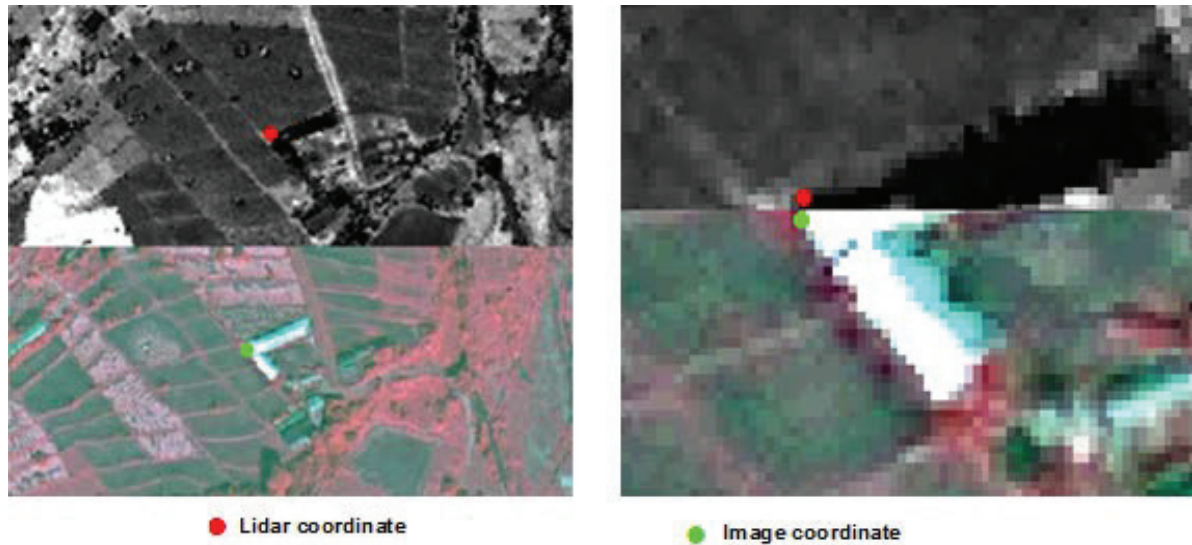


Figure 5-4: Error caused by co-registration

5.7.4. Sun elevation angle and off nadir view

Sun elevation angle and viewing angle of the sensor are most important factors for true vertical projection area of canopy. Viewing angle of WorldView-2 sensor was 25° off-nadir which makes the tree canopy to appear differently and causes confusion for the algorithm in eCognition to recognize the tree. Song *et al.*, (2010) observed that topography, off-nadir viewing and illumination angles make different tree size in the image than the real one as shown in Figure 5-5. Although trees are always vertical regardless of whether they grow on a slope or on a flat surface, topography and off-nadir illumination can change the amount of shadows in the image seen by the sensors. Thus, off nadir viewing angle changes the size of crown projection area on the image which ultimately affects the segmentation and classification accuracy of WorldView-2 image.

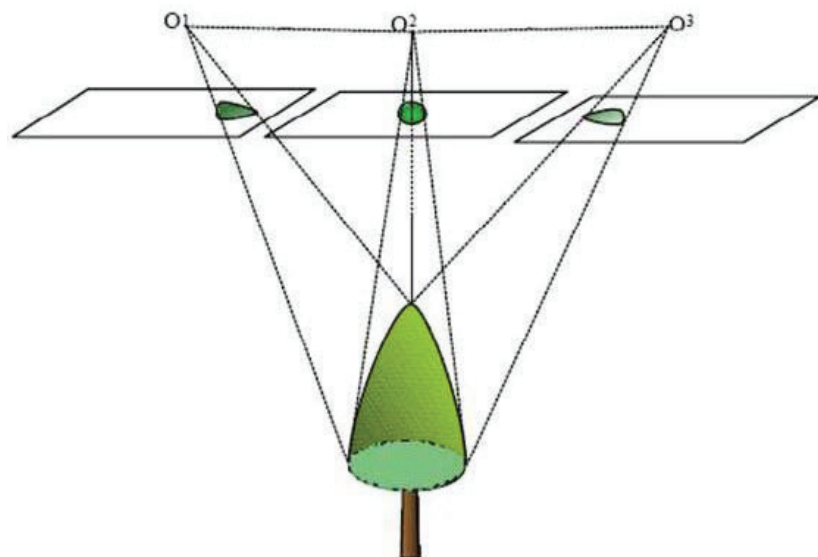


Figure 5-5: Tree crown shape from different angle of view (Li *et al.*, 2008)

5.7.5. Summary of analysis of error

The chronological order of error for estimation of above ground carbon stock in the study area is shown in Table 5-1. The propagation of error starts from field measurement and accumulates at model development which ultimately affects the carbon prediction of the whole study area.

Table 5-1: Several stages of sources of error and uncertainties

Stages of error	Measurements	Impacts	Error propagation
Image acquisition	Off nadir angle, shadow and cloud	Quality of image	
GPS measurement	Location of sample plot	Recognizing tree on image	
Tree measurement	DBH, height and crown width	Quality of field data	
Co-registration of image	Data fusion	Image segmentation	
Tree crown delineation	Extraction of CPA and height	Quality of CPA and height	
Classification	Species identification	Classification accuracy	
Model development	Parameter estimate	Carbon stock estimation	

5.8. Limitation of the research

1. GPS error encountered in the field could not be avoided due to dense canopy, steep slope and atmospheric conditions. A better validation field data leads to a better prediction or modelling.
2. Species wise model was only developed for few dominant tree species of the study area due to less sample measurement of tree parameters. Regression models could not estimate above ground carbon stock for undergrowth and trees less than 10 cm DBH and 5 m height
3. Relationship between tree diversity and carbon stock could not be explored in full fledge due to small number of samples extracted from remote sensing data.

6. CONCLUSIONS AND RECOMMENDATIONS

6.1. Conclusions

WorldView-2 satellite imagery and airborne Lidar data are very promising remote-sensing sources for estimating and mapping the above ground carbon stock of tropical broadleaved forest in Nepal. The species specific regression models developed from CPA and height of the tree using object based image analysis is the main technique to estimate the carbon stock of study area. With respect to this approach, following conclusions were made to address the research questions.

How accurately the height of individual trees can be estimated from the Lidar derived CHM?

The result showed that Lidar derived tree height was able to explain 76% of field measured tree height with RMSE of 3.84 m. Pearson's correlation analysis indicated statistically significant correlation between field height and Lidar derived tree height at $P < 0.05$ whereas F-test showed no difference between means of the two heights.

How accurately WorldView-2 image can differentiate tree species on the basis of spectral separability?

Transformed divergence among six major dominant tree species showed the best average separability of 1970.99 which indicated a good separation among the species. NIR1, NIR2 and Red-Edge of WorldView-2 image were found to be the best bands for spectral separability of different tree species in comparison to other visible bands of the image. Classification accuracy reported as 58.06% and Kappa statistics 0.47 for classifying six dominant tree species whereas overall accuracy of 72.73% and Kappa statistics 0.62 were achieved for classifying three dominant tree species.

How accurate is the segmentation of CPA from WorldView-2 image in combination with Lidar data?

Two types of accuracy assessment for segmentation of image were applied in this study *i.e.* measure of closeness (D value) and 1:1 spatial correspondence. Overall D value for the study area was found to be 0.33 with 0.29 over segmentation and 0.34 under segmentation that means there was 33% error (67% accuracy) in segmentation whereas 76% accuracy of segmentation was obtained from 1:1 spatial correspondence.

What is the relationship between CPA, height and carbon stock of dominant tree species?

Pearson's correlation analysis indicated that there is a strong positive correlation ($r > 0.70$) between height and carbon stock for all five tree species. The correlation between CPA and carbon was 0.70, 0.79 and 0.84 for *Shorea robusta*, *Terminalia tomentosa* and *Schima wallichii* respectively whereas poorer relationship ($r < 0.70$) was found between CPA and height for all the species. However, on average correlation coefficient of CPA and carbon, height and carbon, and CPA and height was found to be 0.73, 0.76 and 0.63 respectively.

Model validation results showed that species wise regression models were able to explain up to 94%, 78%, 76%, 84% and 78% of variation in carbon estimation for *Shorea robusta*, *Lagerstroemia parviflora*, *Terminalia tomentosa*, *Schima wallichii* and others respectively.

How much carbon is stored by each major type of tree species in the study area?

A total of 188485 Mg C carbon was estimated in the study area with an average of 216 Mg C per ha. Approximately 60 % of carbon stock (112637 Mg C) was stored by *Shorea robusta* with 129 Mg C per ha. *Lagerstromea parviflora*, *Terminalia tomentosa*, *Schima wallichii* and other species constitutes about 3717 Mg C, 28945 Mg C, 12436 Mg C and 30749 Mg C respectively.

What is the relationship between tree diversity and carbon stock of each community forests (CF)?

There is no significant relationship between tree diversity and carbon stock of each CF of the study area. Pearson's correlation test and F-test did not indicate any statistically significant relationship between tree diversity and carbon stock of forest at 95% confidence level. However, there is a negatively weak relationship in case of Pragati CF and Nibuwatar CF.

Finally, it can be concluded that correlation among CPA, Lidar derived tree height and carbon measured from field data was found to be significant. Therefore, multiple regression models developed for each species using CPA and Lidar derived height can be used to estimate the carbon stock of similar forest types.

6.2. Recommendations

Use of very high resolution imagery in combination with airborne Lidar data and applying OBIA method is very effective for accurately estimating the species wise carbon stock and thus, is recommended for implementation of REDD+ pilot project in Nepal. However, some recommendations are listed for further research.

- An accurate field validation technique is strongly recommended. For instance differential GPS (DGPS) should be used to minimize the field based location error and recognizing the individual trees on image, Lidar data and field data.
- Co-registration of image and Lidar data should be improved by using DEM of Lidar point cloud data which can eliminate the shift between trees identified on the image and Lidar.
- The Lidar point density per sq m used in this study is relatively low and it thus could not identify the individual trees in the field. In future work, Lidar mapping should be acquired at relatively high point density (preferably at least 5 points per sq m).
- Non-linear multiple regressions are recommended to reflect the true relationship of CPA, height and carbon stock of tree species.
- Sufficient sample size and a range of forest types *i.e.* according to elevation gradient or climatic zone should be preferred to generalize the relationship of tree diversity and carbon stock.

List of References

- Ahamed, T., Tian, L., Zhang, Y., & Ting, K. C. (2011). A review of remote sensing methods for biomass feedstock production. *Biomass and Bioenergy*, 35(7), 2455-2469.
- Amelinckx, S. (2010). *Spatial and Spectral Separability of Grasslands in the inner Turku Archipelago using Landsat Thematic Mapper Satellite Imagery*. MSc University of Turku, Turku, Finland. Retrieved from <http://www.doria.fi/bitstream/handle/10024/63590/MasterThesis2010SimonAmelinckx.pdf?sequence=1>
- Andersen, H.-E., McGaughey, R. J., & Reutebuch, S. E. (2005). Estimating forest canopy fuel parameters using LIDAR data. *Remote Sensing of Environment*, 94(4), 441-449.
- Andersson, K., Evans, T. P., & Richards, K. R. (2009). National forest carbon inventories: policy needs and assessment capacity. *Climatic Change*, 93(1-2), 69-101.
- ANSAB. (2011). The first Forest Carbon Trust Fund in Nepal helps communities benefit from forest conservation and sustainable use Retrieved 22-12-2011, from <http://www.ansab.org/publication/>
- Baccini, A., Friedl, M., Woodcock, C., & Warbington, R. (2004). Forest biomass estimation over regional scales using multisource data. *Geophysical Research Letters*, 31(10), L10501.
- Bachman, C. G. (Ed.). (1979). *Laser radar systems and techniques* (Vol. 1).
- Baral, S. (2011). *Mapping carbon stock using high resolution satellite images in sub - tropical forest of Nepal*. MSc Thesis, University of Twente Faculty of Geo-Information and Earth Observation (ITC), Enschede. Retrieved from http://www.itc.nl/library/papers_2011/msc/nrm/baral.pdf
- Baral, S., Malla, R., & Ranabhat, S. (2010). Above-ground carbon stock assessment in different forest types of Nepal. *Banko Janakari*, 19(2), 10-14.
- Bartelink, H. H. (1996). Allometric relationships on biomass and needle area of Douglas-fir. *Forest Ecology and Management*, 86(1-3), 193-203.
- Brandtberg, T. (2002). Individual tree-based species classification in high spatial resolution aerial images of forests using fuzzy sets. *Fuzzy Sets and Systems*, 132(3), 371-387.
- Brandtberg, T., Warner, T. A., Landenberger, R. E., & McGraw, J. B. (2003). Detection and analysis of individual leaf-off tree crowns in small footprint, high sampling density lidar data from the eastern deciduous forest in North America. *Remote Sensing of Environment*, 85(3), 290-303.
- Brown, S. (1997). Estimating biomass and biomass change of tropical forests: a primer. A Forest Resource Assessment Publication (pp. 55). FAO, Rome.
- Brown, S. (2002). Measuring carbon in forests: current status and future challenges. *Environmental Pollution*, 116(3), 363-372.
- Cairns, M. A., Olmsted, I., Granados, J., & Argaez, J. (2003). Composition and aboveground tree biomass of a dry semi-evergreen forest on Mexico's Yucatan Peninsula. *Forest Ecology and Management*, 186(1-3), 125-132.
- Caparros, A., & Jacquemont, F. (2003). Conflicts between biodiversity and carbon sequestration programs: economic and legal implications. *Ecological Economics*, 46(1), 143-157.
- CBD. (2009). Connecting Biodiversity and Climate Change Mitigation and Adaptation: Report of the Second Ad Hoc Technical Expert Group on Biodiversity and Climate Change. (Vol. Technical Series No. 41, pp. 126 pages). Montreal, Canada.
- Cerbu, G. A., Swallow, B. M., & Thompson, D. Y. (2011). Locating REDD: A global survey and analysis of REDD readiness and demonstration activities. *Environmental Science & Policy*, 14(2), 168-180.
- Chaturvedi, A. N., & Khanna, L. (1982). *Forest mensuration* (Vol. 9): International Book Distributors Dehra Dun, India.
- Chave, J., Condit, R., Aguilar, S., Hernandez, A., et al. (2004). Error propagation and scaling for tropical forest biomass estimates. *Philosophical Transactions of the Royal Society of London. Series B: Biological Sciences*, 359(1443), 409-420.
- Chen, Q., Yang, X. L., Petriu, E. M., & iee. (2004). *Watershed segmentation for binary images with different distance transforms*.
- Chen, X. W. (2006). Tree diversity, carbon storage, and soil nutrient in an old-growth forest at Changbai Mountain, Northeast China. *Communications in Soil Science and Plant Analysis*, 37(3-4), 363-375.
- Clark, D. A., Brown, S., Chambers, J. Q., et al. (2001). Net primary production in tropical forests: an evaluation and synthesis of existing field data. *Ecological Applications*, 11(2), 371-384.
- Clark, M. L., Clark, D. B., & Roberts, D. A. (2004). Small-footprint lidar estimation of sub-canopy elevation and tree height in a tropical rain forest landscape. *Remote Sensing of Environment*, 91(1), 68-89.
- Clinton, N., Holt, A., Scarborough, J., Yan, L., et al. (2010). Accuracy assessment measures for object-based image segmentation goodness. *Photogrammetric Engineering and Remote Sensing*, 76(3), 289-299.

- Culvenor, D. S. (2002). TIDA: an algorithm for the delineation of tree crowns in high spatial resolution remotely sensed imagery. *Computers & Geosciences*, 28(1), 33-44.
- Definiens. (2011). *eCognition Developer 8.7 Reference book*. Munchen, Germany.
- Definiens Imaging. (2004). *eCognition User Guide 4: Concepts and Methods*. Munchen, Germany.
- DigitalGlobe. (2010). WHITE PAPER The Benefits of the 8 Spectral Bands of WorldView-2. Retrieved 15-08-2011, from http://www.digitalglobe.com/downloads/spacecraft/WorldView-2_8-Band_Applications_Whitepaper.pdf
- DoF. (2010). Hamro Ban, Community Forestry Division. Department of Forests. Kathmandu, Nepal.
- Dragut, L., Tiede, D., & Levick, S. R. (2010). ESP: a tool to estimate scale parameter for multiresolution image segmentation of remotely sensed data. *International Journal of Geographical Information Science*, 24(6), 859-871.
- Drake, J. B., Dubayah, R. O., Clark, D. B., Knox, R. G., et al. (2002). Estimation of tropical forest structural characteristics using large-footprint lidar. *Remote Sensing of Environment*, 79(2-3), 305-319.
- Drake, J. B., Knox, R. G., Dubayah, R. O., Clark, D. B., et al. (2003). Above ground biomass estimation in closed canopy neotropical forests using lidar remote sensing: factors affecting the generality of relationships. *Global Ecology and Biogeography*, 12(2), 147-159.
- Du, Y. (2008). *Verification of tsunami reconstruction projects by object - oriented building extraction from high resolution satellite imagery*. ITC, Enschede. Retrieved from http://www.itc.nl/library/papers_2008/msc/gfm/duye.pdf
- Dubayah, R. O., & Drake, J. B. (2000b). Lidar remote sensing for forestry. *Journal of Forestry*, 98(6), 44-46.
- Dubayah, R. O., Knox, R., Hofton, M., Blair, J. B., et al. (2000a). Land surface characterization using lidar remote sensing. *Spatial information for land use management*, 25-38.
- ERDAS. (2011). What's New ERDAS 2011 Software Release Retrieved 15-12-2011, http://www.erdas.com/Libraries/Tech_Docs/What_s_New_in_ERDAS_Software_2011.sflb.as
- Erikson, M. (2004). Species classification of individually segmented tree crowns in high-resolution aerial images using radiometric and morphologic image measures. *Remote Sensing of Environment*, 91(3-4), 469-477.
- FAO. (2010). Global Forest Resource Assessment 2010 : Main Report, 2011-07-28, from <http://www.fao.org/docrep/013/i1757e/i1757e.pdf>
- Gao, H., Siu, W. C., & Hou, C. H. (2001). Improved techniques for automatic image segmentation. *Circuits and Systems for Video Technology, IEEE Transactions on*, 11(12), 1273-1280.
- Gautam, B. R., Tokola, T., Hamalainen, J., M., G., et al. (2010). Integration of airborne LiDAR, satellite imagery, and field measurements using a two-phase sampling method for forest biomass estimation in tropical forests. *Presented at International Symposium on "Benefiting from Earth Observation" 4 - 6 October 2010, Kathmandu, Nepal*
- Gibbs, H. K., Brown, S., Niles, J. O., & Foley, J. A. (2007). Monitoring and estimating tropical forest carbon stocks: making REDD a reality. [Article]. *Environmental Research Letters*, 2(4).
- Gonzalez, P., Asner, G. P., Battles, J. J., Lefsky, M. A., et al. (2010). Forest carbon densities and uncertainties from Lidar, QuickBird, and field measurements in California. *Remote Sensing of Environment*, 114(7), 1561-1575.
- Gougeon, F. A., & Leckie, D. G. (2006). The individual tree crown approach applied to Ikonos images of a coniferous plantation area. *Photogrammetric Engineering and Remote Sensing*, 72(11), 1287-1297.
- Harding, D. J., Blair, J. B., Garvin, J. B., & Lawrence, W. T. (1994). *Laser altimetry waveform measurement of vegetation canopy structure*.
- Hemery, G. E., & Pryor, S. N. (2005). Applications of the crown diameter-stem diameter relationship for different species of broadleaved trees. *Forest Ecology and Management*, 215(1-3), 285-294.
- Heritage, G. L. (2009). *Laser scanning for the environmental sciences*. West Sussex, PO19 8SQ, UK: Blackwell Publishing Ltd.
- Heurich, M., Schneider, T., & Kennel, E. (2003). *Laser scanning for identification of forest structure in the Bavarian forest national park*.
- Holmgren, J., Nilsson, M., & Olsson, H. (2003). Estimation of tree height and stem volume on plots-using airborne laser scanning. *Forest Science*, 49(3), 419-428.
- Holmgren, J., Persson, Å., & Söderman, U. (2008). Species identification of individual trees by combining high resolution LiDAR data with multi-spectral images. *International Journal of Remote Sensing*, 29(5), 1537-1552.
- Houghton, J. T., Meira Filho, L. G., Lim, B., Treanton, K., et al. (1997). Revised 1996 Guidelines for National Greenhouse Gas Inventories. IPCC/OECD/IEA.

- Hudak, A. T., Lefsky, M. A., Cohen, W. B., & Berterretche, M. (2002). Integration of lidar and Landsat ETM+ data for estimating and mapping forest canopy height. *Remote Sensing of Environment*, 82(2-3), 397-416.
- Husch, B., Beers, T. W., & Kershaw, J. A. (2003). *Forest mensuration*: Wiley.
- Hyypä, J., Hyypä, H., Leckie, D., Gougeon, F., et al. (2008). Review of methods of small-footprint airborne laser scanning for extracting forest inventory data in boreal forests. *International Journal of Remote Sensing*, 29(5), 1339-1366.
- ICIMOD, A., FECOFUN. (2011). Monitoring Report on Forest Carbon Stocks Changes in REDD Project Sites (Ludikhola, Kayarkhola and Charnawati). Kathmandu, Nepal.
- IPCC. (2006). 2006 IPCC Guidelines for National Greenhouse Gas Inventories Volume 4 Agriculture, Forestry and Other Land Use Retrieved 03 January, 2012, from http://www.ipcc-nggip.iges.or.jp/public/2006gl/pdf/4_Volume4/V4_04_Ch4_Forest_Land.pdf
- IPCC. (2007). Summary for Policymakers. In: Climate Change 2007: The Physical Science Basis. Contribution of Working Group I to the Fourth Assessment Report of the Intergovernmental Panel on Climate Change. Cambridge University Press, Cambridge, United Kingdom and New York, NY, USA.
- Jensen, J. R. (2005). *Introductory digital image processing: a remote sensing perspective* (3rd ed.): Pearson Prentice Hall, USA.
- Jochem, A., HOLLHAUS, M., RUTZINGER, M., HÖFLE, B., et al. (2010). Estimation of aboveground biomass using airborne LiDAR data.
- Kaul, M., Mohren, G. M. J., & Dadhwal, V. K. (2010). Carbon storage and sequestration potential of selected tree species in India. *Mitigation and Adaptation Strategies for Global Change*, 15(5), 489-510.
- Ke, Y., & Quackenbush, L. J. (2011). A review of methods for automatic individual tree-crown detection and delineation from passive remote sensing. *International Journal of Remote Sensing*, 1-23.
- Ke, Y., Quackenbush, L. J., & Im, J. (2010). Synergistic use of QuickBird multispectral imagery and LIDAR data for object-based forest species classification. *Remote Sensing of Environment*, 114(6), 1141-1154.
- Keene, O. N. (1995). THE LOG TRANSFORMATION IS SPECIAL. *Statistics in Medicine*, 14(8), 811-819.
- Ketterings, Q. M., Coe, R., van Noordwijk, M., Ambagau, Y., et al. (2001). Reducing uncertainty in the use of allometric biomass equations for predicting above-ground tree biomass in mixed secondary forests. *Forest Ecology and Management*, 146(1-3), 199-209.
- Khanal, Y., Sharma, R., & Upadhyaya, C. (2011). Soil and vegetation carbon pools in two community forests of Palpa district, Nepal. *Banko Janakari*, 20(2), 34-40.
- Khatun, K. (2011). Reconciling timber provision with carbon sequestration opportunities in the tropical forests of Central America. *Environmental Science & Policy*, 14(8), 1091-1102.
- Kim, S. R., Kwak, D. A., Lee, W. K., Son, Y., et al. (2010). Estimation of carbon storage based on individual tree detection in *Pinus densiflora* stands using a fusion of aerial photography and LiDAR data (vol 53, pg 885, 2010). *Science China-Life Sciences*, 53(9), 1162-1162.
- Köhl, M., Baldauf, T., Plugge, D., & Krug, J. (2009). Reduced emissions from deforestation and forest degradation (REDD): a climate change mitigation strategy on a critical track. *Carbon Balance and Management*, 4(10).
- Köhl, M., Magnussen, S., & Marchetti, M. (2006). *Sampling methods, remote sensing and GIS multiresource forest inventory*: Springer Verlag.
- Kuuluvainen, T. (1991). Relationships between crown projected area and components of above-ground biomass in Norway spruce trees in even-aged stands: Empirical results and their interpretation. *Forest Ecology and Management*, 40(3-4), 243-260.
- Kwak, D.-A., Lee, W.-K., Lee, J.-H., Biging, G., et al. (2007). Detection of individual trees and estimation of tree height using LiDAR data. *Journal of Forest Research*, 12(6), 425-434.
- Lamonaca, A., Corona, P., & Barbati, A. (2008). Exploring forest structural complexity by multi-scale segmentation of VHR imagery. *Remote Sensing of Environment*, 112(6), 2839-2849.
- Leckie, D., Gougeon, F., Hill, D., Quinn, R., et al. (2003). Combined high-density lidar and multispectral imagery for individual tree crown analysis. *Canadian Journal of Remote Sensing*, 29(5), 633-649.
- Leckie, D. G., Gougeon, F. A., Tims, S., Nelson, T., et al. (2005). Automated tree recognition in old growth conifer stands with high resolution digital imagery. *Remote Sensing of Environment*, 94(3), 311-326.
- Lefsky, M. A., Cohen, W. B., Acker, S. A., Parker, G. G., et al. (1999a). Lidar remote sensing of the canopy structure and biophysical properties of Douglas-fir western hemlock forests. *Remote Sensing of Environment*, 70(3), 339-361.

- Lefsky, M. A., Cohen, W. B., Parker, G. G., & Harding, D. J. (2002). Lidar remote sensing for ecosystem studies. *Bioscience*, 52(1), 19-30.
- Lefsky, M. A., Harding, D., Cohen, W. B., Parker, G., et al. (1999b). Surface lidar remote sensing of basal area and biomass in deciduous forests of eastern Maryland, USA. *Remote Sensing of Environment*, 67(1), 83-98.
- Li, Z., Hayward, R., Zhang, J., & Liu, Y. (2008). *Individual tree crown delineation techniques for vegetation management in power line corridor*.
- Lim, K., Treitz, P., Baldwin, K., Morrison, I., et al. (2003a). Lidar remote sensing of biophysical properties of tolerant northern hardwood forests. *Canadian Journal of Remote Sensing*, 29(5), 658-678.
- Lim, K., Treitz, P., Wulder, M., St-Onge, B., et al. (2003b). LiDAR remote sensing of forest structure. *Progress in Physical Geography*, 27(1), 88-106.
- Liu, J., & Yang, Y. H. (1994). Multiresolution color image segmentation. *Pattern Analysis and Machine Intelligence, IEEE Transactions on*, 16(7), 689-700.
- Lovell, J., Jupp, D. L. B., Culvenor, D., & Coops, N. (2003). Using airborne and ground-based ranging lidar to measure canopy structure in Australian forests. *Canadian Journal of Remote Sensing*, 29(5), 607-622.
- Lu, D. S. (2006). The potential and challenge of remote sensing-based biomass estimation. *International Journal of Remote Sensing*, 27(7), 1297-1328.
- Magurran, A. E. (1988). *Ecological diversity and its measurement*: Princeton University Press, Princeton, NJ.
- Malhi, Y., Meir, P., & Brown, S. (2002). Forests, carbon and global climate. *Philosophical Transactions of the Royal Society of London. Series A: Mathematical, Physical and Engineering Sciences*, 360(1797), 1567.
- maps-gps-info.com. (2012). GPS Accuracy - How Accurate is it? Retrieved 2012-02-01, 2012, from <http://www.maps-gps-info.com/gps-accuracy.html>
- McCombs, J. W., Roberts, S. D., & Evans, D. L. (2003). Influence of fusing lidar and multispectral imagery on remotely sensed estimates of stand density and mean tree height in a managed loblolly pine plantation. *Forest Science*, 49(3), 457-466.
- Means, J. E., Acker, S. A., Fitt, B. J., Renslow, M., et al. (2000). Predicting forest stand characteristics with airborne scanning lidar. *Photogrammetric Engineering and Remote Sensing*, 66(11), 1367-1371.
- Means, J. E., Acker, S. A., Harding, D. J., Blair, J. B., et al. (1999). Use of large-footprint scanning airborne lidar to estimate forest stand characteristics in the Western Cascades of Oregon. *Remote Sensing of Environment*, 67(3), 298-308.
- MOFSC. (2009). Ministry of Forests and Soil Conservation, Government of Nepal.
- Möller, M., Lymburner, L., & Volk, M. (2007). The comparison index: A tool for assessing the accuracy of image segmentation. *International Journal of Applied Earth Observation and Geoinformation*, 9(3), 311-321.
- Muukkonen, P., & Heiskanen, J. (2007). Biomass estimation over a large area based on standwise forest inventory data and ASTER and MODIS satellite data: A possibility to verify carbon inventories. *Remote Sensing of Environment*, 107(4), 617-624.
- Naesset, E., & Bjercknes, K. O. (2001). Estimating tree heights and number of stems in young forest stands using airborne laser scanner data. *Remote Sensing of Environment*, 78(3), 328-340.
- Nakakaawa, C., Aune, J., & Vedeld, P. (2010). Changes in carbon stocks and tree diversity in agro-ecosystems in south western Uganda: what role for carbon sequestration payments? [Article]. *New Forests*, 40(1), 19-44.
- Nelson, R., Krabill, W., & Tonelli, J. (1988). ESTIMATING FOREST BIOMASS AND VOLUME USING AIRBORNE LASER DATA. *Remote Sensing of Environment*, 24(2), 247-267.
- Nilsson, M. (1996). Estimation of tree heights and stand volume using an airborne lidar system. *Remote Sensing of Environment*, 56(1), 1-7.
- Padwick, C., Deskevich, M., & Smallwood, S. (2010). WorldView-2 pan-sharpening. *ASPRS 2010*.
- Panta, M. (2003). *Analysis of forest canopy density and factors affecting it using RS and GIS techniques : a case study from Chitwan district of Nepal*. ITC, Enschede. Retrieved from http://www.itc.nl/library/papers_2003/msc/nrm/panta.pdf
- Patenaude, G., Hill, R., Milne, R., Gaveau, D. L. A., et al. (2004). Quantifying forest above ground carbon content using LiDAR remote sensing. *Remote Sensing of Environment*, 93(3), 368-380.
- Patenaude, G., Milne, R., & Dawson, T. P. (2005). Synthesis of remote sensing approaches for forest carbon estimation: reporting to the Kyoto Protocol. *Environmental Science & Policy*, 8(2), 161-178.
- Persson, Å., Holmgren, J., & Söderman, U. (2002). Detecting and measuring individual trees using an airborne laser scanner. *Photogrammetric Engineering and Remote Sensing*, 68(9), 925-932.
- Persson, Å., Holmgren, J., Söderman, U., & Olsson, H. (2004). Tree species classification of individual trees in Sweden by combining high resolution laser data with high resolution near-infrared digital

- images. *proceedings of the ISPRS working group VIII/2. Laser-Scanners for Forest and Landscape Assessment. Freiburg, Germany, October*, 3-6.
- Pilger, N. (2008). Coupling Lidar and high-resolution digital imagery for biomass estimation in mixed-wood forest environments. *ASPRS Annual Conference, Portland, Oregon, USA: April 28 –May 2, 2008*
- Pohl, C., & Genderen, J. (1998). Review article Multisensor image fusion in remote sensing: concepts, methods and applications. *International Journal of Remote Sensing*, 19(5), 823-854.
- Popescu, S. C. (2007). Estimating biomass of individual pine trees using airborne lidar. *Biomass and Bioenergy*, 31(9), 646-655.
- Popescu, S. C., & Wynne, R. H. (2004a). Seeing the trees in the forest: Using lidar and multispectral data fusion with local filtering and variable window size for estimating tree height. *Photogrammetric Engineering and Remote Sensing*, 70(5), 589-604.
- Popescu, S. C., Wynne, R. H., & Nelson, R. F. (2003). Measuring individual tree crown diameter with lidar and assessing its influence on estimating forest volume and biomass. *Canadian Journal of Remote Sensing*, 29(5), 564-577.
- Popescu, S. C., Wynne, R. H., & Scrivani, J. A. (2004b). Fusion of small-footprint lidar and multispectral data to estimate plot-level volume and biomass in deciduous and pine forests in Virginia, USA. *Forest Science*, 50(4), 551-565.
- Pouliot, D., King, D., Bell, F., & Pitt, D. (2002). Automated tree crown detection and delineation in high-resolution digital camera imagery of coniferous forest regeneration. *Remote Sensing of Environment*, 82(2), 322-334.
- Rahman, R. M., & Saha, S. (2008). Multi-resolution segmentation for object-based classification and accuracy assessment of land use/land cover classification using remotely sensed data. *Journal of the Indian Society of Remote Sensing*, 36(2), 189-201.
- REDD net. (2009). REDD in Nepal: Putting community forestry centre stage? Retrieved 22 July 2011, from <http://redd-net.org/files/REDDinNepal.pdf>
- Rosenqvist, Å., Milne, A., Lucas, R., Imhoff, M., et al. (2003). A review of remote sensing technology in support of the Kyoto Protocol. *Environmental Science & Policy*, 6(5), 441-455.
- Shah, S. K. (2011). *Modelling the relationship between tree canopy projection area and above ground carbon stock using high resolution geoeye satellite images*. MSc Thesis, University of Twente Faculty of Geo-Information and Earth Observation ITC, Enschede. Retrieved from http://www.itc.nl/library/papers_2011/msc/nrm/shah.pdf
- Shannon, C. E., & Weaver, W. (1962). *The mathematical theory of communication* (Vol. 19). Urbana, USA: University of Illinois Press
- Sharma, C. M., Baduni, N. P., Ghildiyal, S. K., et al. (2010). Tree diversity and carbon stocks of some major forest types of Garhwal Himalaya, India. *Forest Ecology and Management*, 260(12), 2170-2179.
- Sharma, E. R., & Pukkala, T. (1990). *Volume Equations and Biomass Prediction of Forest Trees of Nepal*. Kathmandu, Nepal: Forest Survey and Statistics Division, MOFSC.
- Sharma, R. P. (2011). Allometric models for total-tree and component-tree biomass of *Alnus nepalensis* D. Don in Nepal. *The Indian Forester*, 137(12), 1386-1390.
- Shiver, B. D., & Borders, B. E. (1996). *Sampling techniques for forest resource inventory*: John Wiley and Sons.
- Shrestha, B. M., & Singh, B. R. (2008). Soil and vegetation carbon pools in a mountainous watershed of Nepal. *Nutrient Cycling in Agroecosystems*, 81(2), 179-191.
- Shrestha, S. K. (2011). *Carbon stock estimation using very high resolution satellite imagery and individual crown segmentation : a case study of broadleaved and needle leaved forest of Dollakha, Nepal*. MSc Thesis, University of Twente Faculty of Geo-Information and Earth Observation (ITC), Enschede. Retrieved from http://www.itc.nl/library/papers_2011/msc/nrm/shrestha.pdf
- Sierra, C. A., del Valle, J. I., Orrego, S. A., Moreno, F. H., et al. (2007). Total carbon stocks in a tropical forest landscape of the Porc region, Colombia. *Forest Ecology and Management*, 243(2-3), 299-309.
- Simpson, E. H. (1949). Measurement of diversity. *Nature*, 163:688.
- Song, C., Dickinson, M. B., Su, L., Zhang, S., et al. (2010). Estimating average tree crown size using spatial information from Ikonos and QuickBird images: Across-sensor and across-site comparisons. *Remote Sensing of Environment*, 114(5), 1099-1107.
- Steininger, M. (2000). Satellite estimation of tropical secondary forest above-ground biomass: data from Brazil and Bolivia. *International Journal of Remote Sensing*, 21(6-7), 1139-1157.
- Strassburg, B. B. N., Annabel Kelly, Andrew Balmford, Davies, R. G., et al. (2010). Global congruence of carbon storage and biodiversity in terrestrial ecosystems. *Conservation Letters*(3), 98–105.
- Suarez, J. C., Ontiveros, C., Smith, S., & Snape, S. (2005). Use of airborne LiDAR and aerial photography in the estimation of individual tree heights in forestry. *Computers & Geosciences*, 31(2), 253-262.

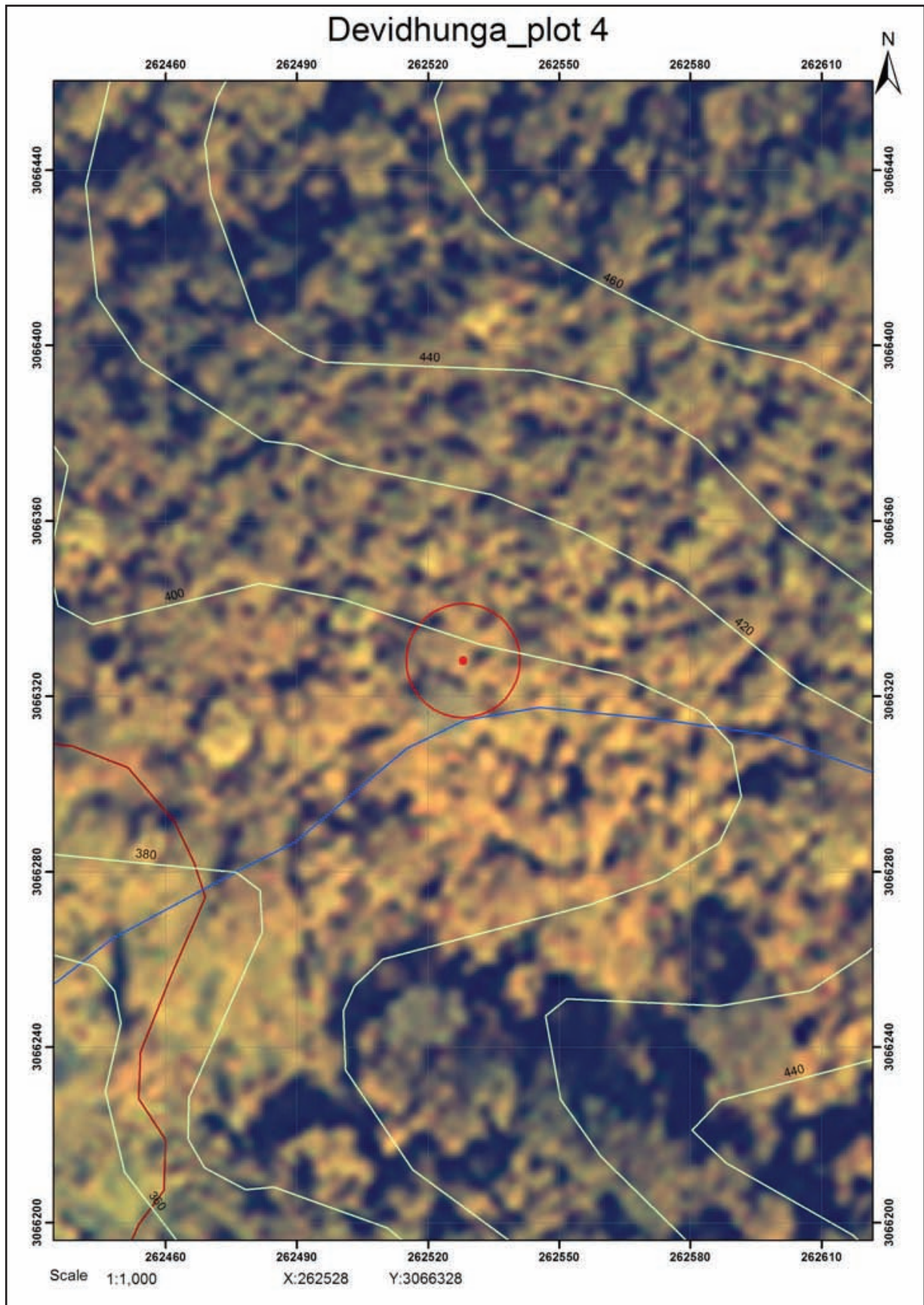
Appendices

Appendix 1: Features of satellite image

Sensor Name	WorldView-2
Launch Information	Date: October 8, 2009 Vandenberg Air Force Base, California, USA
Orbit	Altitude: 770 kilometres, Type: Sun synchronous Period: 100 minutes
Mission Life	7.25 years, including all consumables and degradable (e.g. propellant)
Spectral Range	Panchromatic: 450 – 800 nm Coastal Blue: 400 – 450 nm Blue: 450 – 510 nm Green: 510 – 580 nm Yellow: 585 – 625 nm Red: 630 -690 nm Red-Edge: 705 – 745 nm Near Infrared 1: 770 – 895 nm Near Infrared 2: 860 – 1040 nm
Sensor Resolution (GSD = Ground Sample Distance)	Panchromatic: 0.46 meters GSD at nadir* Multispectral: 1.84 meters GSD at nadir*
Radiometric resolution	11-bits per pixel
Swath Width	16.4 Km at nadir
Max Viewing Angle / Accessible Ground Swath	Nominally +/-45° off-nadir = 1355 km wide swath Higher angles selectively available
Revisit Frequency	1.1 days at 1 meter GSD or less 3.7 days at 20° off-nadir or less (0.52 meter GSD)
Acquisition Time	10:30 am local time; 04:45 GMT
Spacecraft Size, Mass and Power	4.3 meters (14 feet) tall x 2.5 meters (8 feet) across 7.1 meters (23 feet) across the deployed solar arrays 2800 kilograms (6200 pounds) 3.2 kW solar array, 100 Ahr battery
Max Contiguous Area Collected in a Single Pass (30° off-nadir angle)	Mono: 138 x 112 km (8 strips)
Geo-location Accuracy (CE90%)	Specification of 6.5 m CE90, with predicted performance in the range of 4.6 to 10.7 m (15 to 35 feet) CE90, excluding terrain and off-nadir effects With registration to GCPs in image: 2.0 m (6.6 feet)
Onboard Storage	2199 gigabits solid state with EDAC

**Distribution and use of imagery at better than .50 m GSD pan and 2.0 m GSD multispectral is subject to prior approval by the U.S. Government.*

Appendix 2: Printed image of sample plot



Appendix 3: Sample of data collection sheet

Data Collection Sheet

Name of recorder:

Date:

CF Name		Coordinates	X:
Sample plot ID			Y:

Slope (%):

Aspect:

Altitude:

Canopy Density: 1. 2. 3. 4. 5.

Average:

Reference Points:

Bearing:

Distance:

Undergrowth:

S.N.	Species	DBH (cm)	Height (m)	Crown diam (m)	Tree Class*	X_ Coord	Y_ Coord	Remarks
1.								
2.								
3.								
4.								
5.								
6.								
7.								
8.								
9.								
10.								
11.								
12.								
13.								
14.								
15.								

* D=Dominant

CD= Codominant

Others= Dominated or Suppressed

Diversity Index

S. N.	Species	Sapling/ Regeneration	No. of individuals	Relative abundance	Remarks

Appendix 4: Location of sample plots

CF Name	Plot name	X-coordinate	Y-coordinate	CF Name	Plot name	X-coordinate	Y-coordinate
Samphrang	SAM1	263219	3070730	Nibuwatar	NIB16	264729	3067341
Samphrang	SAM2	264232	3070552	Nibuwatar	NIB17	266279	3066543
Samphrang	SAM3	264426	3071262	Nibuwatar	NIB18	263634	3066797
Samphrang	SAM4	264062	3071109	Nibuwatar	NIB19	266131	3065901
Samphrang	SAM5	264155	3071362	Nibuwatar	NIB20	264862	3066165
Janpragati	JAN_1	263330	3070083	Nibuwatar	NIB21	264802	3067632
Janpragati	JAN_2	262273	3070226	Nibuwatar	NIB22	266042	3066109
Janpragati	JAN_3	263158	3070359	Nibuwatar	NIB23	265557	3066212
Pragati	PRA1	261706	3070133	Nibuwatar	NIB24	263815	3067369
Pragati	PRA2	261103	3069195	Nibuwatar	NIB25	265101	3066323
Pragati	PRA3	261867	3070002	Nibuwatar	NIB26	265024	3067175
Pragati	PRA4	261753	3069633	Nibuwatar	NIB27	264707	3066700
Pragati	PRA5	261185	3069470	Devdhunga	DEV1	262850	3067609
Pragati	PRA6	261529	3069649	Devdhunga	DEV2	262774	3067127
Pragati	PRA7	261239	3069282	Devdhunga	DEV3	263292	3065384
Jamuna	JAM1	262652	3069794	Devdhunga	DEV4	262528	3066328
Jamuna	JAM2	262831	3069668	Devdhunga	DEV5	262362	3067320
Jamuna	JAM3	263062	3069976	Devdhunga	DEV6	263185	3066495
Janpragati (B)	JANP1	263735	3068187	Devdhunga	DEV7	263052	3065947
Janpragati (B)	JANP2	263433	3068367	Devdhunga	DEV8	263233	3067037
Janpragati (B)	JANP3	264205	3068184	Devdhunga	DEV9	262497	3067065
Janpragati (B)	JANP4	263980	3068456	Devdhunga	DEV10	262985	3067101
Janpragati (B)	JANP5	263312	3067851	Devdhunga	DEV11	262452	3066558
Janpragati (B)	JANP6	263374	3067702	Devdhunga	DEV12	263620	3066534
Nibuwatar	NIB1	265209	3066098	Devdhunga	DEV13	262805	3067827
Nibuwatar	NIB2	264470	3066725	Devdhunga	DEV14	262398	3067941
Nibuwatar	NIB3	264322	3067913	Devdhunga	DEV15	263449	3066099
Nibuwatar	NIB4	265646	3066052	Devdhunga	DEV16	263232	3067613
Nibuwatar	NIB5	265408	3065941	Devdhunga	DEV17	263330	3065895
Nibuwatar	NIB6	264447	3067706	Devdhunga	DEV18	262944	3066576
Nibuwatar	NIB7	264272	3067708	Devdhunga	DEV19	263307	3066197
Nibuwatar	NIB8	265861	3066137	Devdhunga	DEV20	263415	3066338
Nibuwatar	NIB9	263892	3067796	Devdhunga	DEV21	263357	3066565
Nibuwatar	NIB10	265384	3066539	Devdhunga	DEV22	263540	3065587
Nibuwatar	NIB11	265463	3065741	Devdhunga	DEV23	263697	3066029
Nibuwatar	NIB12	263866	3066459	Devdhunga	DEV24	263704	3066148
Nibuwatar	NIB13	266986	3066327	Devdhunga	DEV25	263461	3065427
Nibuwatar	NIB14	263953	3067587	Devdhunga	DEV26	263136	3066577
Nibuwatar	NIB15	264558	3066228	Devdhunga	DEV27	262979	3066618

Appendix 5: Name list of plant species found in the study area

S. N.	Species	Scientific name	Form of species
1	Aankhatare	<i>Walsura trijuga</i>	Tree (M)
2	Amala	<i>Emblica officinalis</i>	Tree (M)
3	Arkhole	<i>Quercus spicata</i>	Tree (M)
4	Arkhu	<i>Quercus spicata</i>	Tree (M)
5	Asare	<i>Mussaenda frondosa</i>	Shrub
6	Asna	<i>Terminalia tomentosa</i>	Tree (L)
7	Badkaule	<i>Casaria graveolens</i>	Tree (M)
8	Bandare	<i>Cynocardia odorata</i>	Tree (M)
9	Banpipal	<i>Sapium baccatum</i>	Tree (L)
10	Bansupari	<i>Ophiopogon wallichianus</i>	Tree (M)
11	Barro	<i>Terminalia belerica</i>	Tree (L)
12	Bhalayo	<i>Semicarpous anacardium</i>	Tree(M)
13	Bhalebhusha	Vernacular name	Shrub
14	Bhalukath	<i>Sida rhombifolia</i>	Tree (M)
15	Bhellar	Vernacular name	Tree (M)
16	Bhorla	<i>Bauhinia vabilii</i>	Shrub
17	Bilaune	<i>Maesa chisia</i>	Shrub
18	Botdhairo	<i>Lagerstromia parviflora</i>	Tree (M)
19	Champ	<i>Michelia champaca</i>	Tree (L)
20	Chhatiwani	<i>Alstonia scholaris</i>	Tree (L)
21	Chilaune	<i>Schima wallichii</i>	Tree (M)
22	Chiuri	<i>Bassia butyracea</i>	Tree (L)
23	Dabdabe	<i>Bassia butyracea</i>	Tree (M)
24	Dhalnekatus	<i>Castonopsis indica</i>	Tree (M)
25	Dhangero	<i>Dillenia aurea</i>	Tree (S)
26	Dolikath	<i>Dillenia aurea</i>	Tree (M)
27	Dumari	<i>Ficus benjamina</i>	Tree (M)
28	Falame	Vernacular name	Tree (M)
29	Gayo	<i>Bridelia retusa</i>	Tree (M)
30	Gindari	<i>Premna latifolia</i>	Tree (M)
31	Guelo	<i>Elaeagnus latifolia</i>	Tree (M)
32	Harro	<i>Terminalia chebula</i>	Tree (L)
33	Jamun	<i>Syzygium cumini</i>	Tree (L)
34	Jhakrisyaula	<i>Actinodaphne angustifolia</i>	Tree (S)
35	Jhirenge	Vernacular name	Tree (S)
36	Kadam	<i>Anthocephalus cadamba</i>	Tree (L)
37	Kalibakhre	Vernacular name	Tree (S)
38	Kalikath	<i>Myrsine semiserrata</i>	Tree (M)
39	Kalo Siris	<i>Albizia lebbek</i>	Tree (M)
40	Karma	<i>Adina cordifolia</i>	Tree (L)

S. N.	Species	Scientific name	Form of species
41	Khamari	<i>Gmelia arborea</i>	Tree (M)
42	Khasreto	<i>Ficus hispida</i>	Tree (M)
43	Khatire	Vernacular name	Tree (S)
44	Khirro	<i>Holarrhena pubescens</i>	Tree (M)
45	Kukhurekath	Vernacular name	Tree (S)
46	Kummi	<i>Careya arborea</i>	Tree (M)
47	Kutmiro	<i>Litsea polyantha</i>	Tree (M)
48	Kyamuna	<i>Syzygium serasoides</i>	Tree (M)
49	Latikath	<i>Cornus oblonga</i>	Tree (M)
50	Madane	<i>Randia dumetorum</i>	Shrub
51	MasureKatus	<i>Castonopsis tribuloides</i>	Tree (M)
52	Mayankanda	<i>Tetrameles nudiflora</i>	Tree (L)
53	Nimaro	<i>Ficus roxburghii</i>	Tree (M)
54	Odane	Vernacular name	Tree (L)
55	Padake	<i>Albizia julibrissin</i>	Tree (M)
56	Padari	<i>Stereospermum personatum</i>	Tree (M)
57	Parijaat	<i>Nyctanthes arbortristis</i>	Tree (M)
58	Pipal	<i>Ficus religiosa</i>	Tree (L)
59	Rajbriksha	<i>Cassia fistula</i>	Tree (M)
60	Sal	<i>Shorea robusta</i>	Tree (L)
61	Sandan	<i>Ougeinia oojeinensis</i>	Tree (M)
62	Sidhali	Vernacular name	Tree (M)
63	Simal	<i>Bombax ceiba</i>	Tree (L)
64	Sindure	<i>Mallotus philippensis</i>	Tree (M)
65	Singane	<i>Quercus pachyphylla</i>	Tree (L)
66	Tantari	<i>Dillenia pentagyna</i>	Tree (M)
67	Tatelo	<i>Oroxylon indicum</i>	Tree (S)
68	Tendu	<i>Diospyros melanoxylon</i>	Tree (M)
69	Thinke	Vernacular name	Tree (M)
70	Tiari	Vernacular name	Tree (M)
71	Tirchaule	Vernacular name	Tree (S)
72	Tuni	<i>Cedrela toona</i>	Tree (L)

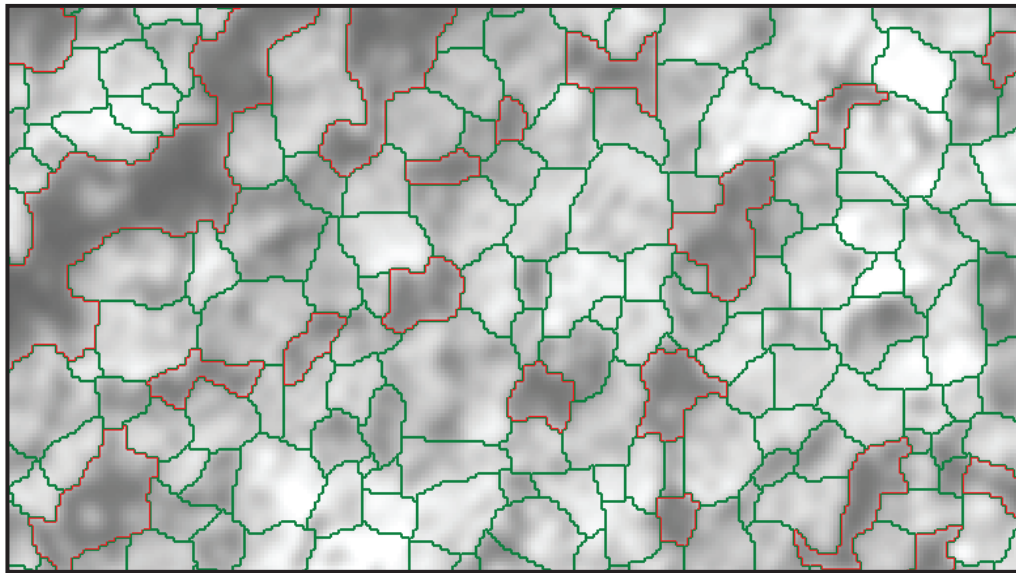
Appendix 6: Descriptive statistics of trees for each CFs

Statistics	DBH (cm)	Height (m)	Crown Diameter (m)
Samphrang CF			
Mean	27.55	10.18	7.02
Minimum	7.00	4.00	2.00
Maximum	86.00	29.10	12.00
Standard Deviation	18.88	5.73	2.99
Number of Trees	70.00	43.00	25.00
Jamuna CF			
Mean	17.33	10.82	4.50
Minimum	6.50	2.00	1.00
Maximum	113.00	35.00	15.50
Standard Deviation	18.79	6.65	4.17
Number of Trees	53.00	25.00	15.00
Janpragati CF			
Mean	17.65	9.48	3.18
Minimum	7.00	5.00	1.50
Maximum	51.50	14.70	10.00
Standard Deviation	8.77	2.50	2.20
Number of Trees	57	36	22
Pragati CF			
Mean	23.04	11.59	4.32
Minimum	6.00	3.00	1.00
Maximum	77.00	30.50	11.00
Standard Deviation	18.98	7.30	2.65
Number of Trees	99.00	78.00	48.00
Janpragati B CF			
Mean	20.21	11.69	4.25
Minimum	5.00	4.80	1.00
Maximum	105.00	23.90	14.00
Standard Deviation	18.66	4.80	3.04
Number of Trees	125.00	78.00	56.00
Devidhunga CF			
Mean	25.93	13.76	5.09
Minimum	7.00	2.00	1.00
Maximum	116.00	33.00	20.00
Standard Deviation	18.08	7.17	3.40
Number of Trees	436.00	221.00	158.00
Nibuwatar CF			
Mean	32.33	14.15	5.03
Minimum	6.00	2.00	1.00
Maximum	152.00	37.00	14.00
Standard Deviation	22.98	6.81	2.77
Number of Trees	307.00	243.00	169.00

Appendix 7: Details of outlier trees

CF Name	Plot No	Tree No	Species	DBH (cm)	Height (m)	Crown diameter (m)
Devidhunga	73	1	<i>Shorea robusta</i>	102	25.7	13
Devidhunga	27	1	<i>Shorea robusta</i>	104	30.8	10
Devidhunga	61	11	<i>Terminalia belerica</i>	105	25.6	20
Devidhunga	30	13	<i>Shorea robusta</i>	116	28.5	11.5
Jamuna	5	25	<i>Shorea robusta</i>	113	35	15.5
Nibuwatar	42	4	<i>Vernacular name</i>	99	20	
Nibuwatar	49	1	<i>Shorea robusta</i>	101	20.9	9
Nibuwatar	48	1	<i>Terminalia tomentosa</i>	105	28.5	10
Nibuwatar	42	2	<i>Vernacular name</i>	111	34	8
Nibuwatar	42	5	<i>Michelia champaca</i>	152	37	14
Janpragati B	36	26	<i>Shorea robusta</i>	105	9.6	
Nibuwatar	48	4	<i>Mallotus philippinensis</i>	11	2	

Appendix 8: Segmentation of Panchromatic WorldView-2 image



Appendix 9: Accuracy assessment of species classification for each CFs

Accuracy assessment for Devidhunga CF

Class Name	<i>Shorea</i>	<i>Terminalia</i>	<i>Lagerstroemia</i>	<i>Mallotus</i>	<i>Semecarpus</i>	Others	Total	Commission Error	User Accuracy
<i>Shorea</i>	6	0	0	0	0	3	9	33.33 %	66.67 %
<i>Terminalia</i>	1	1	0	0	0	2	4	75 %	25 %
<i>Lagerstroemia</i>	0	0	3	0	0	1	4	25 %	75 %
<i>Mallotus</i>	0	0	0	2	0	0	2	0	100 %
<i>Semecarpus</i>	0	0	0	0	1	0	1	0	100 %
<i>Others</i>	0	0	1	1	1	5	8	37.50 %	62.50 %
Unclassified						3	3		
Total	7	1	4	3	2	14	31		
Omission Error (%)	14.29	0	25	33.33	50	64.29			
Producer Accuracy	85.71	100	75	66.67	50	35.71			
Overall Accuracy	58.06 %								
Kappa Statistic	0.4683								

Accuracy assessment for Nibuwatar CF

Class Name	<i>Shorea</i>	<i>Terminalia</i>	<i>Lagerstroemia</i>	<i>Schima</i>	Others	Total	Commission Error	User Accuracy	
<i>Shorea</i>	6	1	1	0	0	8	25 %	75 %	
<i>Terminalia</i>	2	2	0	0	0	4	57.14 %	42.86 %	
<i>Lagerstroemia</i>	0	0	2	0	0	2	0	100 %	
<i>Schima</i>	1	1	0	3	2	7	50 %	50 %	
<i>Others</i>	3	0	1	0	2	6	66.67 %	33.33 %	
Total	12	4	4	3	4	27			
Omission Error (%)	50	50	50	0	50				
Producer Accuracy (%)	50	50	50	100	50				
Overall Accuracy	55.56 %								
Kappa Statistic	0.4255								

Accuracy assessment for Janpragati B CF

Class Name	<i>Shorea robusta</i>	<i>Schima wallichii</i>	Others	Unclassified	Total	Commission Error	User Accuracy
<i>Shorea robusta</i>	3	0	0	0	3	0	100 %
<i>Schima wallichii</i>	0	2	1	0	3	33.33 %	66.67 %
<i>Others</i>	2	0	2	0	4	50 %	50 %
Unclassified	0	0	0	1	1		
Total	5	2	3	1	11		
Omission Error	40 %	0	33.33				
Producer Accuracy	60 %	100 %	66.67				
Overall Accuracy	72.73 %						
Kappa Statistic	0.6207						

Accuracy assessment for Samphrang, Jamuna, Janpragati and Pragati CF

Class Name	<i>Shorea</i>	<i>Terminalia</i>	<i>Lagerstroemia</i>	<i>Mallotus</i>	Others	Total	Commission Error	User Accuracy
<i>Shorea</i>	5	0	1	0	1	7	28.57 %	71.43 %
<i>Terminalia</i>	0	2	0	0	0	2	0 %	100 %
<i>Lagerstroemia</i>	1	0	2	0	1	4	50 %	50 %
<i>Mallotus</i>	0	0	0	2	1	3	33.33 %	66.67 %
Others	2	2	2	1	9	16	43.75 %	56.25 %
Total	8	4	5	3	12	32		
Omission Error (%)	37.5	25	50	60	33.33			
Producer Accuracy (%)	62.5	75	50 %	40	66.67			
Overall Accuracy		62.50 %						
Kappa Statistic		0.4804						

Appendix 10: Details of ANOVA table and regression parameters

Shorea robusta

ANOVA

	df	SS	MS	F	Significance F
Regression	2	92.06343754	46.03172	56.13121	2.22E-14
Residual	59	48.3843361	0.820073		
Total	61	140.4477736			

Regression coefficients

	Coefficients	Standard Error	t Stat	P-value	Lower 95%
Intercept	-0.87673818	0.758643601	-1.15567	0.252477	-2.39478
CHM_log	1.872509034	0.35371466	5.293841	1.85E-06	1.164728
CPA_log	0.59725025	0.193917053	3.079926	0.003142	0.209223

1. *Lagerstroemia parviflora*

ANOVA

	df	SS	MS	F	Significance F
Regression	2	13.834	6.917002	20.76638	2.95E-06
Residual	28	9.326422	0.333087		
Total	30	23.16043			

Regression coefficients

	Coefficients	Standard Error	t Stat	P-value	Lower 95%
Intercept	0.204751	0.725493	0.282224	0.779847	-1.28135
CHM_ht	1.493948	0.382768	3.903014	0.000545	0.709884
CPA_image	0.370105	0.244679	1.512614	0.141584	-0.1311

2. *Terminalia tomentosa*

ANOVA

	df	SS	MS	F	Significance F
Regression	2	9.519374	4.759687	35.18614	2.17E-06
Residual	15	2.029075	0.135272		
Total	17	11.54845			

Regression coefficients

	Coefficients	Standard Error	t Stat	P-value	Lower 95%
Intercept	-0.12553	1.032274	-0.1216	0.904827	-2.32577
CHM_ht	1.847621	0.455095	4.059856	0.001027	0.877609
CPA_image	0.458059	0.173854	2.634729	0.018755	0.087497

3. *Schima wallichii*

ANOVA

	df	SS	MS	F	Significance F
Regression	2	25.22783	12.61391	33.83419	1.94E-07
Residual	22	8.201944	0.372816		
Total	24	33.42977			

Regression coefficients

	Coefficients	Standard Error	t Stat	P-value	Lower 95%
Intercept	-0.14415	0.837675	-0.17209	0.864942	-1.88138
CHM_ht	0.883293	0.406765	2.171506	0.040953	0.039714
CPA_image	1.124459	0.229827	4.892637	6.83E-05	0.647827

4. Others

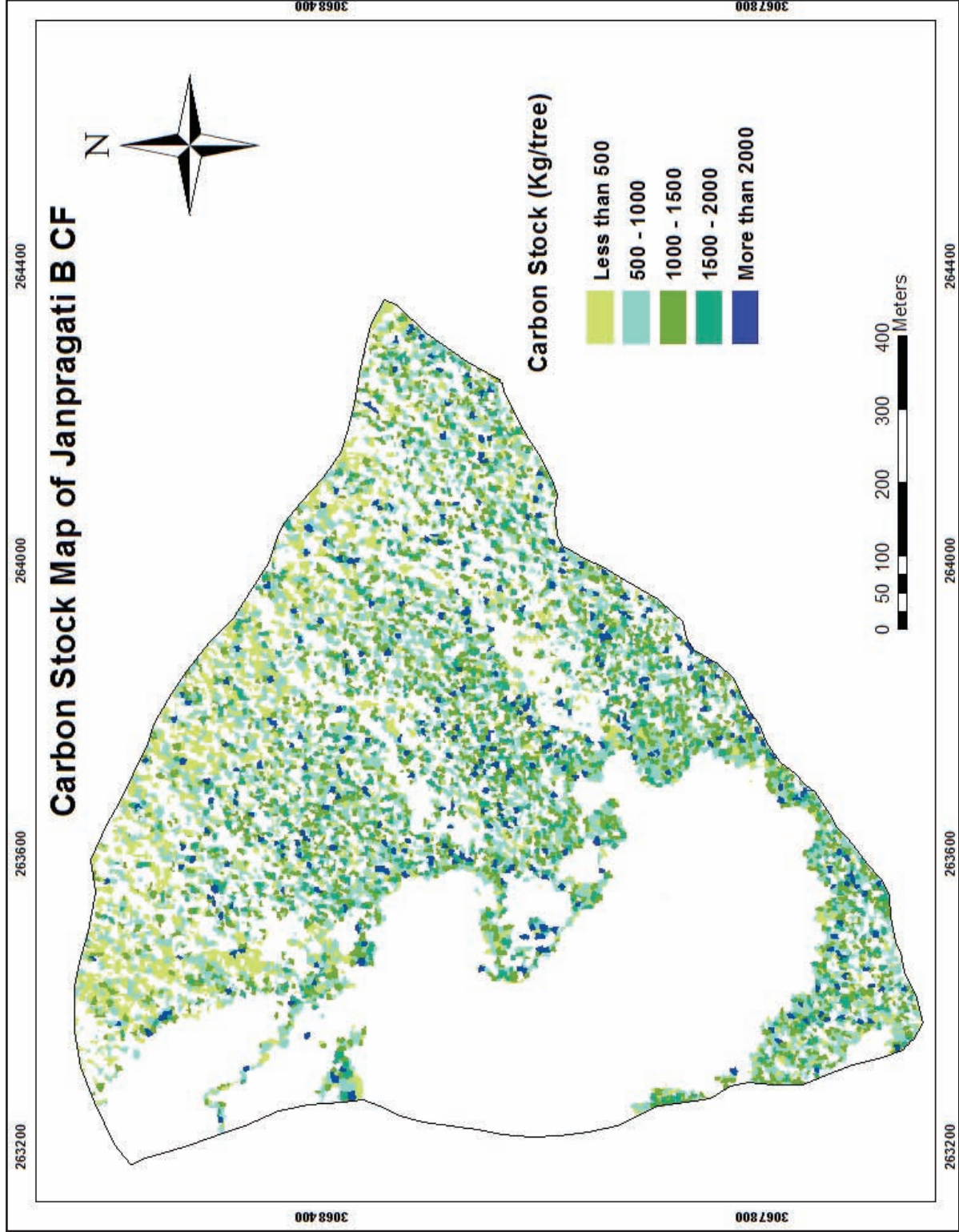
ANOVA

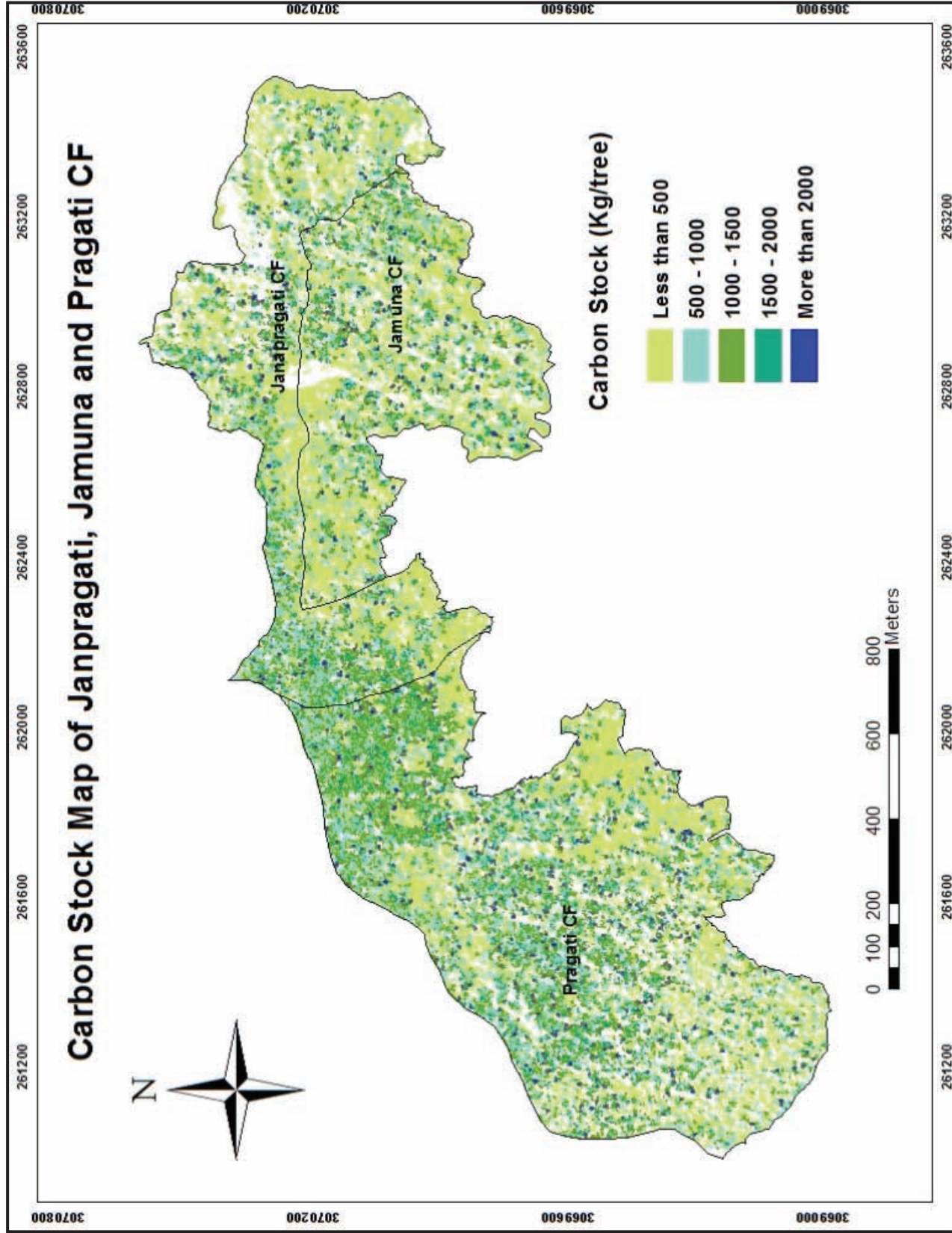
	df	SS	MS	F	Significance F
Regression	2	27.88288	13.94144	43.47844	1.68E-11
Residual	48	15.39129	0.320652		
Total	50	43.27416			

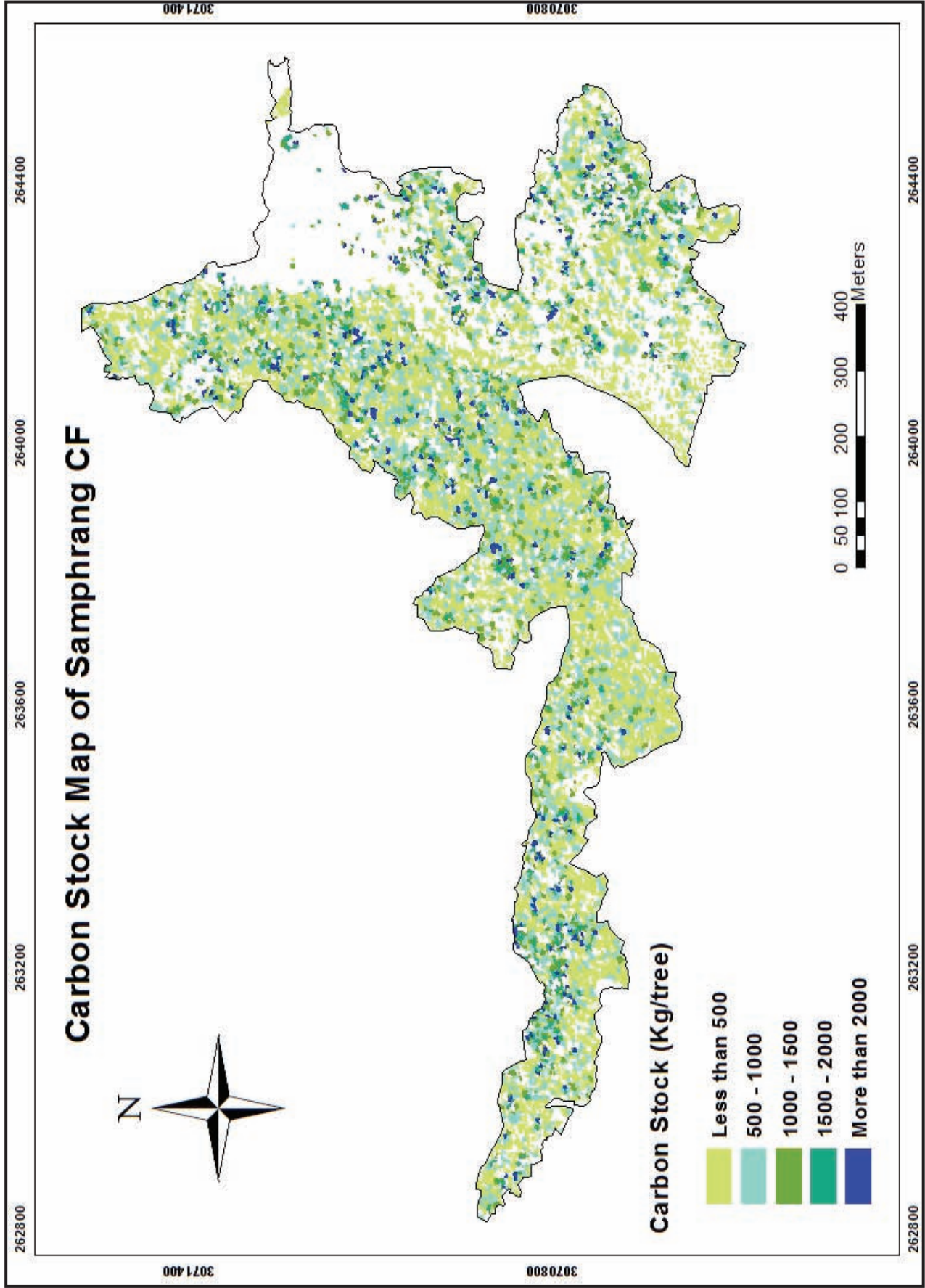
Regression coefficients

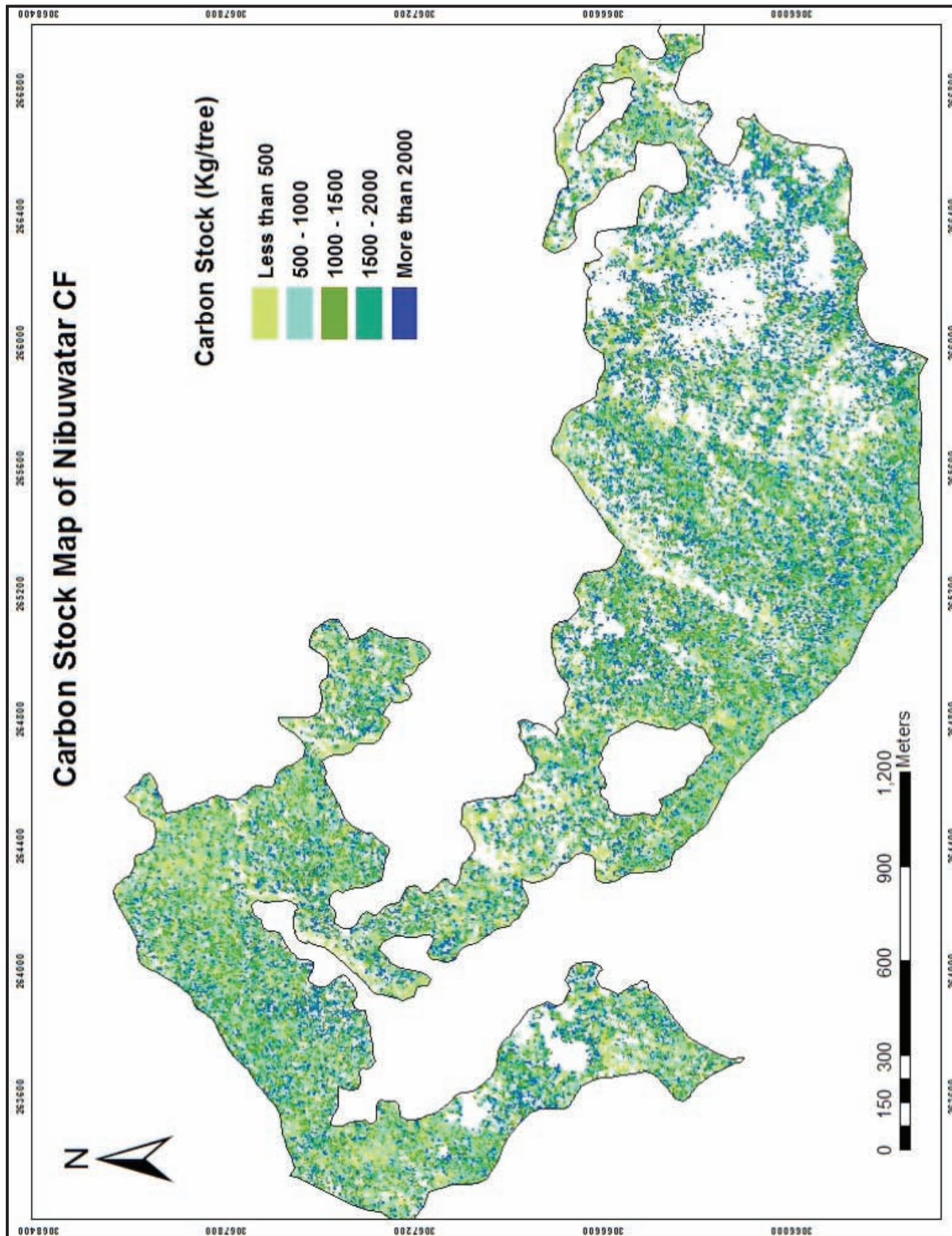
	Coefficients	Standard Error	t Stat	P-value	Lower 95%
Intercept	0.0436	0.60867	0.071631	0.943193	-1.18021
CHM_ht	1.395735	0.291881	4.781868	1.69E-05	0.80887
CPA_image	0.615528	0.153948	3.998295	0.000219	0.305996

Appendix 11: Carbon map of study area (CF wise)









Appendix 12: Photographs from the field

